H3K36-dependent anchoring of the KAT Mst2C is required to maintain the balance between euchromatic and heterochromatic domains in *S. pombe*

Paula Georgescu

München

2019

Aus dem Biomedizinischen Centrum, Lehrstuhl für Physiologische Chemie

Institut der Ludwig-Maximilians-Universität München

Vorstand: Prof. Andreas Ladurner, PhD

H3K36-dependent anchoring of the KAT Mst2C is required to maintain the balance between euchromatic and heterochromatic domains in *S. pombe*

Dissertation

zum Erwerb des Doktorgrades der Naturwissenschaften

an der Medizinischen Fakultät der

Ludwig-Maximilians-Universität zu München

vorgelegt von

Paula Raluca Georgescu

aus

München

2019

Mit Genehmigung der Medizinischen Fakultät

der Universität München

Betreuer: Prof. Andreas Ladurner, PhD

Zweitgutachter: Prof. Dr. rer. nat. Aloys Schepers

Dekan: Prof. Dr. med. dent. Reinhard Hickel

Tag der mündlichen Prüfung: 21.10.2020

Eidesstattliche Versicherung

Georgescu, Paula Raluca

Ich erkläre hiermit an Eides statt,
dass ich die vorliegende Dissertation mit dem Titel

"H3K36-dependent anchoring of the KAT Mst2C is required to maintain the balance between euchromatic and heterochromatic domains in *S. pombe*"

selbständig verfasst, mich außer der angegebenen keiner weiteren Hilfsmittel bedient und alle Erkenntnisse, die aus dem Schrifttum ganz oder annähernd übernommen sind, als solche kenntlich gemacht und nach ihrer Herkunft unter Bezeichnung der Fundstelle einzeln nachgewiesen habe.

Ich erkläre des Weiteren, dass die hier vorgelegte Dissertation nicht in gleicher oder in ähnlicher Form bei einer anderen Stelle zur Erlangung eines akademischen Grades eingereicht wurde.

München, 20.12.2019	Paula Georgescu
Ort, Datum	Unterschrift Doktorandin

Table of contents

1 Summary

1.1 English version

PWWP domains are highly conserved in eukaryotes and act in recruiting histone modifiers to chromatin that is decorated by methylation. In *S. cerevisiae*, the NuA3b subunit Pdp3 targets this H3K14-specific HAT complex histone H3 (di- and) trimethylated at K36, which promotes transcriptional elongation. However, in its *S. pombe* homologue Mst2C the function and target of Pdp3 have yet remained unknown.

In this doctoral thesis, I provide evidence that Mst2C functions in euchromatic and heterochromatic transcription but through entirely different means.

My research revealed that deletion of *pdp3+* in *S. pombe* results in perturbed silencing at pericentromeric and subtelomeric heterochromatin domains. However, this is suppressed in absence of Mst2, a catalytic subunit of Mst2C, which is also required for the functional integrity of the complex. Based on this observation, and in cooperation with the Bühler group in Basel, I studied the distribution of Mst2 and Pdp3 on chromatin. We could show that *pdp3+* deletion or mutation of its PWWP domain led to loss of Mst2 binding and its encroachment on heterochromatin, thereby demonstrating that Mst2 localization to euchromatin is dependent on Pdp3. In addition, I could reveal that the PWWP domain of Pdp3 is able to discriminate between the different methylation states of H3K36. Both binding of Mst2 and of Pdp3 was abolished in a Set2 truncation mutant, which mediates mono and di methylation but not trimethylation of H3K36. Lastly, my collaborators could show that in addition to H3K14, euchromatic Mst2C acetylates the HULC subunit Brl1, thereby promoting transcription and preventing the initiation of ectopic silencing.

Several studies have reported that loss of Set2 results in a silencing defect itself. Through studying heterochromatic transcription in *set2Δ* in conjunction with deletion mutants of *pdp3+*, *mst2+*, and *nto1+* and *ptf2+*, which are essential for Mst2C integrity, I determined that, as in *pdp3Δ*, the silencing defect of *set2Δ* is solely founded in the encroachment of Mst2C on heterochromatin. Intriguingly, deletion of any of the three critical subunits resulted in suppression below the level of found in wild-type strains, implying that Mst2C is required to maintain basal transcription in heterochromatin. Together with the previous observations, this suggests that loss of Pdp3 and Set2

leads a silencing defect via the same pathway that promotes basal transcription. Surprisingly, I found that Mst2C promotes heterochromatin transcription via an entirely different Pdp3-independent mechanism than in euchromatin, as it functions neither through Brl1 nor H3K14ac, but a yet unknown target.

In conclusion, this thesis has demonstrated that Pdp3-dependent anchoring of Mst2C to H3K36me3 has a dual purpose: (a) in euchromatin it prevents formation of ectopic heterochromatin at regions decorated with H3K36me3 and promoting transcription in a Brl1-dependent manner; (b) in heterochromatin, this sequestration protects Mst2C-mediated but Pdp3 and Brl1-independent basal transcription from becoming hyperactivated and interfering with maintenance of this region.

1.2 Deutsche Version

PWWP-Domänen sind in Eukaryoten hochkonserviert und werden dazu verwendet Histonmodifizierer zu mit Methylierung gekennzeichnetem Chromatin zu rekrutieren. In *S. cerevisiae* lotst die Pdp3, eine Untereinheit von NuA3b, diesen H3K14-spezifischen HAT-Komplex zu Histon H3, welches an K36 (di- und) trimethyliert ist, was wiederum transkriptionelle Elongation begünstigt. Jedoch blieben die Funktion und der Interaktionspartner von Pdp3 in seinem Homolog Mst2C in *S. pombe* bis dato bekannt.

Anhand dieser Doktorarbeit liefere ich nun Beweise dafür, dass Mst2C sowohl an euchromatischer als auch an heterochromatischer Transkription beteiligt ist, aber auf gänzlich verschiedene Art und Weise.

Meine Nachforschungen enthüllten, dass Deletion von *pdp3⁺* in *S. pombe* in einer Beeinträchtigung der Stilllegung perizentromerischer and subtelomerer Heterochromatindomänen resultiert. Diese wird bei Fehlen von Mst2, einer katalytischen Untereinheit von Mst2C, welche auch für den Erhalt der Komplexfunktion benötigt wird, supprimiert. Basierend auf dieser Beobachtung untersuchte ich zusammen mit unseren Kollaborationspartnern, der in Basel ansässigen Bühler-Gruppe, die Verteilung von Mst2 und Pdp3 auf Chromatin. Wir konnten zeigen, dass Deletion von *pdp3⁺* oder Mutation seiner PWWP-Domäne zum Verlust der Bindung von Mst2 und einem Vordringen dessen in Heterochromatin führt, wodurch demonstriert wurde, dass die euchromatische Positionierung von Mst2 von Pdp3 abhängt. Darüber hinaus konnte ich enthüllen, dass die PWWP-Domäne von Pdp3 dazu in der Lage ist zwischen den Methylierungsstadien von H3K36 zu unterscheiden.

Sowohl die Anbindung von Mst2 also auch Pdp3 wurden in einer trunkierten Set2-Mutante, welche zwar Mono- und Dimethylierung, jedoch keine Trimethylierung von H3K3 vermitteln kann, aufgehoben. Schlussendlich konnten meine Mitpartner darlegen, dass euchromatisches Mst2C zusätzlich zu H3K14 die HULC-Untereinheit Brl1 acetyliert, wodurch Transkription begünstigt und die Initiierung ektopischer Stilllegung verhindert wird.

Aus einigen Studien ist bekannt, dass der Verlust von Set2 selbst in einem Stilllegungsdefekt resultiert. Dadurch, dass ich heterochromatische Transkription in *set2Δ* im Zusammenhang mit der Deletion von *pdp3⁺*, *mst2⁺*, *nto1⁺* and *ptf2⁺*, welche ebenfalls essentiell für den Erhalt von Mst2C sind, stellte ich fest, dass sich, wie bei *pdp3Δ*, der Stilllegungsdefekt von *set2Δ* allein auf dem Vordringen von Mst2C in Heterochromatin begründet. Interessanterweise resultierte die Deletion jeglicher kritischen Untereinheit in einer Suppression, die unterhalb des Niveaus in Wildtyp lag, was impliziert, dass Mst2C zum Erhalt der basalen Transkription innerhalb von Heterochromatin notwendig ist. Zusammengenommen mit den vorherigen Beobachtungen deutet dies an, dass die Stilllegungsdefekte durch Verlust von Pdp3 und Set2 auf dieselbe Weise entstehen, in der basale Transkription unterstützt wird. Zu meiner Überraschung stellte sich heraus, dass Mst2C basale Transkription von Heterochromatin durch einen völlig anderen Mechanismus vorantreibt als in Euchromatin, da dieser weder über Brl1 noch über H3K14 agiert, sondern über ein noch unbekanntes Zielobjekt.

Im Großen und Ganzen hat diese Arbeit demonstriert, das Pdp3-vermittelte Verankerung von Mst2C an H3K36me3 zwei Aufgaben erfüllt: (a) in Euchromatin verhindert diese die Bildung von ektopischem Heterochromatin in Regionen, die mit H3K36me3 markiert sind; (b) in Heterochromatin, schützt diese Abtrennung davor, dass Mst2-vermittelte, aber Pdp3- und Brl1-unabhängige basale Transkription hyperaktiviert wird und dadurch mit der Instandhaltung dieser Region interferiert.

2 Introduction

2.1 Spatial regulation of chromatin

2.1.1 From nucleosome to chromatin

Genetic information is encoded by deoxyribonucleic acid (DNA) and stored as macromolecular chromosomes inside the nucleus of every eukaryotic cell. Chromosomes consist of millions of base pairs (bp) and require multiple layers of organization to fit into the nucleus but also to remain accessible to transcription, DNA replication and repair processes. When DNA is visualized under an electron microscope, it appears as a 10-nm fiber that resembles beads on a string [1]. These beads constitute the nucleosomes that consist of DNA and an octamer of four different histone proteins (i.e. the canonical histones H2A, H2B, H3, and H4) [2]. Prior to nucleosome assembly histones H2A and H2B as well as H3 and H4 form a heterodimer via handshake of a histone fold domain in their respective C-terminal region [3]. This is followed by tetramerization of two H3-H4 dimers and the binding 147 bp of DNA as well as of one H2A-H2B dimer above and below the tetramer-DNA axis, resulting in nucleosomes [4]. Nucleosomes are highly stable, as the negatively charged phosphate backbone of the DNA interacts with basic surface residues exposed on the outward surface of the histone octamer [5], [6]. The N-termini of the histones protrude from the nucleosome and are often post-translationally modified (see chapters 2.1.3 and 2.1.4). The nucleosome core particle together with two linker H1 histones and 10 bp of DNA on both ends forms the chromatosome, which assists in the formation of higher order nucleosome structures [7]. Chromatosomes together with the connecting linker DNA form the nucleosomal arrays [8].The nucleosome arrays and their interacting proteins, such as nucleosome remodelers and proteins that bind to modified histones, together form the nuclear structure known as chromatin [9].

2.1.2 Chromatin states are determined by chromatin organization

Chromatin is present in either 'open' or 'closed' conformation. Domains with the former trait are known as euchromatin (EC) and the latter as heterochromatin (HC). The composition of EC and HC differs regarding DNA modifications, posttranslational protein modifications, and associated proteins. Though these modifications primarily have regulatory functions, many eukaryotes have co-evolved interacting factors that

are specific to subnuclear compartments. Thus, HC and EC are delegated to one of three main areas of the nucleus: (i) the nuclear interior (ii) the periphery or (iii) the nucleolus [10].

2.1.2.1 Heterochromatin is often located at the nuclear periphery

Transcriptionally silent heterochromatin comes in two main variants, facultative and constitutive. Facultative HC consists of inactive genes whose expression is specific to other tissues. Constitutive HC is gene poor and enriched in repetitive DNA sequences. Long interspersed nuclear elements (LINEs), and long terminal repeats (LTRs) fall under this category [11], [12]. The periphery of the nucleolus is specifically involved in the silencing of ribosomal RNA (rRNA) but also contributes to X chromosome inactivation [13], [14]. In many eukaryotic cells constitutive HC is located at the nuclear periphery, a stable protein network below the inner membrane that consisting of filaments called lamins and integral proteins of the inner nuclear membrane [15], [16]. The nuclear lamina acts as a central hub for many processes, in particular chromosome positioning within the nucleus and chromatin regulation [16]. Repressed chromatin can be recruited to the nuclear periphery by interaction with peripheral proteins, such as Lamin-associated proteins (e.g. PRR14) and the lamin B receptor (LBR), which binds to heterochromatin protein 1 (HP1), a reader of H3K9 di- and trimethylation and hallmark of constitutive heterochromatin [17]. Chromatin recruitment is further assisted by LAP2-emerin-MAN1 (LEM) domain proteins reviewed in [15]. Certain LEM domain proteins may also be involved HC maintenance, as recently shown the yeast *Schizosaccharomyces pombe* (*S. pombe*); interestingly, however, silencing by these proteins is mediated not by the LEM domain but a different nucleoplasmic domain [18]. Finally, telomeres and subtelomeres, which flank the chromosome ends in eukaryotes, are also heterochromatic and often localized at the nuclear periphery reviewed in [19].

Both euchromatin and heterochromatin are further regulated by the interplay of transcription factors (TFs), posttranslational (histone) modifications (PTMs), PTM binding proteins and enzymes that are guided by TFs or bind to PTMs themselves.

2.1.2.2 Nuclear sub-compartments and coordination of transcriptional processes promote transcription efficiency

EC is gene-rich and actively transcribed into protein-coding or non-coding ribonucleic acid (RNA). EC is replicated during early S phase and constitutes the majority of genes,

which are either tissue-specific or constitutively expressed in all cell types (housekeeping genes), e.g. cytoskeletal genes [20]–[22]. According to some models, transcription of genes takes place in distinct nuclear foci known as transcription factories that contain enzymes and factors required for transcription, e.g. the RNA polymerase complex (RNAP) that mediates transcription and various factors involved in the transcription initiation process [23]–[25]. These factories are stable subcompartments in the nucleus and need to be contacted by the genes [25], [26]. The genes, while co-regulated, often stem from different chromosomes and migrate from the rest of the chromosome to co-localize in these factories, thereby inducing an adjustment of the nuclear architecture to facilitate the migration [27]–[29]. Genes are composed of the promoter to which the RNAP is recruited, the 5' untranslated region (5'-UTR), the gene body comprising the coding sequence (known as open reading frame or gene body), the 3'-UTR, and the terminator sequence. Following initiation, the transcribing polymerase passes into the adjacent nuclear compartment space, where other transcription steps, such as elongation, take place [24]. In parallel, the transcription machinery coordinates RNA nascence co-transcriptionally with the spliceosome, a multi-subunit ribozyme complex that removes introns from the nascent precursor messenger RNA (pre-mRNA) to generate mature mRNA [30]. Lastly, the mRNA is associates with the TREX complex, which mediates the nuclear export of mRNA [31]. mRNA transcripts include both UTRs, though only the codons contained in the gene body will be translated from RNA to protein.

2.1.3 Spatial regulation inside heterochromatin

Heterochromatin is not only topologically separated from euchromatin but also controlled by a complex network of regulatory mechanisms to differentiate it from euchromatin. While some of the mechanisms in HC regulation have a rather broad function, others are specific for facultative or constitutive heterochromatin.

2.1.3.1 Facultative heterochromatin is regulated by Polycomb proteins

Facultative HC is formed during cellular differentiation and development. Throughout embryogenesis, cells of multicellular eukaryotic organisms differentiate from a totipotent zygote via pluripotent stem cells and progenitors into somatic cells [32]. Cellular differentiation requires transcription of genes with tissue-specific functions, whereas genes required for other cell types are inactivated. This necessitates gene expression to be coordinated at the level of TF binding and chromatin modification.

Lineage-specific TFs activate transcription of genes that promote differentiation to the next developmental stage of a specific cell type. For example, the TF p63 promotes the recruitment of remodelers to activate transcription at genes involved in murine keratinocyte differentiation [33].

Facultative heterochromatin is formed during differentiation and early development (reviewed in [34]). During embryogenesis, lineage-specific TFs establish specific gene expression patterns through enhancer interactions [35], [36]. These TF-enhancer interactions are relatively short-lived; thus, a second layer of regulation is required to maintain a stable memory of lineage-specific gene patterns. Genes are either silenced via Polycomb group (PcG) proteins or activated via Trithorax group (TrxG) proteins, which is achieved through modifications of PcG/TrxG response elements (PRE/TRE) [34].

Prominent examples of lineage-commitment are the Hox genes in Drosophila whose study led to the discovery of the PcG repressor complexes (reviewed in [37]). Two main repressor complexes are known, PRC1 and PRC2. PRC2 contains a SET domain lysine methyltransferase (KMT) that mediates H3K27me3 at PREs. H3K37me3 is recognized by the chromodomain subunit CBX of PRC1. PRC1 also contains the ubiquitin ligase RING1 that monoubiquitylates histone H2A (H2Aub); however, the function of this modification is unclear, as it is not required for silencing [38], [39]. Recent studies suggest that PRC1 mediates silencing primarily through the compaction of heterochromatin, which is dependent on the PRC1 subunits Cbx2 and Phc1 (in *Drosphila* Psc and Ph, respectively). They act as bridge between nucleosomes and promote self-interaction of PRC1, respectively, resulting in the formation of globular domains for neighboring PRC1 domains and looping of non-PRC1 regions by distal PRC1 domains interacting with each other [40], [41].

In Drosophila, PRC2 is recruited to PREs assisted by interaction with other proteins, like Pho, a DNA-binder and interactor of the nucleosome remodeler Brama, which is targeted to histone acetylation marks at promoter regions [42], [43]. Such PRE-binding factors have not been found in mammals, but alternative binding modes seem to exist. For instance, the murine PCL3/Phf19 Tudor domain subunit recruits PRC2 to H3K36me3 at specific target genes [44]. Another prominent example is the long non-coding RNA (lncRNA)-mediated PcG recruitment linked to sex chromosome dosage compensation. This takes place during X chromosome inactivation in females to assure similar levels of X chromosomal transcripts in males and females. This

mechanism involves the lncRNA *Xist,* which is encoded in the X inactivation center (*Xic*) on the X chromosome to act as a nucleation site for heterochromatin formation reviewed in [45].

2.1.3.2 Constitutive heterochromatin is continuously present

While facultative heterochromatin regions differ between different cell types, pericentromeric DNA and telomeres are persistently silenced throughout development.

2.1.3.2.1 DNA methylation and histone methylation influence each other

Pericentromeric DNA consists of tandem repetitive elements that evolved from transposons but differ in sequence composition and number of repeats between species [46]. Due to their repetitive nature these tandem repeats, as well as transposons, are prone to recombination such as insertions or deletions; therefore they need to be silenced to maintain genome integrity [47], [48].

A hallmark of constitutive heterochromatin is methylation at H3K9, which can be present as mono-, di- and trimethylated. In higher eukaryotes, the three different states of H3K9me are established by more than a single KMT. A study in murine cells uncovered that H3K9me1 is conferred redundantly by the cytosolic KMTs Prdm3 and Prdm16 prior to import of histone H3 into the nucleus [49]. H3K9me2 is mediated by the GLP/G9a (also known as EHMT1/EHMT2) complex [50], [51]. Lastly, Suv39h1 and Suv39h2 (Su(var)3-9 in *Drosophila*) as well as Setdb1 mediate trimethylation of H3K9. These enzymes share a conserved catalytic region, the Su(var)3–9, Enhancer of *zeste* (E(z)) and *trithorax* (trx) (SET) domain (Tschiersch et al., 1994). In *S. pombe*, all three methylation steps are mediated by a sole SET domain KMT, Clr4; in contrast, *S. cerevisiae* does not possess H3K9 methylation [52]–[54].

In mammals and other species, H3K9me occurs in conjunction with DNA methylation at C5 of cytosine bases (which is absent in Drosophila and fission yeast; reviewed in [55]). During embryogenesis, most germline-specific chromatin marks, including DNA methylation, are first removed, which allows that lineage-specific *de novo* formation of heterochromatin during differentiation. However, as DNA methyltransferases do not recognize specific DNA motifs, DNA methylation needs to be directed by other means. Establishment of DNA methylation partially depends on preexisting histone methyl-lysine marks that direct DNA methyltransferases to specific positions, although this process is not fully understood. The maintaining DNA methyltransferase Dnmt1 is recruited to newly replicated hemi-methylated DNA by Uhrf1 [56], [57]. In contrast, the

de novo methylating enzymes, Dnmt3A and Dnmt3B, possess an N-terminal ADD (ATRX, DNMT3, DNMT3L) domain and a C-terminal PWWP (proline-tryptophan-tryptophan-proline) domain. The PWWP domains of Dnmt3A and Dnmt3B recognize H3K36me3, although Dnmt3B also binds nonspecifically to DNA [58], [59]. Dnmt3L forms a complex with Dnmt3A or Dnmt3B at later developmental stages, thereby controlling binding and the activity of these DNA methylases. Chromatin binding of Dnmt3A and Dnmt3B is further regulated by their ADD domains, which bind to H3K4me0 but cannot recognize H3K4me2 or H3K4me3 [60]. Recent insights into mammalian DNMT3A suggest that ADD-binding to H3K4me0 alleviates autoinhibition of its catalytic domain [61]. Conversely, CpG islands, which are void of DNA methylation, are specifically trimethylated at H3K4, thereby preventing the recruitment of Dnmt proteins and their interference with transcription [62]. A similar mechanism may act at CEN chromatin, which is methylated at H3K4 as well [63].

DNA methylation assists in the deposition of methyl-lysine marks as the ADD domains of Dnmt3A and Dnmt3B have been shown to recruit Suv39h1 and Setdb1, thereby acting as a nucleation site for H3K9 methylation [64], [65]. Furthermore, both Dnmt3s interact with heterochromatin protein 1 (HP1), which binds to H3K9me3 via its chromodomain and is another conserved hallmark of heterochromatin. HP proteins in turn can interact with each other via their chromoshadow domains and promote heterochromatin spreading [65]. Moreover, DNA methylation itself is recognized by specific proteins, such as MeCP2, which is known to recruit histone deacetylases and Suv39h1/2, adding another layer of heterochromatin formation at pericentromeres [66].

2.1.3.2.2 RNA interference and H3K9me2/me3

In several organisms, including nematodes, flies, fungi, and plants, silencing of transposons by RNA interference (RNAi) is highly conserved. RNAi is often induced by small interference RNAs (siRNA). These are generated from double-stranded DNAs by different mechanisms. Either siRNAs are excised from transcripts of inverted repeats that folded back into a hairpin; or they result from bidirectional transcription; alternatively they are generated from single-stranded RNA transcripts by use of an RNA-dependent RNA polymerase (RdRP) reviewed in [67]–[70]. The last option occurs for example in *S. pombe* where the nucleation site stems from a nascent transcript, which is first recognized by through base pairing by the RNA-induced transcriptional silencing complex (RITS), a paralog of the RNA-induced silencing complex (RISC)

[71]. RITS then recruits an RdRP that synthesizes a complementary strand. Perfectly paired double-stranded RNA is cleaved by a Dicer ribonuclease (Dcr1) into to 22 nucleotides long fragments with a characteristic 2-bp 3' overhang [72]. The siRNA duplex is passed onto the intermediary complex (ARC) that contains an Argonaute protein (Ago1) whose slicing activity is inhibited by the other two subunits Arb1 and Arb2 [73]–[75]. Once loaded on ARC, the passenger strand of the siRNA duplex strand is removed, resulting in Arb1/2 release. Ago1 with the bound single-stranded siRNA assembles with Chp1 and Tas3 into RITS [76]. Chp1 possesses a chromodomain that interacts with methylated histones as well as DNA, while Tas3 mediates *cis*-spreading of the complex through self-association [77], [78]. The loaded siRNA is complementary to heterochromatic transcripts and guides RITS to heterochromatin together with Chp1. In addition, through interaction with the bridging factor Stc1, Ago1 recruits CLRC, a complex comprising the KMT Clr4 and a ubiquitin ligase, resulting in the establishment of H3K9me2/H3K9me3 [79]–[81]. This induces a feed-forward loop, as the HP proteins Swi6 and Chp2 as well as Chp1, and Clr4 itself, each contain chromodomains that bind H3K9me2/me3 (see Figure 1).
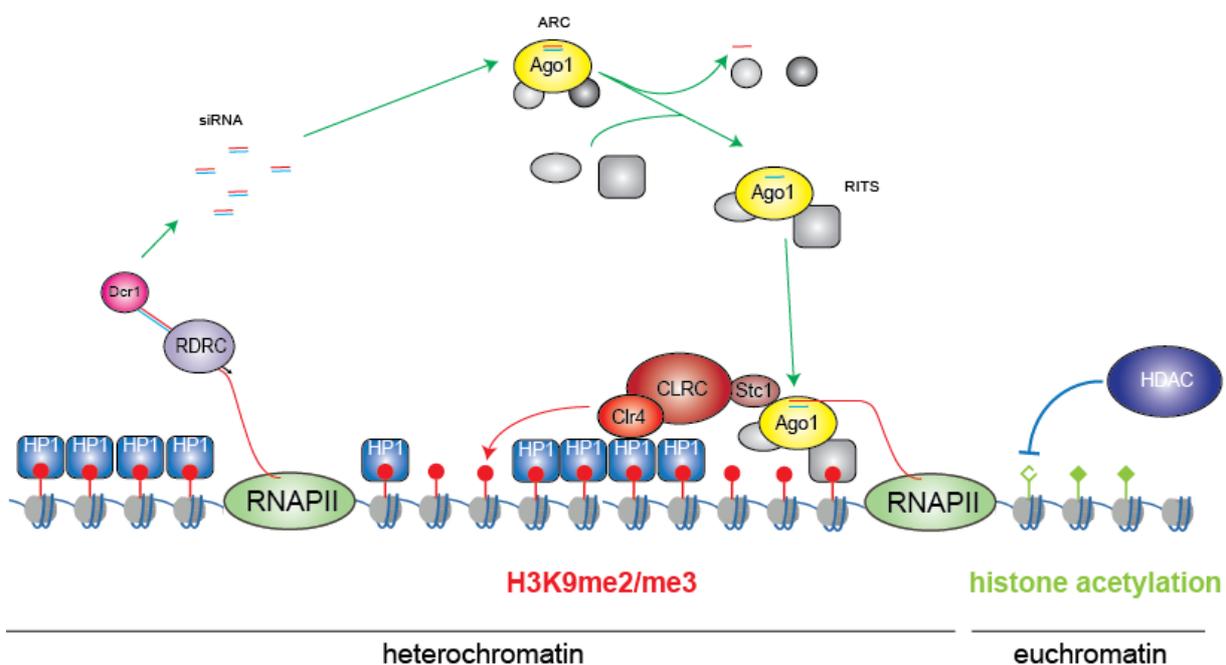
Figure 1 - Overview of the RNAi pathway in *S. pombe*: Nascent HC RNA is recognized by RDRC, which synthesizes a complimentary strand; the dsRNA is sheared into siRNA by Dcr1 and then loaded onto the ARC complex containing Ago1; the passenger strand is discarded and Ago1 forms the RITS complex with two other subunits; RITS is recruited to HC via recognition of nascent RNA by Ago1 and interaction with H2K9me2; Ago1 recruits CLRC via the bridging factor Stc1, which then methylates H3K9.

2.1.3.2.3 Telomeric and subtelomeric silencing

Due to DNA polymerase needing an RNA primer for its annealing, the 5' end of the lagging strand of a linear chromosome would not be replicated and the chromosome would lose genetic information with each cell duplication (replication end problem). However, observations in vivo show the opposite as with each replication cycle, the 3'-ends of a chromosome are shortened reviewed in [82]. To prevent the shortening of the 5'-end an RNA-dependent DNA polymerase, called telomerase, adds DNA repeats to the chromosomal 3'-ends. These tandem repeats and the 5'-region of the lagging strand are then replicated by DNA polymerase, thereby leading to an extension of the telomeres and continuous protection of the chromosome ends [83]. However, the free telomeric ends resemble DNA double strand (dsDNA) breaks and can result in inter- or intrachromosomal fusions if recognized by the DNA repair machinery. This is counteracted by binding of the highly conserved shelterin complex, comprised of dsDNA and ssDNA binding proteins interconnected by bridging proteins, which also acts as a recruiting platform for telomerase [84], [85], reviewed in [86]. An electron microscopy study in mammalians revealed that here shelterin also promotes the formation t-loops by the telomeric ssDNA strand invading the dsDNA repeats, thereby adding another layer of protection [87].

In *S. pombe*, the shelterin complex recruits besides telomerase in addition CLRC and the multifunctional repressor complex SHREC, which contains the HDAC Clr3, via the shelterin subunit Ccq1 [88]–[91]. Among other functions, the mutually exclusive binding of SHREC and telomerase contributes to modulating the activity of telomerase [89], [90], [92].

Both telomeres and the adjacent subtelomeric region, which is gene-poor and repeat-rich, have several hallmarks of constitutive heterochromatin in common with centromeric heterochromatin. In higher eukaryotes, decoration of telomeric and subtelomeric HC with H3K20me3, H3K9me3 and HP1 proteins regulates telomere length and contributes to protection against telomeric damage and sister chromatid exchange [93], [94], reviewed in [95]. Furthermore, subtelomeric HC DNA is methylated, which also negatively regulates telomere length [96]. In fungi, presence of HC hallmarks differs between the species with some displaying H3K9me at subtelomeric HC such as *S. pombe* and *Neurospora crassa* (*N. crassa*) while others are marked by DNA methylation, e.g. *N. crassa* or the formation of HC requires a different set of factors altogether (*S. cerevisiae*) reviewed in [47].

2.1.3.2.4 Other constitutive silencing mechanisms

Centromeres, telomeres and subtelomeres are often located to the nuclear periphery via specific recruiting mechanisms. Two examples for perinuclear heterochromatin can be found in *S. pombe*, which may also be conserved in higher eukaryotes. The LEM domain (see section 1.1.2.1) of the transmembrane factor Lem2, which sits in the inner nuclear envelope, interacts with centromeres and recruits them to the nuclear envelope, whereas the telomeric dsDNA binder and TRF homolog Taz1 associates with members of the peripheral bouquet complex via the bridging protein Rap1 [18], [97], [98]. The localization to the nuclear periphery is of great importance for the formation and maintenance of HC, as this environment is enriched for HDACs, such as HDAC3 for which a study in mammals has indicated direct association with nuclear envelope proteins [99], [100]. Hypoacetylation by HDACs promotes heterochromatin formation, e.g. deacetylation of H3K9ac makes the lysine residue available for subsequent methylation reactions, whereas removal of H3K14ac prevents histone turnover [43], [101], [102].

2.1.4   Regulation of euchromatic transcription

Euchromatin consists of cell type-specific genes and the housekeeping genes, i.e. genes that are essential for cell survival and constitutively transcribed into mRNA, as well as various other RNAs that don't encode proteins [21], [103]. Euchromatin is more dispersed across the chromosomes than heterochromatin, which can result in genes encoding similarly regulated proteins being located on different chromosomes. Moreover, transcribed DNA needs to be accessible to the transcription machinery, which requires bypassing nucleosomes. To control all these aspects of euchromatic transcription cells have evolved many different regulatory mechanisms, of which underlying principles will be described in the following chapters.

2.1.4.1 Regulation of transcription factors

Initiation of transcription and regulation of transcriptional elongation in euchromatin require transcription factors [104]. Except for pioneer factors, TFs bind only to nucleosome-free DNA sequences. In contrast, pioneer factors have the capacity to bind to nucleosomal (closed) DNA and open it up, which otherwise may happen only through spontaneous unwrapping of the nucleosome [105]–[107]. When DNA is accessible, regulatory transcription factors come into play. General or basal TFs are ubiquitously present in every cell and constitutively expressed. They bind to a

consensus sequence, e.g. the TATA box, in the promoter region of protein coding genes and assemble into a pre-initiation complex with RNAPII, which is needed to position RNAPII at the transcriptional start site [108], [109]. Unlike general TFs, specific transcription factors interact with a discrete set of loci within a cell. They are involved in multiple processes including cell development, differentiation, oxidative stress, and apoptosis [110], [111].

Specific transcription factors that negatively regulate transcription are called repressors. They interact with binding sites termed silencers situated close to or within the gene they regulate. Examples for silencers have been reported for promoter regions, introns and exons as well as the 3'-UTR of certain genes reviewed in [112].

In contrast, activators bind to promoter-proximal recognition sites or to enhancers and recruit the RNAP II machinery. Enhancers are comprised of several TF binding motives that are located up to over a million base pairs upstream or downstream of the transcription start site on the same chromosome, thus acting *in cis* [113]–[115]. In few cases, enhancers may also regulate gene expression from a different chromosome *in trans* [116]. Multiple TFs can co-localize to a single enhancer, with the binding pattern dependent on the differentiation state, such as seen for hematopoiesis [117]. The enhancer then brings the transcription factors into promoter vicinity where the TFs act as effectors through recruitment of nucleosome remodelers that co-activate transcription by modulating nucleosome occupation and composition [118], [119].

2.1.4.2 Nucleosome remodelers and their interplay with histone marks

Nucleosomes pose an obstacle not only for RNA polymerases during transcription initiation, but also interfere with DNA polymerase during replication and the repair machinery during the DNA damage response. Minor and major grooves of the DNA change their shapes when wound around the histone octamer and thus cannot be recognized by DNA binding proteins [120]. While some pioneer factors (see section 2.1.4.1) can intrinsically bind to closed chromatin, most DNA interacting proteins are not capable of removing or shifting nucleosomes [121]. For that purpose, the pioneer factors recruit nucleosome remodelers, a family of ATPases that use the energy stored in ATP to break the hydrogen bonds between the DNA backbone and histone residues [6], [121], [122]. Remodeler functions entail the deposition and removal of histones, sliding nucleosomes along the DNA, positioning of nucleosomes, and the exchange of histone variants [122]. Remodelers are often part of complexes with multiple subunits

that specify their function. For example, the remodeling enzyme ISWI can act in transcription, DNA replication, DNA repair, and other pathways, depending on the presence of other proteins with which this remodeler forms a complex [123].

Furthermore, remodeling functions are often coordinated with covalent modifications of the protruding histone N-termini. Histone marks include methylation, acetylation, phosphorylation, ADP-ribosylation, sumoylation, and ubiquitylation, with more marks still being discovered [124], [125]. Though not all these marks are recognized by remodelers, there are well documented examples where binding modules in one of its subunits mediate the recognition of a specific posttranslational histone modification (PTM) and assist in the chromatin recruitment of the remodeler. One example is the *S. cerevisiae* ISWI family remodeler Isw1b. This remodeler is specifically recruited to trimethylated H3K36 (H3K36me3) via the PWWP domain of its subunit Ioc4 and suppresses histone exchange and cryptic transcription [126]. Comparable to Isw1b, studies in *S. cerevisiae* have demonstrated that Swi/Snf complexes are only efficiently retained at promoters when interacting with a transcription factor or via histone acetylation that is recognized by the bromodomain of one of the complex subunits [127]. In agreement, acetylated lysine histone residues K9 and K14 on histone H3 as well as K12 and K16 on histone H4 are mostly enriched at the promoter region and 5'-end of genes and decline towards the 3'-end [43], [128]. Swi/Snf complexes are recruited by transcriptional activators and promote transcription by making the promoter accessible via nucleosome sliding [129]. The recruitment of SWR chaperones relies partially on acetylated histones, which the complexes recognize via bromodomain subunits BRD proteins in higher eukaryotes and Brd1 in *S. cerevisiae* [130].

In conclusion, cross-talk between remodelers and histone acetylation marks is a conserved mechanism that directs nucleosome remodelers to their target site.

2.1.4.3 Writers that read – How histone acetylation and methylation are functionally linked

Lysine acetyltransferase (KAT) complexes are histone writers that mediate the acetylation of histones and are needed to retain remodelers at promoters. KATs are recruited through their interaction with effectors, i.e. proteins that recognize specific histone modifications and interact with the enzyme complex or are part of the complex itself [119]. Recruitment can also occur via the binding to transcription factors [131]. For example, this is the case for the co-activator SAGA (Spt-Ada-Gcn5

acetyltransferase) complex, which contains the highly conserved KAT GCN5 (general control of amino-acid synthesis 5), and the *S. cerevisiae* NuA4 (Nucleosome Acetylation at histone 4) complex, which contains the MYST (Moz-Ybf2/Sas3-Sas2-Tip60) family member Esa1 as its catalytic subunit. Both SAGA and NuA4 are recruited by transcription factors like Gal4 and Gcn4, or the viral TF VP16 [132]–[135]. Alternatively, enzymes can bind their target sites through recognition of other histone marks, such as H3K4me and H3K36me (methylated histone H3 lysine 4 and lysine 36), as seen for the mammalian MYST complexes MOZ/MORF and HBO1–BRPF1 (see chapter 2.1.4.5 for details on H3K36me) [136]–[138]. This type of recruitment is highly conserved and has also been reported for *S. cerevisiae*, where both complexes share the homologous MYST family member Sas3 [139]–[141]. H3K4 and H3K36 can be mono, di- or trimethylated. Both marks are associated with active transcription. Methylation of H3K4 is mediated by the Set1/COMPASS complex (Set1C) family of KMTs whereas each state of H3K36me is regulated by different enzymes in higher eukaryotes and a single enzyme in yeast (see chapter 2.1.4.5). Like other lysine residues, H3K4me3 is and found at promoters and the 5' region of genes [128], [142]. H3K4me2 is situated further downstream of H3K4me3 and targets NuA4 to promoters in *S. cerevisiae* [143]. H3K4me2 also correlates with transcription factor binding sites in humans [144]. In contrast to H3K4me3, H3K36me3 is usually found along the gene body, increasing towards the 3'-end [128], [145]. The level of H3K36me3 correlates with the gene's transcription frequency [146]. Unlike H3K36me3, H3K36me2 appears to inversely correlated with transcription with less expressed genes displaying a higher level of H3K36me2 than higher expressed loci [128]. H3K36me is involved in a variety of different processes with H3K36me3 promoting transcription whereas H3K36me2 rather acts in inducing its suppression (for details see chapter 2.1.4.5).

This specific recruitment of proteins via interaction with distinct histone modifications to induce downstream events, which was also noted for heterochromatic H3K9me and chromodomains, has come to be known as the 'histone code' [147], [148]. A further layer of regulation is added by the interaction of histone modifications with other enzymes that also modify nucleosomes.

2.1.4.4 The Paf1 regulatory mechanism – an example for histone cross-talk

Deposition of H3K4 is regulated by the highly conserved RNAP II associated factor complex (Paf1C), which is has multiple functions (see Figure 2).
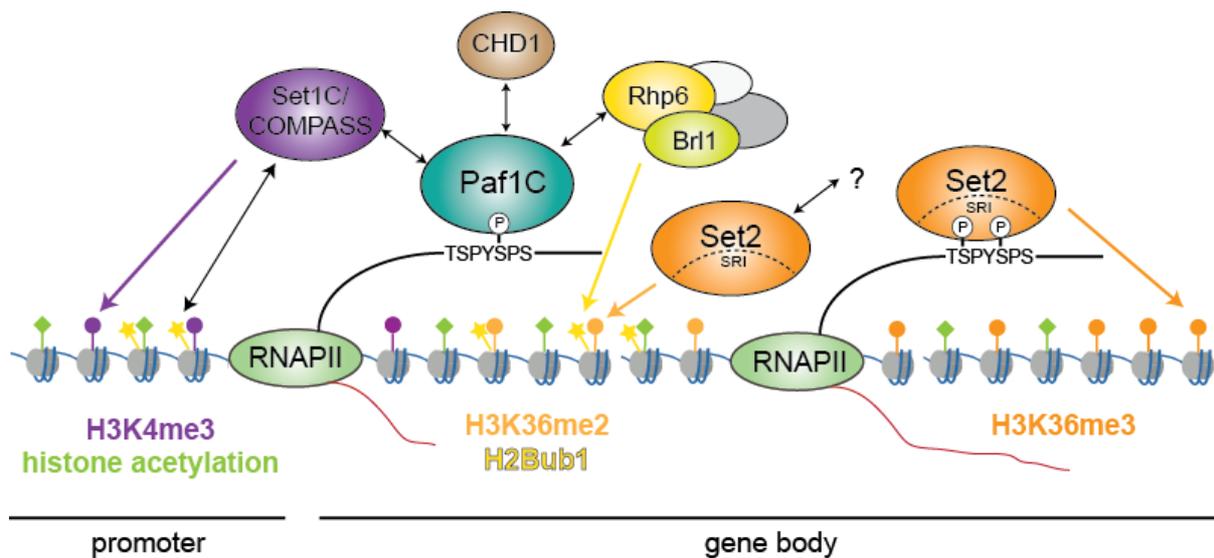
Figure 2: Overview of pathways promoting transcription, here in S. pombe - Paf1C recognizes the RNAPII-CTD phosphorylated at S5 and recruits the COMPASS complex, the remodeller CHD1 and the ubiquitin ligase HULC to initiating RNAPII, which mediate deposition of H3K4me3, promoter escape of RNAPII, and H2Bub1, respectively; Set2 is recruited directly to the elongating RNAPII via interaction of its SRI domain with the CTD phosphorylated at S2 and S5 and co-transcriptionally mediates H3K36me3; H3K36me2 is deposited by a different mechanism.

Paf1C is required for the control of histone H2B monoubiquitylation (H2Bub). H2Bub is a highly conserved euchromatic mark in eukaryotes. It is enriched over gene bodies and its level strongly correlates with transcription [149], [150]. Ubiquitylation of H2B is mediated by the E2-E3 ligase RAD6-RNF20/40 in humans, and homologs exist in *S. cerevisiae* (Rad6-Bre1) and *S. pombe* (HULC) [151]–[154]. Studies in *S. cerevisiae* and in flies revealed that the Paf1C subunit Rtf1 directly interacts with the E3 Rad6 [155], [156]. Through the interaction with Paf1C, the Rad6-Bre1 complex travels along with the initiating and elongating RNAPII and modifies H2B co-transcriptionally [155]. Further, Paf1C genetically interacts with the KMT Dot1 (Dot1L in humans, Dot1p in *S. cerevisiae*), which mediates methylation of H3K79 and is involved in multiple euchromatic regulatory processes [157]–[159]. Both Set1C/COMPASS and Dot1 need H2Bub for their function. Human Dot1L interacts with H2Bub and uses it as a pivot to rotate into position for downstream interactions of Dot1L with histone H4 and H3K79 [160]. In *S. cerevisiae*, H2Bub acts as a binding partner for COMPASS, which facilitates its recruitment to chromatin and promotes the methylation of all three stages of H3K4 [161]. Paf1C also physically interacts with Set1; however as Paf1C promotes H2Bub and Set1C recognizes the phosphorylated C-terminal domain (CTD) of Rpb1,

the largest subunit of RNAP II, it is unclear whether this physical interaction plays a role in the recruitment to early elongating RNAP II [153], [162]–[164]. Lastly, in humans, both Paf1C and H3K4me3 interact with the chromatin remodeler CHD1, thereby recruiting this remodeler to promoter and 5'-regions of genes during early elongation. At promoters CHD1 assists RNAPII in escaping the nucleosome barrier, while within the gene body it is needed to maintain the boundary between H3K4me3 and H3K36me3 [165], [166].

2.1.4.5 H3K36 methylation – at the crossroads between different pathways

The methylation state and localization of lysine position 36 of histone H3 (H3K36me) is controlled by a network of regulatory mechanisms that are highly conserved in eukaryotes [167], [168].

Trimethylation of H3K36 is carried out by the SET2BD family of KMTs throughout all eukaryotes [167], [169]. Usually, H3K36me3 is mediated by a single KMT in any given higher eukaryote at H3K36 residues that were previously mono- and demethylated; however, mono- and dimethylation are in general deposited by more than one enzyme [168]. For example, in humans, three different KMTs, NSD1 to NSD3 (nuclear receptor binding SET domain proteins), are responsible for mono- and/or dimethylation of H3K36 [170]–[172]. In contrast, in yeast, this redundancy is not present and all methylation stages are carried out by single enzyme, Set2 [167], [169]. Demethylation of histones is mediated by the Jumonji domain of lysine demethylases (KDMs), e.g. the conserved H3K36me3 and H3K9me3-specific JMJD2A and the H3K36me2-specific JMJD5, to restrict the downstream processes of H3K36me3 [173]–[175].

Trimethylation by Set2 is coupled to active transcription. Set2 is recruited to transcribing RNAP II via interaction of the Set2 Rpb1 interacting (SRI) domain with the CTD of elongating RNAP II that is phosphorylated at serine two and five [176], [177]. This interaction not only controls the localization of Set2 but also contributes to its protein stability [178]. Secondly, a study in *S. cerevisiae* has shown that part of the SRI domain of Set2 interacts with linker DNA thereby providing further substrate specificity for nucleosomes over free histones and histone octamers [179]. Moreover, an AID (autoinhibitory domain) that is situated between the SET domain and the WW domain of Set2 blocks its activity when not bound to the CTD [179]. The level of H3K36me3 is also negatively regulated by proteolysis, as a recent study revealed that human SPOP,

the E3 subunit of the ubiquitin ligase complex SPOP/CUL3/ROC1, targets SETD2 for proteasomal degradation [180].

Lastly, another layer of control links H3K36me3 to Paf1C. A study in *S. cerevisiae* revealed that H3K36me3 levels on chromatin are significantly reduced when Paf1 or Ctr9 are lacking, while the loss of other subunits has only a moderate or no effect [181]. Another study in mouse embryos focusing on Ctr9 suggests that Paf1C is required to control the levels of H3K36me3 during development, possibly in connection with the Paf1C-CHD1 interaction [166], [182]. This complex level of control for the different stages of H3K36me, particularly for H3K36me3, suggests that they are required for different pathways that may even counteract each other.

Indeed, all three stages of H3K36me have distinct functions. H3K36me1 acts as a substrate for H3K36me2-specific KMTs (e.g. NSD1) and may also be recognized as a secondary substrate along H3K36me2 by the binding sites of certain proteins, such as the human DNA methylhydroxylase TET2 [170], [183]. H3K36me2 is involved in both acetylation and deacetylation of histones. In *S. cerevisiae*, H3K36me2 is sufficient to recruit the chromodomain protein Eaf3, which is part of the histone lysine deacetylase (HDAC) Rdp3S [184]. Rdp3S recruitment in turn prevents transcription from cryptic start sites through deacetylation of histone H4 [185]. Moreover, H3K36me2, in conjunction with H3K4me2/me3, is one of the histone marks that is needed for the recruitment of *S. cerevisiae* NuA4 and is also required for acetylation of H4K16ac during the larval stage in *Drosophila* [143], [186]. Thus, dimethylation can have different functions, depending on whether the modification overlaps with H3K4me2/me3 or not.

The strict control of H3K36me3 levels highlights its importance in chromatin regulation. H3K36me3 is needed for processes that promote transcriptional silencing, as described for *S. cerevisiae* ISWI remodeler Isw1b [126] (see also 2.1.4.2). H3K36me3 also interacts with the DNA methyltransferases Dnmt3A, which recognize the mark via its PWWP domain, and a subunit of PRC2; thus, it is also required for processes involving facultative silencing [58], [187], [188].

In addition, exons are enriched for H3K36me3 while introns are depleted for this mark [55]. The maintenance of this distribution is critical as it promotes intron retention whereas its increase at specific splice sites results in aberrant splicing via exon exclusion [180], [189], [190].

Lastly, H3K36me3 is involved in DNA damage response and histone acetylation, as binding partner of the transcriptional co-activator LEDGF [191]–[194].

In conclusion, like H3K4me, H3K36me is essential in the control of transcriptional processes. However, H3K36me, particularly H3K36me3, participates in different regulatory pathways depending on both its methylation state and chromatin context.

2.2 Chromatin reader domains are conserved through evolution

Regulatory mechanisms require fine-tuning on chromatin. They often depend on proper chromatin effectors, e.g. nucleosome remodelers or histone writers, such as a KAT or KMT, which are recruited to either HC or EC. To this end, proteins contain specific domains that discriminate between PTMs, such as acetylation and methylation, or even different methylation states. These domains are conserved from yeast to mammals and classified into different families based on the composition of their histone-binding pocket and their secondary and tertiary structure.

The PWWP domain, a member of the Royal family of methyllysine binders, is one such example and is found in many regulatory factors, such as the above mentioned LEDGF and the Dnmts [195]. PWWP domains owe their name to the presence of a conserved proline-tryptophan-tryptophan-proline motif (see Figure 3A). The domain itself spans 100-130 amino acids and is folded into a five-stranded β-barrel, followed by a bundle of two to five α-helices (Figure 3B and 3C)[196]–[198]. Methyllysine binders often employ an aromatic cage for substrate recognition; this pocket comprises two to four residues depending on the binding motif [199]. The aromatic cage of PWWP domains consists of three residues (Figure 3A) [197], [200]. The first and third residues is either tyrosine, tryptophan, or phenylalanine, whereas the second residue is either a tryptophan or tyrosine. The first aromatic residue precedes the first proline of the PWWP motif and is part of the loop between the β_1 and β_2 strand of the beta-barrel structure. The second aromatic residue comprises the amino acid in the third position of the PWWP motif and is part of the β_2 strand and the third aromatic residue, which is part of the β_3 strand, is located further downstream.

A

```
DNM3A_HUMAN   263 E-PVGSDAGDKNATKAGDDEPEYEDGRGFGIGELVWGKLRGFSWWPGRIVSWWMTGR---   318
DNM3B_HUMAN   196 Q-QGGMESPQVEADSGDGDSSEYQDGKEFGIGDLVWGKIKGFSWWPAMVVSWKATSK---   251
NSD1_HUMAN    294 ELPGTSSSS-TSQELPFCQPKKKSTPLKYBVGDLIWAKFKRRPWWPCRICSDPLINTHSK  352
NSD2_HUMAN    199 KIPAKKESC-------PNTGRDKDHLLKYNVGDLVWSKVSGYPWWPCMVSADPLLHSYTK  251
NSD3_HUMAN    240 EEPVLKEEAPVQPILSSVPTTEVSTGVKFQVGDLVWSKVGTYPWWPCMVSSDPQLEVHTK  299
PDP1_SCHPO     29 NIPSVV-EE--SKDN--L---EQASADDRLNFGDRILVKAPGYPWWPALLLRRKETKDSL-  80
PDP2_SCHPO     99 -IKSQKSEK--SNGN-ARKETKQSERVNYKPGMRVLTKMSGFPWWPSMVVTESKMTSVAR  154
PDP3_SCHPO     38 NLRDV---K--KKGKQLAYVPRTSPRKSYKNGEYVLAKMSSFPWWPARVASQKSIPTEVR   92
PSIP1_HUMAN     1 -----------------------MTRDFKPGDLIFAKMKGYPHWPARVDEVP---DGA-   32
YL455_YEAST     1 -----------------------MTKDIRTGDLVLCKVGSFPPWPAVVFPQRLLRNDVY   36
                                                          *  : *     ** :
```

```
DNM3A_HUMAN   319 -----SRAAEGTRWVMWFGD-GKFSVVCVEKLMPLSSFCSAFHQATY--------NKQPM  364
DNM3B_HUMAN   252 -----RQAMSGMRWVQWFGD-GKFSEVSADKLVALGLFSQHFNLATF--------NKLVS  297
NSD1_HUMAN    353 MKVS-NRRPYRQYYVEAFGDPSERAWVAGKAIVMFEGRHQFEELPVLRRRGK---QKEKG  408
NSD2_HUMAN    252 LKGQ--KKSARQYHVQFFGDAPERAWIFEKSLVAFEGEGQFEKLCQESAKQAPTKAEKIK  309
NSD3_HUMAN    300 IN----TRGAREYHVQFFSNQPERAWVHEKRVREYKGHKQYEELLABATKQASNHSEKQK  355
PDP1_SCHPO     81 -NT--NSSFNVLYKVLFFPD-FNFAWVKRNSVKPLLDSEIAK-------FL-GSSK---  124
PDP2_SCHPO    155 KSK--PKRAGTFYPVIFFPN-KEYLWTGSDSLTPLTSEAISQ-------FL-EKPK---  199
PDP3_SCHPO     93 ERLKRNFRMDNGIFVQFLPS-RDYAIISSSNVLPLTVDESRF-------IL-DHDLSTK  142
PSIP1_HUMAN    33 -----VKPPTNKLPIFFFGT-HETAFLGPKDIFPYSENKEKY-------GKPNKRK---   75
YL455_YEAST    37 -----RKRKSNCVAVCFTND-PTYYWEQPSRLKELDQDSIHN-------FILEHSKN--   80
                                      :  :            . :
```

B   **C**

Figure 3: Aromatic cage of PWWP domain proteins - (A) Positioning of the aromatic residues comprising the aromatic cage within an amino sequence context and relative to the PWWP motif, aromatic residues are shown in red in different species; (B) Solution NMR structure of Pdp1 PWWP domain visualized with NGL, DOI: 10.2210/pdb2l89/pdb, retrieved from rcsb.org/pdb/ on December 4, 2017; (C) Solution NMR structure of Pdp2 PWWP domain visualized with NGL, DOI: 10.2210/pdb1h3z/pdb, retrieved from rcsb.org/pdb/ on December 4, 2017.

The structures of other Royal family members, like the Tudor domain or the chromodomain, use a similar arrangement of β strands, α-helices, and positions of the binding residues but are otherwise diverged from each other during evolution [195]. Many PWWP domain proteins bind specifically to H3K36me3, e.g. mammalian Dnmt3A, whereas only few members recognize H3K79me3 or H4K20me3 [197], [198], [200]. In contrast, chromodomains preferentially interact with H3K9me2/me3 or H3K27me3, e.g. in HP1 or PRC2, respectively.

2.3 The reader writer problem

A confounding observation is that many histone writers can read the same histone PTM they deposit. However, if the writer recognizes its own mark then deposition should theoretically not be possible to write the mark in the first place as general consensus is that recruitment to chromatin mediates histone writer activity. Nonetheless, many histone writers display such a target specificity. The mammalian methyltransferase Suv39h and fission yeast Clr4 recognize H3K9me2/me3 through their chromodomain [201], [202]. Similarly, the *S. pombe* PWWP domain protein Pdp1 is recruited to H4K20me1, the mark that is deposited by its binding partner Set9 [197]. Such modifiers are often part of a feedforward loop (see also 2.1.4.4). For instance, in fission yeast, the bridging protein Stc1 mediates the interaction between the Clr4-containing CLRC complex and the RITS complex, which is recruited to nascent HC transcripts via Ago1 and to H3K9me2 via Chp1, resulting in increased H3K9 methylation [79], [81]. In mammals, Dnmt3A interacts with Suv39h1 and HP1 proteins, thereby feeding a similar loop [64]. It is also possible that the interaction with the chromatin marks deposited by these enzymes keep them in place, thereby preventing the breakdown of the loop; an example is H3K9me2 in a *dcr1∆* or *stc1∆* mutant [79]. In a *dcr1∆* mutant siRNA cannot be generated anymore resulting in a cease of RITS recruitment. In a *stc1∆* mutant CLRC cannot be recruited to HC. Though loss of either protein results in de-repression of centromeric HC, H3K9me2 is maintained at a reduced level (~35% in *dcr1∆* and ~50% in *stc1∆*) due to direct recruitment of Clr4 via its chromodomain.

Considering the presence of such a loop for HC, the question arises whether more such connections exist that have not yet been discovered. However, the complexity of the regulatory pathways and the redundancy of the factors involved, e.g. three different H3K9me2 and H3K9me3 HMTs each in humans, further complicate the elucidation of interconnections between mechanisms.

2.4 *S. pombe* as a model for the study of chromatin regulation

Model organisms that harbor conserved mechanisms of higher eukaryotes but are less complex can facilitate the identification of novel regulatory factors. A powerful genetic model system is *S. pombe*. Compared with the human genome, which is made up of 3.1 billion base pairs arranged on 23 chromosomes that encode around 19 – 20,000 genes, the *S. pombe* genome consists of 12.6 million base pairs, which are organized

into three chromosomes and encodes 5064 protein-coding genes [203]–[205]. Also, many chromatin factors are not essential for survival, thus allowing studies with null mutants, e.g. *clr4Δ*. Additionally, similar to higher eukaryotes a vast array of genomic tools is available to generate mutants, reporter strains and epitope-tagged strains in *S. pombe*, including the use of homologous recombination and CRISPR [206], [207]. Compared to higher eukaryotes, such as mouse cells which need 14 kb of homologous flanking sequences for successful insertion into a targeted locus, *S. pombe* requires only 600 bp, and *S. pombe* cells have a much shorter division time than higher eukaryotes (2 h compared to 24 h in humans) [208]–[210]. Thus, genetic modification of *S. pombe* requires much less time and effort than for higher eukaryotes.
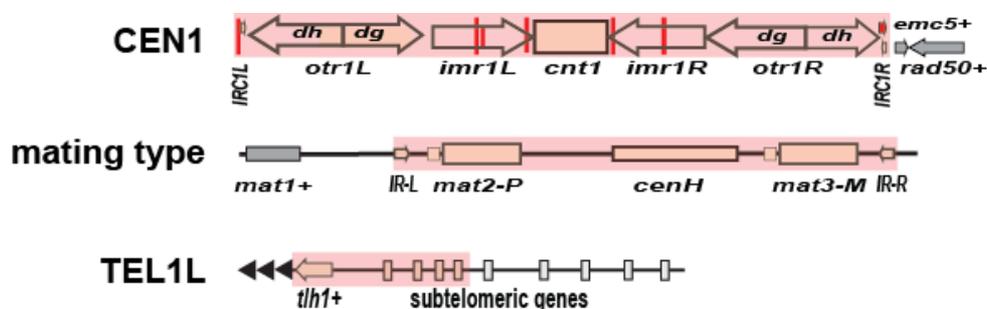
Figure 4: Overview of constitutive heterochromatin in *S. pombe* - Shown are the two heterochromatic regions used of this study and the mating type locus with the heterochromatic domains shaded in red, red stripes – tRNA, grey – euchromatic genes: top – centromeric region of chromosome 1, heterochromatic repeats: sequences depicted as red stripes, *imr*- innermost repeats, *otr* – outer repeats, *IRC* – inverted repeats at centromeres; middle – mating type locus, *mat1*[+] locus – actively transcribed mating type, mat2-P and mat3-M - silenced mating type cassettes, *cenH* - *dg/dh*-like region, *IR* – inverted repeats; bottom – subtelomeric region of the left arm of telomere 1.

Like in higher eukaryotes, constitutive heterochromatin in *S. pombe* is found at the pericentromeres and the subtelomeric regions. A third region of constitutive heterochromatin is located at the mating type locus. In contrast to higher eukaryotes, where only the pericentromeric region is clearly defined, this applies to all constitutive heterochromatin regions in *S. pombe*, making it excellently suited for studying silencing mechanisms (see Figure 4).

Pericentromeric DNA is organized into four kinds of non-coding repeats: (i) the inner most repeats (*imr*) that flank the centromere on each chromosome; the outer repeats (*otr*) that flank the *imr* and consist of (ii) *dg* repeats and (iii) *dh* repeats; (iv) the inverted centromeric repeats (*IRC*) that flank pericentromeric HC on each side and act as a physical boundary to euchromatin [47].

The mating type locus contains the actively transcribed *mat1* locus and the two transcriptionally silent mating type loci (mat2-P and mat3-M), which each contains a cassette (*h+* and *h-*, respectively) with copies of the two mating type genes. These copies are used as templates for mating type switching [211]. The central part of the mating locus contains the *cenH* region, which consists of sequences homologous to the pericentromeric dg/dh repeat [212]. The mat locus is flanked by another set of IR domains that function as boundaries [213]. The telomeres of *S. pombe* are comprised of G/T rich heterogeneous tandem repeats ($G_{0-6}GGTTACAC_{0-1}$) [214], [215]. This is different from mammals, whose telomeres usually only consist of the repeat GGGTTA [216]. Nonetheless, telomere protection via the shelterin complex works similar in mammals and *S. pombe* [216], [217]. The subtelomeric region of *S. pombe* comprises the TAS (telomere associated repeats), which together with the telomeric repeats give rise to TERRA and other telomeric RNAs, pseudogenes and repetitive sequences (long terminal repeats, LTRs) but also mostly genes that are upregulated during meiosis but silenced during the mitotic cell cycle [218], [219]. In case of chromosome 3, the subtelomeric region contains in addition the rDNA repeats, which are also heterochromatic. Furthermore, in addition to the *dg/dh repeats* and the *dg/dh*-like *cenH* region at pericentromeres and the mating type locus, respectively, the *tlh1+ and tlh2+* genes present on the subtelomeric arms of chromosome 1 and 2 (and probably chromosome 3) may act as the telomeric nucleation site for heterochromatin formation and spreading, as they are partially homologous to *dg/dh* reviewed in [67], [212], [220]. Comparable to higher eukaryotes, *S. pombe* also possesses facultative HC in the form of heterochromatin islands, which include several meiotic genes that directly neighbor euchromatic genes [221]. Two other types of HC have been reported, however these form only temporarily during G1 phase and in certain exosome mutants [222], [223]. Many key HC factors are conserved in *S. pombe* and well characterized, for instance HP1 proteins, KMTs , KDMs, HDACs, and the RNAi machinery [71], [224], [225]. Conversely, silencing in *S. pombe* is less complex than in higher eukaryotes, as it lacks DNA methylation and PcG proteins. Instead, *S. pombe* employs RNAi to establish de novo heterochromatin at the pericentromeres (and to some extent at the mating type locus and subtelomeres). *S. pombe* has two HP1 proteins, Swi6 and Chp2 [226]. Chp1, although a chromodomain protein, lacks the chromoshadow domain and forms with Ago1 and Tas3 the RITS complex involved in RNAi [226], [227]. Swi6 plays an important role during heterochromatin spreading but has also been shown to retain

pericentromeric transcripts to promote their degradation [228], [229]. Both Swi6 and Chp2 bind the *S. pombe* specific-boundary factor Epe1, a putative H3K9me demethylase, which antagonizes heterochromatin spreading beyond the endogenous boundaries [229]–[232]. In addition, Chp2 recruits the multifunctional SHREC complex, which promotes heterochromatin formation. SHREC is orthologous to NuRD and contains the H3K14ac-specific HDAC Clr3 and the nucleosome remodeler Mit1 [88], [233]. The HDAC Sir2, the homolog of *S. cerevisiae* Sir2, deacetylates H3K14ac as well as H3K9ac, H4K16ac and H3K4ac [43], [234], [235]. Especially the deacetylation of H3K9ac and H3K14ac have been shown to oppose heterochromatin assembly in *S. pombe* [101], [234], [235].

Many of the histone marks found in higher eukaryotes are conserved as well. For example, HC is marked by H3K9me2/me3 and H4K20me3, whereas H3K4me3 as well as H3K14ac and H3K9ac decorate promoter regions, and H3K36me2 and H3K36me3 are distributed throughout the gene body [43], [128]. However, in contrast to the redundancy of KMTs in higher eukaryotes, all three methylation stages are conferred by single copy enzyme, which are a homolog of the trimethylase found in higher eukaryotes: In HC, H3K9me and H4K20me are mediated by Clr4 and Set9, respectively; in EC, Set1 deposits H3K4me, whereas Set2 methylates H3K36 [74], [169], [236], [237].

The *S. pombe* genome also contains three known KATs, the SAGA complex subunit Gcn5 and two MYST family members, Mst1 and Mst2; among which only Mst1 is essential [238], [239]. Mst1 is a homolog of the *S. cerevisiae* HAT complex NuA4 and acetylates H3K4 and histone H4 [240], [241]. Gcn5, named after its homologs in higher eukaryotes, and Mst2 both acetylate H3K14 with Gcn5 additionally targeting H3K9 [238], [239], [242].

To summarize, *S. pombe* is highly suitable to study HC formation and its spatiotemporal regulation, as many hallmarks of EC and HC are conserved, and critical factors are often encoded by single-copy genes, resulting in reduced complexity.

2.5 The Mst2 HAT complex is a known anti-silencing factor

In *S. cerevisiae*, the HAT complex NuA3 is present as two subcomplexes that target different chromatin regions: NuA3a contains the PHD finger domain protein Yng1p that recruits NuA3 to H3K4me3 at promoter regions, whereas NuA3b binds to H3K36me3 (and to a lesser degree H3K36me2) via its PWWP subunit Pdp3p (Figure 5A and 5B)

[140], [243]. Additionally, both subcomplexes contain the PHD domain protein Nto1, which binds to H3K4me and H3K36me via its two PHD domains [244]. In *S. pombe*, NuA3 is named after its catalytic HAT subunit as Mst2 complex (hereafter Mst2C). Mst2C lacks a corresponding Yng1 subunit but contains a homolog of Pdp3; in addition, it comprises two *pombe*-specific subunits (Figure 5C) [245].
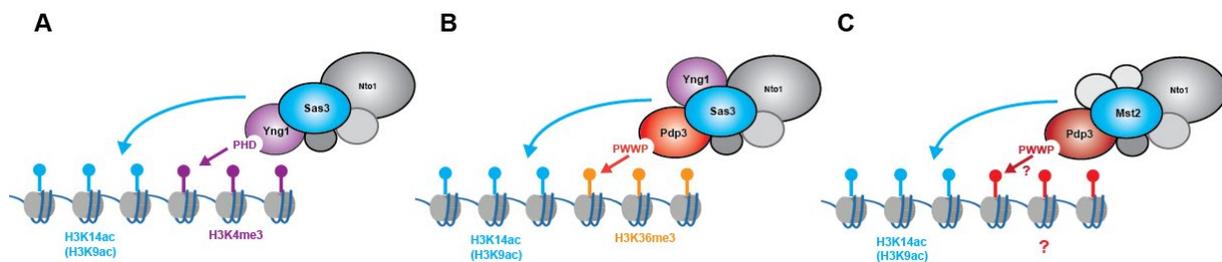
Figure 5: Comparison of recruitment strategies between *S. cerevisiae* NuA3 and *S. pombe* Mst2C - (A) NuA3a is recruited to H3K4me3 via the PHD domain protein Yng1; (B) NuA3b is recruited to H3K36me3 via the PWWP domain protein Pdp3, though Yng1 is still present; (C) function of Pdp3 within Mst2C is unclear, but it is possibly involved in the complex' recruitment; homologous subunits of the complexes are similarly colored.

An early study proposed that Mst2 requires the presence of other Mst2C subunits to function as immunoprecipitated Mst2-HA did display HAT activity in *in vitro* assays [238]. This notion was confirmed by the discovery that Mst2C is catalytically inactive in absence of Nto1 or the *pombe*-specific Ptf2 [245]. *In vivo*, Mst2 acts redundantly with the HAT Gcn5: H3K14ac is maintained in single mutants but lost in the *gcn5Δ mst2Δ* double mutant [245].

H3K14ac plays a role in DNA damage response by increasing chromatin accessibility and promoting the recruitment of the RSC remodeler [245]. However, Mst2 also appears to promote transcription, as *mst2Δ* cells display reduced H3K9ac and H4ac levels, both marks of active promoters, at two loci telomere-distal of *tlh1+* [43], [128], [238], [242]. This anti-silencing function of Mst2C appears to oppose RNAi, as loss of *mst2+* suppresses the silencing defect caused by the lack of components of the RNAi pathway [242]. Silencing in RNAi-deficient cells is also rescued by a catalytically inactive mst2-E274Q mutant but, surprisingly, not by the loss of *gcn5*. In contrast to the silencing defects in RNAi mutants, loss of silencing in HDAC mutants cannot be rescued by concomitant deletion of *mst2+* [242]. Together, this implies that Mst2C antagonizes heterochromatin in a manner that requires its HAT activity but is independent of H3K14 acetylation.

The anti-silencing function of Mst2C is not directly linked to H3K9me deposition, since loss of Mst2 does not rescue silencing defects in mutants lacking CLRC or HP1 [238], [242]. Rather, Mst2C acts redundantly with Epe1 in the maintenance of heterochromatin boundaries, as loss of Mst2, like that of Epe1, results in H3K9me2 spreading [230], [231], [246], [247]. Furthermore, while H3K9me2 levels in *mst2Δ* and *epe1Δ* are comparable at pericentromeres, mating type, and meiotic islands (e.g. *mei4+*), they are drastically increased at subtelomeric regions in an *mst2Δ* single mutant [247]. Thus, while not directly involved in H3K9me deposition, Mst2 acts redundantly with Epe1 in the prevention of H3K9me spreading as well as the ectopic formation of heterochromatin.

Moreover, loss of both Mst2 and Epe1 results in the silencing of genes that neighbor meiotic islands through H3K9me2 spreading, indicating that Mst2 also counteracts ectopic silencing [247]. Lastly, Mst2C has also been reported to mediate maintenance of heterochromatin boundaries through promoting nucleosome turnover and impedes ectopic heterochromatin formation [101].

Thus, Mst2C is an H3K14-specific HAT but has another target that opposes RNAi and H3K9me2-speading as well as the retention of nucleosomes. However, the molecular mechanism by which Mst2C antagonizes heterochromatin has not yet been elucidated.

2.6 Aims and objectives of this study

While Mst2C acts in promoting transcription, the loss its subunit Pdp3 causes paradoxically a defect in heterochromatin silencing [231]. As PWWP domain proteins are known to affect the localization of chromatin-modifying enzymes, it seems plausible that Pdp3 fulfills a similar function for Mst2C [140]. This raised the question whether Pdp3 acts as a specification factor of Mst2C through anchoring to euchromatin. This hypothesis makes the prediction that loss of Pdp3 causes relocalization of Mst2 and in turn perturbs silencing through aberrant acetylation at heterochromatin. The overall goal of my thesis was to test this hypothesis. In particular, I sought to examine whether Pdp3 sequesters Mst2C to euchromatin and whether the silencing defect of *pdp3Δ* can be alleviated by eliminating Mst2 or any of the other complex subunits.

Revealing the mechanism by which Pdp3 acts within Mst2C makes it necessary to know where Mst2 is localized on chromatin and which histone modification is recognized by Pdp3. If Pdp3 recruits Mst2 to chromatin, their binding profiles should

be similar to each other. If Pdp3 recruits Mst2C to chromatin via its PWWP domain, then binding of Mst2 should be lost in a strain lacking Pdp3 and as a result encroach on heterochromatin. Further, Pdp3 should no longer interact with chromatin in strains with a mutated PWWP domain. Lastly, neither Mst2 nor Pdp3 should be detectable on chromatin in strains that lack the target of Pdp3, i.e. a specific methylated histone residue [200].

Once the histone modification that recruits Pdp3 has been identified, genetic interaction studies can be applied to further explore the functional relationship. A double deletion mutant of the histone-modifying enzyme (likely a KMT) and *pdp3*$^+$ would be expected to be epistatic with its single mutant, as the KMT would function upstream of Pdp3. In contrast, concomitant deletion of *mst2*$^+$ should rescue the silencing defect the mutant lacking the KMT*,* as seen for *pdp3*Δ.

Finally, if delocalization of Mst2 is responsible for the silencing defect in *pdp3*Δ, this suggests that perturbed silencing is mediated through its unrestrained KAT activity. While Mst2 has been shown to acetylate histone H3K14, previous studies suggested that H3K14ac by Mst2 is not involved in HC de-repression. Thus, identifying the relevant acetylation target is critical to fully understand the molecular mechanism.

3 Materials and methods

3.1 Microbiological methods

3.1.1 *E. coli* methods

3.1.1.1 Bacterial strains

Table 1: Electrocompetent *E. coli* strain

name	genotype	source
XL1 blue	recA1; endA1; gyrA96; thi-1; hsdR17; supE44; relA1; lac[F´ proAB lacIqZ**Δ**M15 Tn10(Tetr)]	Stratagene

3.1.1.2 Plasmids

Table 2: Plasmids used and generated during the study

strain designation	plasmid	genotype	source
ESB96	pFA6a-NATMX6	ori, ampR, natR	[248]
ESB251	pRS416	CEN, URA3, ampR	Stratagene
ESB466	pRS416-CBP-FLAG-pdp3	CEN, URA3, ampR, natMX:2xFLAG-CBP-Pdp3	this study
ESB467	pRS416-CBP-FLAG-pdp3_F109A	CEN, URA3, ampR, natMX:CBP-2xFLAG-pdp3_F109A	this study
ESB468	pRS416-mst2-CBP-FLAG	CEN, URA3, ampR, mst2-CBP-2xFLAG:natMX	this study

3.1.1.3 Media

Table 3: LB liquid media

compound	amount	final concentration
tryptone	10 g	10 g/l
yeast extract	5 g	5 g/l
NaCl	10 g	10 g/l
ddH$_2$O	up to 1000 ml	-
Ampicilline (50 mg/ml) [for LB+Amp)	1 ml	50 µg/ml

LB non-selective stored at RT, LB+Amp stored at 4ºC

Table 4: LB + Amp plates

compound	amount	final concentration
tryptone	10 g	10 g/l
yeast extract	5 g	5 g/l
NaCl	10 g	10 g/l
Agar (Serva)	15 g	1.5 %
ddH$_2$O	up to 1000 ml	-
Ampicilline (50 mg/ml)	1 ml	50 µg/ml

stored at 4ºC

3.1.1.4 Growth and storage of strains

For colony growth, cells were plated onto LB media containing antibiotic and incubated at 37 °C overnight. For maxipreps (section 3.3.2.1), 50 ml of medium were inoculated from the -80ºC stock using a sterile pipet tip to add a small amount of cells directly to the medium. For minipreps, 2 ml of medium were inoculated with a single colony, using a sterile pipet tip as well. The cells were grown overnight at 37 ºC and 200 rpm (rounds per minute). For long-term storage, 125 µl of cells suspended in LB (+ antibiotic), e.g. from a miniprep, were mixed with 1.275 ml of filtered and cold 20% glycerol and stored at -80 ºC.

3.1.1.5 Transformation of plasmids via electroporation

For propagation in *E. coli*, DNA was extracted from 1/3 to 1/2 of a plate of *S. cerevisiae* transformants using the Smash and Grab method (section 3.3.2.3) and resuspended in 50 µl ddH$_2$O. 10 µl were placed on a filter disc (Millipore 0.05µm VMWP; Cat#: VMWP02500) swimming on 100 ml of H$_2$O and dialyzed for 10 minutes. The rest was stored at -20ºC. Electrocompetent XL1blue cells (Table 1) were thawed on ice and aliquoted to 40 µl per transformation. 10 µl of dialyzed plasmid were mixed with the thawed cells and pipetted into sterile electroporation cuvettes (Bio-rad #165-2089; brown cap). The cells were electroporated using a Bio-Rad Gene Pulser Electroporation system (1.8 kV, 200 Ohm, 25 µF). Immediately after electroporation the transformants were mixed with 400 µl of RT LB medium (Table 3) and transferred to a fresh 1.5 ml tube. For recovery, the cells were incubated for 45 min at 37ºC and constant agitation. 40 µl of cells were plated onto LB + Amp (Table 4) as a 1:10 plate while the rest of the cells were spun down and about 200 µl of supernatant were removed. The cells were resuspended again and plated onto LB + Amp as 9:10 plate. The colonies were grown over night at 37 ºC. All inoculation steps were performed using aseptic laboratory techniques [249].

3.1.2 S. cerevisiae methods

3.1.2.1 Strains

Table 5: *S. cerevisiae* strain for homologous recombination

Strain designation	genotype	source
YSB92	BHM1669 (pEG202) [W303]	Sigma-Aldrich

3.1.2.2 Media

Table 6: YPD liquid media

compound	amount	final concentration
yeast extract	10 g	10 g/l
Bacto peptone	20 g	2 %
amino acids	10 ml each	see amino acids table
ddH$_2$O	up to 950 ml	-
40 % glucose	50 ml (directly before use)	2 %

common RT stock

Table 7: SD plates

compound	amount	final concentration
yeast nitrogen base w/o amino acids	6.7 g	6.7 g/l
agar (Serva)	20 g	2 %
amino acid or uracil	10 ml each	20-200 mg/ml depending on the compound
ddH$_2$O	850 ml	-

common 4ºC stock

Table 8: SC-ura plates

compound	amount	final concentration
yeast nitrogen base w/o amino acids	6.7 g	6.7 g/l
agar (Serva)	20 g	2 %
amino acid	10 ml each	20-200 mg/ml depending on the amino acid
ddH$_2$O	850 ml	-

common 4ºC stock

10 ml per amino acid and of uracil were added from 100 ml preparations of 100x stock solutions as required (all reagents were purchased from Sigma-Aldrich).

Table 9: amino acids and uracil

compound	amount	final concentration (in 1l media)
Arginine HCl	200 mg	2 mg/ml
Isoleucine	300 mg	3 mg/ml
Lysine HCl	300 mg	3 mg/ml
Methionine	200 mg	2 mg/ml
Phenylalanine	500 mg	5 mg/ml
Threonine	2000 mg	20 mg/ml
Tyrosine	300 mg	3 mg/ml
Uracil	200 mg	2 mg/ml
Valine	1500 mg	15 mg/ml

common RT stock

The compounds were mixed in by stirring and brought to 950ml with ddH$_2$O. The pH was adjusted to 5.8 with HCl and the mixture autoclaved. 50 ml 40% glucose were added after cooling the mixture to 55ºC before pouring.

3.1.2.3 Growth of strains

Solid cultures were inoculated from -80 °C stock by streaking the cell onto SD plates (Table 7) using a sterile 2-ml serological glass pipette. For liquid cultures, 2-ml of YPD was inoculated from plate. The preculture was grown overnight at 30ºC on a turning

wheel. In the morning 1.25 ml of the preculture were diluted 1:40 in 50 ml of YPD medium (Table 6) in a 250 ml flask. The OD_{600} (optical cell density at 600 nm) was measured using an OD600 DiluPhotometer™ (*IMPLEN*). The culture was then grown at 30 C and 160 rpm until the desired OD_{600}. All inoculation and measurement steps were performed using aseptic laboratory techniques [249].

3.1.2.4 Plasmid generation via homologous recombination

To increase the rate of successful transformants in *S. pombe*, the mutants were first constructed in *S. cerevisiae*, then propagated in *E. coli* to produce a high quantity of material for transformation. To this end, the shuffle vector pRS416, which is propagated both in *S. cerevisiae* and *E. coli*, was used as backbone plasmid for molecular cloning (Sikorski and Hieter, 1989). *S. cerevisiae* was used as it has a 10-fold higher capacity for homologous recombination than *S. pombe*, thus requiring shorter homologous domains for recombination (50 bp compared 500 bp for *S. pombe*). Plasmids containing FLAG-tagged *pdp3+*, *pdp3+*_F109A or *mst2+* were generated by homologous recombination with the shuffle vector pRS416 (markers *URA3* and *amp^R*) in the *S. cerevisiae* W303 strain (Table 5). pRS416 was linearized with EcoI-HF (see section 3.3.4.1), tested for linearization by agarose gel electrophoresis and purified (see sections 3.3.4.3 and 3.3.4.4). The cells were grown to an OD of at least 0.6, then pelleted and washed twice with 25 ml of ddH_2O at room temperature and 400xg for 5 min. The cells were resuspended in 500 µl H_2O, aliquoted to 100 µl each and pelleted again for 1.5 min at 400 x g. The pellets were then treated with a lithium acetate, polyethylene glycol mix containing the DNA fragments (250 µl 50% PEG 3350, 5 µl boiled 10 mg/ml single-stranded DNA, 36 µl of 1 M LiOAc, 500 ng per DNA fragment in a total of 50 µl ddH_2O). The mix was vortexed and incubated for 40 min at 42°C on a heating block. After incubation the transformed cells were spun down for 2 min at 400xg and washed with 500 µl of sterile ddH_2O. Lastly, the cells were resuspended in 100 µl of ddH_2O and plated onto SC-ura (Table 8). These plates were grown at 30°C for four days.

3.1.3 *S. pombe* methods

3.1.3.1 Strains

Strains of the *Bioneer* collection are derived from the SP286 background (*M (h-), smt0, ade6-M210, leu1-32, ura4-D18*). The reporter gene strains are derived from the wild

type strain 972 (*M(h-), ade6-M210, leu1-32, ura4-D18*). Table 10 comprises all strains that were utilized during this study.

Table 10: *S. pombe* strains used in the study.

name	genotype	use	source	applied in Figure
PSB065	*h⁺, imr1L::ura4⁺*	gene reporter assay, RT-qPCR	Braun Lab	1B, 1D, 4D, 5A, 5E, 6A-6C
PSB090	*h⁺, imr1L::ura4⁺, clr4Δ*	positive control for gene reporter assay	Braun Lab	1B
PSB582	*h⁻ SPSQ (cyhR), SPL42 (cyhS), hphMX::cen1, imr1L(NcoI)::ura4⁺, otr1R(SphI)::ade6⁺, leu1-32, ura4-DS/E ade6-M210*	SGA, gene reporter assay, RT-qPCR, ChIP-qPCR	Braun Lab	1D, 2C, 3B, 3C, 7A-7C, 8A, 8B
PSB619	*h⁺, pdp3Δ::kanMX*	gene reporter assay, deletion cassette donor, marker switch	Bioneer	1B
PSB623	*h⁺, pdp3Δ::natMX*	deletion cassette donor	Braun Lab	-
PSB657	*h⁺, imr1L::ura4⁺, pdp3Δ::natMX*	gene reporter assay, RT-qPCR	Braun Lab	1B, 1D, 4D, 5A
PSB658	*imr1L::ura4⁺, pdp3Δ::natMX*	gene reporter assay	Braun Lab	1B
PSB689	*h⁻, SPSQ (cyhR), SPL42 (cyhS), hphMX::cen1, imr1L(NcoI)::ura4⁺, otr1R(SphI)::ade6⁺, leu1-32, ura4-DS/E, ade6-M210, pdp3Δ::natMX*	gene reporter assay, RT-qPCR, SGA	Braun Lab	1D, 2C, 3B, 3C, 7B, 8A, 8B
PSB955	*h⁺, SPSQ (cyhR)), hphMX::cen1, imr1L(NcoI)::ura4⁺, otr1R(SphI)::ade6⁺, leu1-32, ura4-DS/E, ade6-M210, pdp3Δ::natMX, mst2Δ::kanMX*	ChIP-qPCR	this study	9G-9I, 10H
PSB969	*h⁺, SPSQ (cyhR)), hphMX::cen1, imr1L(NcoI)::ura4⁺, otr1R(SphI)::ade6⁺, leu1-32, ura4-DS/E, ade6-M210, mst2Δ::kanMX*	ChIP-qPCR, deletion cassette donor, marker switch	this study	9D-9F, 10C
PSB972	*h⁺, SPSQ (cyhR)), hphMX::cen1, imr1L(NcoI)::ura4⁺, otr1R(SphI)::ade6⁺, leu1-32, ura4-DS/E, ade6-M210, eaf6Δ::kanMX*	genotyping, deletion cassette donor, marker switch	this study	-
PSB975	*h⁺, SPSQ (cyhR)), hphMX::cen1, imr1L(NcoI)::ura4⁺, otr1R(SphI)::ade6⁺, leu1-32, ura4-DS/E, ade6-M210, nto1Δ::kanMX*	genotyping, deletion cassette donor, marker switch	this study	-
PSB978	*h⁺, SPSQ (cyhR)), hphMX::cen1, imr1L(NcoI)::ura4⁺, otr1R(SphI)::ade6⁺, leu1-32, ura4-DS/E, ade6-M210, ptf1Δ::kanMX*	genotyping, deletion cassette donor, marker switch	this study	-
PSB981	*h⁺, SPSQ (cyhR)), hphMX::cen1, imr1L(NcoI)::ura4⁺, otr1R(SphI)::ade6⁺, leu1-32, ura4-DS/E, ade6-M210, ptf2Δ::kanMX*	genotyping, deletion cassette, donor, marker switch	this study	-
PSB984	*h⁺, SPSQ (cyhR)), hphMX::cen1, imr1L(NcoI)::ura4⁺, otr1R(SphI)::ade6⁺, leu1-32, ura4-DS/E, ade6-M210, tfg3Δ::kanMX*	genotyping, deletion cassette donor, marker switch	this study	-
PSB1042	*h⁺, SPSQ (cyhR)), hphMX::cen1, imr1L(NcoI)::ura4⁺, otr1R(SphI)::ade6⁺, leu1-32, ura4-DS/E, ade6-M210, mst2Δ::natMX*	genotyping, deletion cassette donor	this study	-
PSB1044	*h⁺, SPSQ (cyhR)), hphMX::cen1, imr1L(NcoI)::ura4⁺, otr1R(SphI)::ade6⁺, leu1-32, ura4-DS/E, ade6-M210, eaf6Δ::natMX*	genotyping, deletion cassette donor	this study	-

name	genotype	use	source	applied in Figure
PSB1046	*h$^+$, SPSQ (cyhR)), hphMX::cen1, imr1L(NcoI)::ura4$^+$, otr1R(SphI)::ade6$^+$, leu1-32, ura4-DS/E, ade6-M210, nto1Δ::natMX*	genotyping, deletion cassette donor	this study	-
PSB1050	*h$^+$, SPSQ (cyhR)), hphMX::cen1, imr1L(NcoI)::ura4$^+$, otr1R(SphI)::ade6$^+$, leu1-32, ura4-DS/E, ade6-M210, ptf2Δ::natMX*	genotyping, deletion cassette donor	this study	-
PSB1122	*h$^-$ SPSQ (cyhR), SPL42 (cyhS), hphMX::cen1, imr1L(NcoI)::ura4$^+$, otr1R(SphI)::ade6$^+$, leu1-32, ura4-DS/E, ade6-M210, mst2Δ::natMX*	SGA, gene reporter assay, RT-qPCR, ChIP	this study	2C, 3B, 3C, 7A, 8A, 8B
PSB1124	*h$^-$ SPSQ (cyhR), SPL42 (cyhS), hphMX::cen1, imr1L(NcoI)::ura4$^+$, otr1R(SphI)::ade6$^+$, leu1-32, ura4-DS/E, ade6-M210, eaf6Δ::natMX*	SGA	this study	2C
PSB1127	*h$^-$ SPSQ (cyhR), SPL42 (cyhS), hphMX::cen1, imr1L(NcoI)::ura4$^+$, otr1R(SphI)::ade6$^+$, leu1-32, ura4-DS/E, ade6-M210, nto1Δ::natMX*	SGA	this study	2C, 7B
PSB1130	*h$^-$ SPSQ (cyhR), SPL42 (cyhS), hphMX::cen1, imr1L(NcoI)::ura4$^+$, otr1R(SphI)::ade6$^+$, leu1-32, ura4-DS/E, ade6-M210, pdf2Δ::natMX*	SGA	this study	2C, 7B
PSB1303	*h$^+$, SPSQ (cyhR)), hphMX::cen1, imr1L(NcoI)::ura4$^+$, otr1R(SphI)::ade6$^+$, leu1-32, ura4-DS/E, ade6-M210*	ChIP-qPCR	this study	9A-9I, 10C, 10F, 10H
PSB1305	*h$^+$, SPSQ (cyhR)), hphMX::cen1, imr1L(NcoI)::ura4$^+$, otr1R(SphI)::ade6$^+$, leu1-32, ura4-DS/E ade6-M210, pdp3Δ::kanMX*	ChIP-qPCR	this study	9A-9C, 10F
PSB1524	*h$^+$, SPSQ (cyhR), hphMX::cen1, imr1L(NcoI)::ura4$^+$, otr1R(SphI)::ade6$^+$, leu1-32, ura4-DS/E, ade6-M210, clr3Δ::kanMX*	ChIP-qPCR	this study	8A, 8B
PSB1696	*h$^+$, imr1L(NcoI)::ura4$^+$, otr1R(SphI)::ade6$^+$, leu1-32, ura4-DS/E, ade6-M210, natMX::CBP-2xFLAG-pdp3*	ChIP-qPCR	this study	4D, 5A, 5E, 6A-6C, 10A, 10D
PSB1698	*h$^+$, imr1L(NcoI)::ura4$^+$, otr1R(SphI)::ade6$^+$, leu1-32, ura4-DS/E, ade6-M210, natMX::CBP-2xFLAG-pdp3_F109A*	ChIP-qPCR	this study	5E, 6A-6C, 10A
PSB1769	*h$^+$, imr1L(NcoI)::ura4$^+$, otr1R(SphI)::ade6$^+$ leu1-32 ura4-DS/E ade6-M210, natMX::CBP-2xFLAG-pdp3, set2Δ::kanMX*	ChIP-qPCR	this study	5A, 6A, 6B, 10D
PSB1817	*h$^+$ imr1L(NcoI)::ura4$^+$, otr1R(SphI)::ade6$^+$, leu1-32, ura4-DS/E, ade6-M210, natMX::CBP-2xFLAG-pdp3, set2-SRIΔ:kanMX*	ChIP-qPCR	this study	5A, 6A, 6B, 10D
PSB1782	*h$^-$, leu1-32, ura4-D18, ade6-704, trp1$^+$::ade6$^+$*	ChIP-qPCR	Buehler Lab	4E, 4F, 6A-6C, 10B, 10E
PSB1855	*h$^-$, leu1-32, ura4-D18, ade6-704, trp1$^+$::ade6$^+$, mst2-CBP-2xFLAG::natMX*	ChIP-qPCR	this study	4E, 4F, 5B, 5C, 6A-6C, 10B, 10E, 10G
PSB1870	*h$^-$, leu1-32, ura4-D18, ade6-704, trp1$^+$::ade6$^+$, mst2-FLAG::natMX, set2Δ::kanMX*	ChIP-qPCR	this study	5B, 5C, 6A, 6B, 10E, 10G
PSB1871	*h$^-$, leu1-32, ura4-D18, ade6-704, trp1$^+$::ade6$^+$, mst2-FLAG::natMX, pdp3Δ::kanMX*	ChIP-qPCR	this study	4E, 4F, 6A, 6B, 10B
PSB1882	*h$^-$, leu1-32, ura4-D18, ade6-704, trp1$^+$::ade6$^+$, mst2-FLAG::natMX, set2-SRIΔ::kanMX*	ChIP-qPCR	this study	5B, 5C, 6A, 6B, 10G
PSB2099	*h$^-$, SPSQ (cyhR) SPL42 (cyhS), hphMX::cen1, imr1L(NcoI)::ura4$^+$, otr1R(SphI)::ade6$^+$, leu1-32, ura4-DS/E ade6-M210, pdp3Δ::natMX mst2Δ::kanMX*	RT-qPCR	this study	3B, 3C
PSB2111	*h$^-$ SPSQ (cyhR), SPL42 (cyhS), hphMX::cen1, imr1L(NcoI)::ura4$^+$, otr1R(SphI)::ade6$^+$, leu1-32, ura4-DS/E ade6-M210, set2Δ::kanMX*	RT-qPCR	this study	7A, 7B

name	genotype	use	source	applied in Figure
PSB2113	*h⁻ SPSQ (cyhR), SPL42 (cyhS), hphMX::cen1, imr1L(NcoI)::ura4⁺, otr1R(SphI)::ade6⁺, leu1-32, ura4-DS/E ade6-M210, set2∆::kanMX, pdp3∆::natMX*	RT-qPCR	this study	7B
PSB2115	*h- SPSQ (cyhR), SPL42 (cyhS), hphMX::cen1, imr1L(NcoI)::ura4+, otr1R(SphI)::ade6+, leu1-32, ura4-DS/E, ade6-M210, nto1∆::natMX, set2∆::kanMX*	RT-qPCR	this study	7B
PSB2131	*h⁻ SPSQ (cyhR), SPL42 (cyhS), hphMX::cen1, imr1L(NcoI)::ura4⁺, otr1R(SphI)::ade6⁺, leu1-32, ura4-DS/E ade6-M210, set2∆::kanMX, mst2∆::natMX*	RT-qPCR	this study	7A
PSB2325	*h⁻, SPSQ (cyhR) SPL42 (cyhS) hphMX::cen1, imr1L(NcoI)::ura4⁺ otr1R(SphI)::ade6⁺, leu1-32, ura4-DS/E, ade6-M210, ptf2∆::natMX, set2∆::kanMX*	RT-qPCR	this study	7B
PSB2356 (spb426)	*h⁻, leu1-32, ura4-D18, ade6-704, trip1⁺::ade6+, shade6-250/natMX*	RT-qPCR	this study	7C
PSB2357 (spb2982)	*h⁻, leu1-32, ura4-D18, ade6-704, trp1⁺::ade6⁺, nmt1⁺::ade6-hp⁺::natMX, brl1-K242R*	RT-qPCR	this study	7C
PSB2568 (spb2983)	*h-, leu1-32, ura4-D18, ade6-704, trp1⁺::ade6⁺, nmt1⁺::ade6-hp⁺::natMX, brl1-K242Q*	RT-qPCR	this study	7C
PSB2361	*h⁻, leu1-32, ura4-D18, ade6-704, trp1⁺::ade6⁺, shade6-250/natMX, set2∆::kanMX*	RT-qPCR	this study	7C
PSB2363	*h-, leu1-32, ura4-D18, ade6-704, trp1⁺::ade6⁺, nmt1⁺::ade6-hp⁺::natMX, brl1-K242R, set2∆::kanMX*	RT-qPCR	this study	7C
PSB2565	*h⁻, leu1-32, ura4-D18, ade6-704, trp1⁺::ade6⁺, nmt1⁺::ade6-hp⁺::natMX, brl1-K242Q, set2∆::kanMX*	RT-qPCR	this study	7C

3.1.3.2 Media

YES (yeast extract with supplements) liquid media was prepared as a 2x stock without glucose and distributed to 500 ml per 1 l bottle before autoclaving. The glucose was added directly before use and the bottle filled up to 1 l with ddH$_2$O. The amounts listed are required for 3 liters of 2xYES.

Table 11: 2x YES liquid media (3 l)

compound	amount	final concentration
yeast extract (Serva)	30 g	10 g/l
SP Supplements	6 g	2 g/l
1M KH$_2$PO$_4$	350 ml	112 mM
ddH$_2$O	2650 ml	-

All *S. pombe* solid media was prepared with a Masterclave® 09 (*bioMérieux Deutschland GmbH*) at 4 liters of media volume. The amounts listed are required for one liter of media. The media was dispensed to 35 ml per round plate and 50 ml per square plate using a peristaltic pump (*bioMérieux Deutschland GmbH*) with a sterilized medium sized outlet to keep media volumes constant and throughout experiments and thus any gained data more reproducible. All pouring steps were performed in the sterile field of a Bunsen burner flame.

Table 12: YES plates

compound	amount	final concentration
yeast extract (Serva)	6 g	5g/l
SP Supplements	1 g	1 g/l
agar (Serva)	20 g	2%
1M KH$_2$PO$_4$	56 ml	56 mM
ddH$_2$O	875 - x ml	-
glucose 40%*	75 ml	3%

YES non-selective stored at RT, selective plates stored at 4ºC

x represents the added volume of antibiotic, cycloheximide or 5-FOA per liter medium.

Table 13: Selective reagents

compound	amount	solvent	final concentration
cycloheximide (50 mg/ml)	2 ml	DMSO	100 mg/l
Geneticin G418 (50 mg/ml)	2 ml	liquid stock	100 mg/l
cloNAT (50 mg/ml)	2 ml	sterile H$_2$O	100 mg/l
hygromycin B (50 mg/ml)	2 ml	liquid stock	100 mg/l
5-fluoroorotic acid	250 ml	sterile H$_2$O (Dissolve 1 g per 250 ml by prewarming at 62°C for 1h in a shaking water bath. Then, add to pouring temperature media and mix for 10 minutes before dispensing)	250 mg/l

Stored at 4ºC

Table 14: SPAS plates

compound	amount	final concentration
KH$_2$PO$_4$	1 g	1g/l
SP Supplements	1 g	1 g/l
agar (Serva)	20 g	2%
ddH$_2$O	975 ml	-
1000x Vitamin mix	1 g	1/1000
glucose 40%	25 ml	1%

Stored at 4ºC

The vitamin mix was prepared according to Table 15.

Table 15:1000x vitamin mix

compound	amount	final concentration
Biotin	0.01 g	0.04 mM
Pantothenic Acid	1 g	81.2 mM
myo-Inositol	10 g	4.2 mM
Nicotinic Acid	10 g	81.2 mM

Stored at 4ºC

Table 16: EMM (Edinburgh minimal medium) plates

compound	amount	final concentration
EMM-Gluc (ForMedium)	12.3 g	1g/l
SP Supplements	1 g	1 g/l
agar (Otto Norwald)	20 g	2%
glucose hexahydrate	20 g	20 g/l
ddH$_2$O	1000 ml (750 ml for EMM+FOA)	-

Stored at 4ºC

For EMM + FOA plates 5-FOA was prepared and added similarly to YES + FOA.

Table 17: EMM-ura plates

compound	amount	final concentration
EMM-Gluc (ForMedium)	12.3 g	1g/l
Each His Leu Ade Lys	0.225 g	225 mg/l
agar (Otto Norwald)	20 g	2%
glucose hexahydrate	20 g	20 g/l
ddH$_2$O	1000 ml	-

Stored at 4ºC

3.1.3.3 Growth of strains

Solid cultures were inoculated from -80 °C stock by streaking the cell onto YES plates (Table 12) using a sterile 2-ml serological glass pipette. The plates were incubated for 2-3 days at 30 °C. For liquid cultures, a sterile 250-ml flask 50 ml or a 500-ml flask or 100 ml of YES (Table 11) was inoculated directly from plate to an OD$_{600}$ of 0.03 to 0.1 using autoclaved wooden sticks. The optical cell density was measured using an OD600 DiluPhotometer™ (*IMPLEN*). The liquid cultures were incubated at 30 °C and 150-160 rpm. In the morning the OD$_{600}$ measured again and harvested at an OD$_{600}$ of 0.4-0.8. Cultures between and OD$_{600}$ of 0.8 and 1.0 back-diluted to 0.2 grow for two more division cycles (4-5 hours). For experiments requiring more than one culture to be at a similar OD$_{600}$ all cultures were discarded if one culture was completely overgrown (OD$_{600}$ >1.0). For slow growing cultures, 10 µl of culture were tested for bacteria contamination under a light microscope (40x magnification). All inoculation and measurement steps were performed using aseptic laboratory techniques [249].

3.1.3.4 Homologous recombination via gap gene repair

To introduce deletions into a reporter strain, the endogenous locus of the strain was replaced by the deletion cassette via homologous recombination. To this end the deletion cassette was amplified from either a confirmed library strain for *kanMX* resistance using KO primers, or the strain was first transformed with a *natMX* cassette amplified from pFA(*natMX6*) and then amplified with KO primers. Double mutants were generated by successive transformation of confirmed re-KO. To insert a tagged construct into *S. pombe*, the respective null mutant was transformed with the digested construct plasmid. Before transformation the concentration of the plasmid was measured, and 5 µg of plasmid treated with PmeI to liberate the mutant construct (see section 3.3.4.1). The insert was not separated from the backbone after enzyme digestion.

For the transformation, liquid cultures were harvested at an OD of 0.4 - 0.8. To this end, the cultures were transferred to a 50 ml-tube and the cells were pelleted by centrifugation (5 min at 400xg), washed in 10 ml ddH$_2$O and after a second centrifugation step washed again in 5 ml LiOAc/TE solution (Table 18). The pellets were then resuspended LiOAc/TE again. An aliquot of 100 µl of cells per transformation was transferred to a new reaction tube and 20 µl of PCR product of digested construct (~2 µg of plasmid) and 10 µl denatured Carrier DNA (10 mg/ml) were added. The reaction mix was vortexed and then incubated at room temperature for 15 min.

Table 18: LiOAc/TE solution (100 ml)

compound	volume	final concentration
1M lithium acetate (pH 7.5), autoclaved	10 ml	100 mM
1M TRIS/HCl (pH 8.0), autoclaved	1 ml	10 mM
0.5M EDTA (pH 8.0), autoclaved	200 µl	0.1 mM
ddH2O), autoclaved	88.8 ml	-

Stored at 4ºC

Table 19: PEG/LiOAc solution (100 ml)

compound	volume	final concentration
50% PEG 3350	80 ml	40 % (v/v)
1M lithium acetate (pH 7.5), autoclaved	10 ml	100 mM
1M TRIS/HCl (pH 8.0), autoclaved	1 ml	10 mM
0.M EDTA (pH 8.0), autoclaved	200 µl	0.1 mM
ddH$_2$O), autoclaved	8.8 ml	-

Stored at 4ºC

Following the addition of 5-fold the total volume of reaction mix of PEG/LiOAc solution (Table 19) and mixing the cells were incubated at 30°C for 30 min, after which 9/100 of the reaction volume of DMSO were added. The cells were incubated at 42°C for 10 min and recovered by pelleting them (3 min at 400X*g*) to discard the supernatant and washing them in 500 µl YES. The cells were then resuspended in 100 µl YES and plated onto non-selective YES medium (Table 12).

The cells were grown for 2 days at 30°C to allow for recovery. The success of the recombination process was determined by replica-plating the colonies onto selective YES medium and incubating the plates for 2-3 days at 30°C. To gain mutants of a single population, colonies were picked and single-streaked onto selective media (6 streaks per plate). The streaks were incubated for 3 days at 30°C. One colony per streak was patched. To assure that the cassette was inserted at the right locus, a sample of each patch was streaked onto the previously used selective medium for the former marker followed by non-selective medium to control for presence of cells for the streak.

The DNA of cells positive for growth was extracted via zymolyase prep (section 3.3.2.2) and tested by diagnostic PCR (3.3.3.2).

3.1.3.5 Synthetic genetics array (SGA)

Null mutant cassettes of *pdp3⁺, mst2⁺, eaf6⁺, nto1⁺*, and *ptf2⁺* with a replacement of the ORF with a *natMX* resistance were first integrated into PSB582, an *imr::ura4⁺* reporter strain with its reporter genetically linked to a *hygR* resistance cassette against hygromycin B (HYG), which allows to select for the reporter's presence during the SGA. The strain has an *h⁻* mating type and additionally contains a dominant negative allele of a cycloheximide (Cyh) sensitive ribosomal subunit (*cyh^S*) within its mating type locus [250]. YES plates with and without antibiotics were prepared according to Table 12 and Table 13.

A fresh deletion library and a query plate of the same age were prepared, as mating requires relatively young cells. Query strain cells (the mutant of interest as well as a wild-type control) were freshly grown for 2-3 days at 30ºC on YES plates. These cells were used to inoculate a 50 ml YES culture, which was grown over night. On the next day, a *Rotor* HAD station (*Singer*) was used to replicate a deletion library (*Bioneer,* 3. generation) onto YES + G418 plates. The query strains were pinned from the culture onto EMM plates (Table 16). Both sets of plates were then incubated for 2 days at 30°C. The plates were used as a source to mate the *Bioneer* strains with the query strains on SPAS (Table 14). The mated strains were left to sporulate for 3 days at room temperature. For the germination, the spores were replica plated onto YES + Cyh to select against diploids and *h⁻* cells as both carry the *cyh^S* allele. The haploid cells were incubated at 30°C for 2 days and then went through three selection steps via replica plating and 2 days of incubation at 30°C. The first and third selection entails plating on YES plates that contained NAT, G418, Cyh and HYG. To select for the deletions, the mating type and for the presence of the *imr::ura4⁺* reporter gene. In the second step the mutants were replica-plated onto EMM-*ura* (Table 17) to select against mutants, which have a mutation inside their *ura4⁺* gene. After two days growth at 30°C, the mutants were tested for growth in absence and presence of 5-FOA (see and Table 12 Table 16). Pictures were taken of all plates on the 2ⁿᵈ to 4ᵗʰ day of the reporter assay.

3.1.3.6 *ura4⁺* gene reporter assays

For the purpose of verifying the phenotypic effect of single and double mutants in SGAs the deletion cassettes of interest were transformed into a reporter strain with

imr1L::ura4+ background as they have the same reporter gene location (PSB65 for Figure 6, PSB582 for Figure 7). For that purpose, strains were freshly grown on YES media for 2-3 days at 30ºC. A small number of cells was resuspended in 1 ml of YES and the OD_{600} measured. 200º µl YES were added to a 96-well flat-bottom plate was. The resuspension was diluted to an OD_{600} of 0.2 in the first well and then used as starting culture for a 1:5 serial dilution. The cells were plated onto non-selective EMM medium (N/S) and EMM medium containing 5-FOA (see Table 12 and Table 16) by using a sterilized pin array (stamp, pin diameter 0.3 cm). The pin array was sterilized by dipping it briefly in 100 % ethanol, flaming it off and cooling the array down on non-selective medium. The serial dilution was prepared during the cooling phase by transferring 50 µl of culture with a multi-channel pipet to the next well and mixing it in. The pin array was dipped briefly into the wells and left on the plate for 25 s each. The cells were incubated at 30 C for 3-5 days and then photographed.

3.2 Protein biochemical methods

3.2.1 Chromatin immunoprecipitation (ChIP)

3.2.1.1 Buffers

Table 20: 10xPBS (1 l)

compound	amount	final concentration
NaCl	80.0 g	1.37 M
$Na_2HPO_4 \cdot 2H_2O$	14.4 g	92 mM
KCl	2.0 g	27 mM
KH_2PO_4	2.4 g	18 mM
ddH$_2$O, autoclaved	Up to 1 l	-

Sterile filtered and stored at RT

Table 21: Quenching solution (500 ml)

compound	amount	final concentration
Glycine	93.84 g	2.5M
ddH$_2$O, autoclaved	Up to 500 ml	-

Sterile filtered and stored at RT

Table 22: Lysis buffer (500 ml)

compound	volume [ml]	final concentration
0.5 M HEPES/KOH pH 7.5, sterile filtered	50	50 mM
5 M NaCl, autoclaved	14	140 mM
0.5 M EDTA, autoclaved	1	1 mM
10 % Triton X-100	50	1 %
10 % Na-Deoxycholate	5	0.1 %
ddH$_2$O, autoclaved	380	-

Stored at 4ºC

Table 23: Lysis buffer - high salt (500 ml)

compound	volume [ml]	final concentration
0.5 M HEPES/KOH pH 7.5, sterile filtered	50	50 mM
5 M NaCl, autoclaved	50	500 mM
0.5 M EDTA, autoclaved	1	1 mM
10 % Triton X-100	50	1 %
10 % Na-Deoxycholate	5	0.1 %
ddH$_2$O, autoclaved	344	-

Stored at 4ºC

Table 24: Wash buffer (500 ml)

compound	volume [ml]	final concentration
1 M TRIS/HCl, pH 8.0	5	10 mM
4 M LiCl, autoclaved	31.25	250 mM
0.5 M EDTA, autoclaved	1	1 mM
10 % NP-40	25	0.5 %
10 % Na-Deoxycholate	25	0.5 %
ddH$_2$O, autoclaved	417.75	-

Stored at 4ºC

Table 25: TE (100 ml)

compound	volume [ml]	final concentration
1 M TRIS/HCl, pH 8.0	1	10 mM
0.5 M EDTA, autoclaved	0.2	1 mM
ddH$_2$O, autoclaved	98.8	-

Stored at RT

Table 26: TE + 1 % SDS (100 ml)

compound	volume [ml]	final concentration
1 M TRIS/HCl, pH 8.0	1	10 mM
0.5 M EDTA, autoclaved	0.2	1 mM
10 % SDS, autoclaved	10	1 %
ddH$_2$O, autoclaved	88.5	-

Stored at RT

Table 27: Elution buffer 3 (100 ml)

compound	volume [ml]	final concentration
1 M TRIS/HCl, pH 8.0	5	50 mM
0.5 M EDTA, autoclaved	2	10 mM
10 % SDS, autoclaved	8	0.8 %
ddH$_2$O, autoclaved	85	-

Stored at RT

3.2.1.2 Procedure

100 ml-cultures were inoculated to an OD$_{600}$ of 0.03 to 0.1 from freshly grown plates and harvested at an OD$_{600}$ of 0.4-0.8 (14-16 hrs at 30ºC). The chromatin was cross-linked with formaldehyde for 10 min at a final concentration of 1% (stock is 37%) with occasional mixing. The cross-linking reaction was quenched by adding 2.5 M glycine (Table 21) to a final conc. of 125 mM and incubating for 10 min with occasional mixing. The cells were centrifuged for 5 min at 700xg at 4°C and the pellets resuspended in 25 ml ice-cold PBS (see Table 20) and the aliquots pooled. The cells were washed

again with 50 ml PBS, resuspended in 1 ml ice-cold PBS. to 1.5-ml screw-cap tubes, pelleted, and frozen pellets in liquid nitrogen to be stored at -80ºC.

The frozen cell pellets were resuspended in 500 µl of ice-cold lysis buffer (Table 22) with Protease Inhibitors (1 mM AEBSF, 100 µg/ml Leupeptin, 400 µl/10 ml lysis buffer of a 1 pill/2 ml resuspension of Roche complete protease inhibitor cocktail). Approximately 500 µl of zirconia beads were added and the cells broken up in a *Precyllis 24* (*Peqlab*) for 4x 30 s (program 1: 6,800) with 5 min rest on ice. The lysate was extracted by puncturing the bottoms of the tubes with a hot 30-gauge needle and placing the tubes in 2-ml microtubes. These were spun at 700xg and 4°C for 3 min. To separate the zirconia beads from the lysates, the bottoms of the tubes were punctured with a hot 22-gauge needle and inserted into 2-ml micro tubes. These were centrifuged at 700xg for 3 min. The lysates including debris were transferred to polystyrene sonicaton tubes (*Active Motif Inc.*) and sheered using a Q800R1 sonicator (*QSonica*) with the settings: 30 min, 30-sec on /off cycles, 90% amplitude. After sonication the lysate was transferred into a new tube and spun down for 10 min at 16,00xg and the supernatant transferred. The step was repeated again, and the cleared lysate diluted in a final volume 540 µl lysis buffer with inhibitors. 40 µl of lysate were treated with 160 µl of TE/1% SDS solution (Table 26) as "Input DNA" sample and stored at -20ºC. 2 µg of the following antibodies was used per IP (source, identifier, and cell lysates corresponding to different amounts of OD_{600} in brackets): αFLAG to target FLAG-Pdp3 (*Sigma-Aldrich*, F3165; 30 ODs); αH3K14ac (*Abcam plc,* ab52946, 10 ODs); αH3K36me3 (*Abcam plc,* ab9050, 5 ODs); αH3 (*Active Motif Inc.*, 61475, 5 ODs); αH3K9me[2] (*Abcam plc*, ab1220, 15 ODs). For ChIP experiments targeting Mst2-FLAG, 4 µg of αFLAG and volume of cell lysate corresponding to 50 ODs were used. The IPs with their respective antibody were transferred to a nutator in the cold room and incubated with αFLAG for 4 h and/or for a minimum of 1.5 h with all histone and histone modification antibodies.

The cross-linked DNA was immunoprecipitated with 25 µl Dynabeads Protein G (*Life Technologies™). To this end, the beads were washed twice with 10x the total bead volume of PBS + 1% Tween20 and resuspended in 100 µl lysis buffer per 25 µl beads. The beads were added to the IPs and the samples incubated overnight at 4ºC while nutating. Using a magnetic bead rack the beads were then washed with 1 ml each of the following buffers (ice-cold) for 1 min each on a nutator: 2x with Lysis buffer (Table 22), 2x with high salt Lysis buffer (Table 23), 2x with Wash buffer (Table 24). Then the

beads were washed once with 150 ml TE (Table 25) and transferred to a new reaction tube and the TE removed. 200 µl Elution buffer (Table 27) were added after which the IPs and the inputs were incubated for 10 min at 95°C and max. rpm to elute. The eluted IPs were spun down shortly and transferred to new reaction tubes. The beads were discarded. The IP and "input DNA" samples were incubated for 3 h at 65ºC to abolish the crosslink.

To denature the chromatin bound proteins, 40 µg Proteinase K (10 µl of a freshly prepared 4 mg/ml solution) were added to each sample, and the samples incubated for 2x 1 hr at 55ºC with a vortexing step in between.

The IPs and inputs were cleaned with a ChIP DNA Clean & Concentrator™ kit (Zymo Research). The DNA was eluted with 50 µl elution buffer for input and 25 µl for IP'd DNA.

3.2.2   Denaturing TCA precipitation

Total proteins of exponentially growing cells of an OD_{600} 0.4 to 0.6 were extracted from 10 ml of culture by pelleting them for 5 min at 700xg. The pellets were flash-frozen in liquid nitrogen and stored at -80ºC for later extraction. The samples were resuspended in 1 ml of ice-cold ddH_2O and mix of 138.75 µl 2N NaOH and 11.25 µl β-mercaptoethanol was added to each sample. The samples were incubated on ice for 15 min with occasional vortexing. 150 µl of 55 % trichloroacetic acid (TCA) were added to each sample. The samples were incubated on ice for another 15 min with occasional mixing. The samples were centrifugated for 15 min at 4 °C and maximum speed. The supernatant was removed with a pipette, the pellet spun again for 5 min and the rest of the supernatant removed. The pellets were resuspended in 1 ml of ice-cold 100% acetone, spun down at maximum speed for 15 min and the supernatant discarded. As before the sample were spun down for another 5 min and the supernatant discarded. Fresh HU (hydroxyurea) buffer (Table 29) was warmed to 65 °C. The samples were resuspended in HU Buffer to a final concentration of 0.1 OD/µl by pipetting up down. The samples were boiled for 5 min at 65ºC before storing them at -20°C.

3.2.3 NuPAGE

3.2.3.1 Buffers

Table 28: 7x BisTris buffer

compound	amount	final concentration
BisTris (MW=209.24 g/mol) in 160 ml H_2O	104.62 g	2.5 M
37 % HCl	20 ml	1.5 M
37 % HCl, dropwise	adjust to pH 6.5-6.8	1.5 M
ddH$_2$O, autoclaved	fill up to 200 ml total volume	-

Stored at 4ºC

Table 29: HU loading buffer (10 ml)

compound	amount	final concentration
Phosphate buffer, pH 6.8	-	200 mM
urea	4.81 g	8 M
10 % SDS, autoclaved	5 ml	5 %
0.5 M EDTA, autoclaved	20 µl	1 mM EDTA
Bromphenol blue	-	-
1 M DTT	added freshly before use	100mM

Stored at -20ºC

Table 30: 20x MOPS running buffer (100 ml)

compound	volume [ml]	final concentration
1 M TRIS/HCl, pH 8.0	5	50 mM
0.5 M EDTA, autoclaved	2	10 mM
10 % SDS, autoclaved	8	0.8 %
ddH$_2$O, autoclaved	85	-

Stored at 4ºC

3.2.3.2 Procedure

NuPAGE (polyacrylamide gel electrophoresis) gels were cast and run using a Mini-PROTEAN® Tetra Handcast System (*Bio-Rad*). The gels were prepared in 50-ml conical tubes using the following recipes. The preparation of 7x BisTris buffer is found in Table 28. The resolving gel was poured into the casting chambers to the upper edge of the clamp overlay every single gel by with 500 µl isopropanol. The gels were left to polymerize for at least 2 hours. The isopropanol was drained, and chamber rinsed with deionized water. Excess water was removed with strips of Whatman paper. The stacking gel was poured onto the resolving gel and the combs added. The composition of resolving and stacking gels are noted in Table 31. The acrylamide was left to polymerize for 3 h. Remaining polyacrylamide was rinsed off with H_2O and the gels were stored overnight at 4ºC wrapped in moist paper towels inside a sealable plastic bag.

For the running, the inner and outer chamber were filled with 1x MOPS buffer (see Table 30) and a stirring rod added. 500 µl of 200x reducing agent (1 M DTT) were added to the inner (cathode) chamber (chamber volume is approximately 100 ml).

The samples were boiled for at least 5 min at 65 ºC and 0.5 ODs per sample were loaded. The gels were run at 4 W constant for 1 gel or 7 W for 2 gels for 2 h 40 min in the cold room.

Table 31: Recipe for NuPAGE gels (2 gels)

compounds	resolving gel (10 %)	stacking gel (4 %)
AA/bis	3.33 ml	1.32 ml
7x BisTris buffer	0.94 ml	0.94 ml
H_2O	5.66 ml	7.68 ml
TEMED	20 µl	20 µl
APS	40 µl	40 µl

3.2.4 Western blot

3.2.4.1 Buffers

Table 32: 10x Transfer buffer for WB (1 l)

compound	amount	final concentration
TRIS/HCl	24.2 g	50 mM
glycine	112.6 g	10 mM
SDS	8 g	28 mM
ddH$_2$O, autoclaved	up to 1l	-

Stored at RT

Table 33: 1x Transfer buffer for WB (1 l)

compound	volume [ml]	final concentration
10x Transfer buffer	100	1x
100% methanol	200	20%
ddH$_2$O, autoclaved	700	-

Stored at 4ºC

Table 34: 10x TBS for anti-FLAG immunoblotting

compound	amount	final concentration
TRIS/HCl, pH 8.0	60.6 g	0.5 M
NaCl	80.7 g	1.38 M
KCl	2.0 g	27 mM
ddH$_2$O, autoclaved	up to 1 l	-

Stored at RT

3.2.4.2 Procedure

The proteins were blotted onto an Immobilon-P PVDF (polyvinylidene fluoride) membrane (*Millipore*) using semidry blotting for 1h at 250 mA and room temperature (for buffer see Table 33). The membranes were blocked with 3 % Milk in TBS (see

Table 34) and incubated with anti-αFLAG (*Sigma*, F3165, 1:1,000) and goat anti-mouse IgG (H + L)-HRP conjugate (*Bio-Rad*, #1706516, 1:10'000) according to the manual for the αFLAG antibody though incubation with αFLAG occurred overnight at 4ºC on a nutator. The antibody was detected using Immobilon HRP substrate (Millipore) on a Fusion FX Vilber Lourmat CCD camera (~ 5 min).

3.3 Molecular biological methods

3.3.1 Reverse transcription

The strains were woken up on YES and grown at 30°C for 3 days. Streaks from these freshly grown plates were used for a maximum of 4 days to inoculate 50 ml YES liquid medium to a starting OD_{600} of 0.02 to 0.08 depending on the individual strain. The cultures were grown 14-16 hours at 30ºC and 150 rpm. The cells were harvested at an OD_{600} of 0.4 - 0.8, transferred to 50 ml conical tubes and centrifuged at 700xg for 5 min, the cell pellets washed once with 50 ml ice-cold H_2O, transferred to 1.5 screw cap tubes, spun down at maximum speed for 14 s in a tabletop centrifuge. The pellets were flash frozen in liquid N_2 and stored at -80ºC.

For RNA extraction, the pellets were thawed by resuspending them in 1 ml ice-cold TRIzol. 250 µl zirconia beads were added and the cells broken up in a *Precyllis 24* (Peqlab) for 3x30 s (program 1:6800) with 5 min rest on ice. The tubes were centrifuged at 12,000xg at 4ºC for 10 min and the cleared lysate moved a new 1.5-ml micro tube and immediately mixed after adding 200 µl chloroform. The mix incubated at room temperature for 10 min, and spun at 12,000xg at 4ºC for 10 min. The aqueous phase was treated with another 500 µl of chloroform, briefly vortexed and spun at 12,000xg at 4ºC for 10 min. The aqueous phase was extracted, treated with 500 µl isopropanol, mixed and incubated on ice for 15 min to precipitate all nucleic acids. The nucleic acids were pelleted by centrifugation (5 min, 12,000xg) and washed by resuspending the pellet twice in 1 ml of RNAse-free 70 % ethanol. The supernatant was removed with a pipette, and the pellets were carefully dried without heat in a Speedvac RVC 2-25 (*Christ*). The pellets were then resuspended in 60 µl RNase-free H_2O and incubated at 55ºC for 30 min to make sure that the RNA/DNA mix was totally dissolved.

Directly before the next step the RNA yield was determined using a Nanodrop 2000. 20 µg of RNA mix was treated with a *TURBO DNA-free™* kit (*Ambion*) mostly following the manufacturer's instructions. However, instead of 1 µl DNAseI for 1 h, 0.5 µl TURBO

DNA-free DNaseI were pipetted into each sample and the samples were incubated at 37ºC for 30 min, before repeating the procedure. DNaseI was inactivated by adding 6 µl of TURBO DNase inactivation reagent and incubating the samples at room temperature for 10 min, occasionally resuspending the beads by vortexing them shortly. The samples were spun down according to the manufacturer's instructions and 35 µl of supernatant were transferred to a fresh tube (~15 ug RNA).

The cDNA was synthesized using SuperScript™ III Reverse Transcriptase (*Invitrogen*). 5 µg total RNA (i.e. 11 µl of the TURBO DNase treatment reaction) were mixed with 1 µl of oligo-(dT)$_{20}$ primers (50 µM) and 1 µl of 10 mM dNTP mix and heated to inactivate any residual DNaseI (Table 36, top half). A master mix was prepared for the other reaction components (see Table 35) of which 7 µl were added to each sample and the RNA transcribed to cDNA (Table 36, bottom half):

Table 35: reaction mix for one RT reaction

components	volume
5x first strand buffer	4 µl
0.1 M DTT	1 µl
RNAseIN	1 µl
SuperScript III	0.25 µl
RNAse-free H$_2$O	0.75 µl

Table 36: Program for reverse transcription

step	duration
Heat lid to 110.0 ºC	-
Pause at 70.0 ºC	-
70 ºC	10 min
Pause at 8.0 ºC	-
50 ºC	1 h
70 ºC	15 min
Store forever at 8 ºC	

3.3.2 DNA isolation

3.3.2.1 Isolation of plasmid DNA from *E. coli*

For minipreps, plasmid was extracted from 1 ml of culture using a mi-Plasmid Miniprep Kit (*metabion*) according to instructions. For maxipreps, cells were grown in 50 ml medium, harvested, and the plasmid extracted with the vacuum method of the PureYield™ Plasmid Midiprep System (*Promega*). The plasmid was eluted with 500 ml of 55ºC ddH$_2$O and stored at -20ºC.

3.3.2.2 Isolation of *S. pombe* DNA with Zymolyase

A pipet tip of solid yeast culture was resuspended in 15µl of Zymolyase solution (2.5 mg/ml in 0.1 M sodium phosphate buffer, pH 7.5) in either 8-strips or 96-well plates. This was incubated in a PCR machine first at 37ºC for 20 min and then at 95ªC for 5 min. The supernatant was used as template for diagnostic PCR (3.3.3.2). To this end, the Zymolyase prep was diluted 1:10 by addition of 135 µl of ddH$_2$O, mixed through

inversion and spun down to pellet cell debris to clear the supernatant. The supernatant was used for a maximum of two days before discarding.

3.3.2.3 Isolation of crude DNA from yeast

For *S. pombe*, strains were patched onto a YES (yeast extract containing supplements) media plate containing the antibiotics in case of a null mutant strain or a tagged strain. After 3 days of incubation at 30°C the genomic DNA was extracted. For *S. cerevisae*, this method was used to extract DNA of 1/3 of the cells from transformants generated in section 3.1.2.4. The cells were resuspended in 200 µl of breaking buffer (Table 37) after which 200 µl of zirconia beads and 200 µl equilibrated phenol were added. The cells were lysed by vortexing for 2-5 min after which 200 µl water were added. The organic and aqueous phases were separated in a microfuge at top speed for 5 min. 350 µl of supernatant were mixed with 1 ml of ice-cold 100% ethanol via vortexing to precipitate the DNA and spun at top speed for 10 min. The supernatant was discarded, the pellet washed with 500 µl of ice-cold 70% ethanol and spun at top speed for 5 min. Lastly, the pellet was first dried in a speedvac (37°C, 5 min), the resuspended in 50 µl Tris, pH 7.5 for longer stability during storage and stored at -20°C when not in use.

Table 37: Breaking buffer (100 ml)

compound	volume [ml]	final concentration
10 %Triton X-100	20	2 % (v/v)
10 % Sodium dodecyl sulphate (SDS), autoclaved	10	1 % (v/v)
1 M TRIS/HCl (pH 8.0), autoclaved	1	10 mM
0.5 M EDTA (pH 8.0), autoclaved	2	1 mM
5 M NaCl, autoclaved	2	100 mM
ddH$_2$O, autoclaved	62	-

Stored at RT

3.3.2.4 Isolation of high purity DNA from *S. pombe*

To procure DNA template of high purity for the amplification of DNA fragments for plasmid generation in S. cerevisiae, S. pombe DNA was purified from solid culture according to protocol using the Yeast DNA Extraction Kit (*Thermo Scientific™*) and resuspended in 50 µl of 10 mM Tris, pH 7.5. The DNA was stored at -20ºC.

3.3.3 Polymerase chain reaction

3.3.3.1 Primer preparation

All primers used in this study were produced by *metabion*. The 100 µM stocks were resuspended in 10 mM Tris, pH 7.5 to 8.0. Any further dilutions specified in the methods were prepared in autoclaved ddH$_2$O. All stocks were stored at -20 ºC.

3.3.3.2 Diagnostic PCR

Diagnostic PCRs were used to test the presence or insertion of deletion cassettes and of mutant constructs at the correct locus in *S. pombe* cells. To this end flanking PCRs of the 5' and 3' junction of the locus was conducted. For deletion cassettes, primer pairs consisted of the 5' or 3' junction specific Chk primer and a respective reverse or forward primer annealing to the resistance cassette. This was used for testing *Bioneer* library mutants and transformations of deletion cassettes. The ORF primers were used as a control for loss of the coding region.

For the Mst2-FLAG strain, the selection marker was inserted after the FLAG tag. A pairing of 5' Chk primer and the reverse ORF primer was used for the 5' junction and the 3' junction was tested with a primer pair consisting of a forward primer annealing to natMX and the 3' Chk primer. For the FLAG-Pdp3 strains the selection marker was inserted before the gene and the FLAG tag. The junction primers consisted of the of Chk primer and natMX-internal reverse primer for the 5' junction and a Pdp3 internal forward primer (pdp3_seq_4) and the Chk primer for the 3' junction. The reactions were prepared according to Table 38 using Zymolyase preps (chapter 3.3.2.2) as template. The PCRs were performed in a peqSTAR 96X HPL using a 2xFAST PCR Kit (both *PEQLAB Biotechnologie GMBH*). The preparations and PCR products were discarded after successful amplification.

Table 38: Reaction mix for diagnostic PCR

solution	volume [µl]
2xFAST (*PEQLAB Biotechnologie GMBH*)	4
DNA template (1:10 dilution)	2
primer for/rev mix (1 µM)	2

Table 39: PCR program for 1.5 kb amplicons

step	duration
Heat lid to 110.0 ºC	-
Pause at 95.0 ºC	-
95 ºC	3 min
Start loop, 30x	
95 ºC	15 s
48 ºC	15 s
72 ºC	15 – 45 s depending on amplicon length
Close loop	
72 ºC	30 s
Store forever at 8 ºC	

Table 40: Primers utilized for diagnostic PCR.

oligo no	name	gene	for rev	total sequence	source
Sg739	MX6-1 (5' junction)	*kan*	rev	GCACGTCAAGACTGTCAAGG	Braun Lab
Sg780	NatR_Rev(5'junction)	*nat*	rev	AGCCGTGTCGTCAAGAGTGG	Braun Lab
Sg781	NatR_For(3'junction)	*nat*	for	CGCTCTACATGAGCATGC	Braun Lab
Sg909	SPCC24B10.18_WT_int_F	*SPCC24B10.18*	for	GCTGCAACTGTCAAATATTCGGTG	Braun Lab
Sg910	SPCC24B10.18_WT_int_R	*SPCC24B10.18*	rev	AACGACTCAATGCTTTCCCTCCTT	Braun Lab
Sg915	SPAC23D3.01_WT_int_F	*pdp3*[+]	for	ACAATTAGCGTATGTTCCGAGGAC	Braun Lab
Sg916	SPAC23D3.01_WT_int_R	*pdp3*[+]	rev	GGTCGTTGCTTCGATGTTTGAGAA	Braun Lab
Sg969	ura4-ORF-F	*ura4*	for	GCTAGAGCTGAGGGGATGAA	Braun Lab
Sg970	ura4-ORF-R	*ura4*	rev	CCCGTCTCCTTTAACATCCA	Braun Lab
Sg1262	mst2_Chk_F	*mst2*[+]	for	CAACAACAAGAGTGTTTCAGAGGA	this study
Sg1263	mst2_Chk_R	*mst2*[+]	rev	CTAAATTACCTCCAAAGCACCCGT	this study
Sg1266	mst2_WTint_F	*mst2*[+]	for	TGGGTCTATTAACTAAAGGGCAAG	this study
Sg1267	mst2_WTint_R	*mst2*[+]	rev	TTGCCGTTGACCATCAACTTCAAA	this study
Sg1268	eaf6_Chk_F	*eaf6*[+]	for	CAGAAGATTTCCACCAGCAAAGAT	this study
Sg1269	eaf6_Chk_R	*eaf6*[+]	rev	GGGTGATGACTTTGGATTTGTAAC	this study
Sg1272	eaf6_WTint_F	*eaf6*[+]	for	AAGCGACAATTGTTGGAAACTTCG	this study
Sg1273	eaf6_WTint_R	*eaf6*[+]	rev	GGTTGATTAAATGATGCTAGCGCA	this study
Sg1274	nto1_Chk_F	*nto1*[+]	for	GGTCATAACCCTATGTATTCCGAA	this study
Sg1275	nto1_Chk_R	*nto1*[+]	rev	CATCACCTGAAGTGAAATCGAAGA	this study
Sg1278	nto1_WTint_F	*nto1*[+]	for	CCAGACCTACAAATAGACGAACCT	this study
Sg1279	nto1_WTint_R	*nto1*[+]	rev	GAACAGAAGTGTTACAGTTATCGC	this study
Sg1280	tfg3_Chk_F	*tfg3*[+]	for	GGGATAAACTCTTACCTCTGCATA	this study
Sg1281	tfg3_Chk_R	*tfg3*[+]	rev	TATCCCGGTCAAGTTTGCAGGAAA	this study
Sg1284	tfg3_WTint_F	*tfg3*[+]	for	ACTTTGGCATTATACAGGATGCTC	this study
Sg1285	tfg3_WTint_R	*tfg3*[+]	rev	CTGGCCTAGTAGCATTGATATTCT	this study
Sg1286	ptf1_Chk_F	*ptf1*[+]	for	ACAATACCTACACTCAGTTGCTAC	this study
Sg1287	ptf1_Chk_R	*ptf1*[+]	rev	TGGGGAGTTAGGTGAAGAAAGAAA	this study
Sg1290	ptf1_WTint_F	*ptf1*[+]	for	ATTACACTCCAGGATTCCAATGAC	this study
Sg1291	ptf1_WTint_R	*ptf1*[+]	rev	CCACTTGAAAGGATGATTACACGA	this study
Sg1292	ptf2_Chk_F	*ptf2*[+]	for	CCCATCATTCGCATTGTAAACTAC	this study
Sg1293	ptf2_Chk_R	*ptf2*[+]	rev	GACACTGAGTGTATGGTATTGTAC	this study

oligo no	name	gene	for rev	total sequence	source
Sg1296	ptf2_WTint_F	*ptf2+*	for	AATTTAAATACCGCTGCCAGGTTG	this study
Sg1297	ptf2_WTint_R	*ptf2+*	rev	GGAGAAATAAACCTTGGGGAGTAA	this study
Sg1663	set2_chk_F	*set2+*	for	AGCACGCTGACTGCCTCACTCAAA	this study
Sg1664	set2_Chk_R	*set2+*	rev	GGGTATTAACTTAACTGCCGCTGA	this study
Sg1665	set2_WT_int_F	*set2+*	for	GTCGGTTCATCACCATCTTCTTCG	this study
Sg1666	set2_WT_int_R	*set2+*	rev	CTCACTATCGTATTGTCGCATACG	this study
Sg1824	clr3_Chk_F	*clr3+*	for	GGTTGATGAGCTATTAACCCTCTA	Braun Lab
Sg1825	clr3_Chk_R	*clr3+*	rev	ATCTCACGTGCTAACCATTACACC	Braun Lab
Sg1828	clr3_WTint_F	*clr3+*	for	ATAACGAATCCCATGAAATGTCGC	Braun Lab
Sg1829	clr3_WTint_R	*clr3+*	rev	CTTGCGGTTACAGAAACATTGTTG	Braun Lab

3.3.3.3 PCR for the amplification of deletion cassettes

Deletion cassettes were amplified using the KAPA2G Robust PCR Kit (*PEQLAB Biotechnologie GMBH*) from relatively crude DNA samples (see chapter 3.3.2.3). The PCRs were performed in a peqSTAR 96X HPL (*PEQLAB Biotechnologie GMBH*). The reaction mix and program are listed below (Table 41 and Table 42). The KAPA B buffer was always used in conjunction with Enhancer. For templates problematic in amplification, GC buffer was employed instead of KAPA B and Enhancer. The cassettes were amplified using KO primers (see Table 43). The PCR products were directly used without further purification.

Table 41: Reaction mix for 50 µl KAPA2G Robust PCR

solution	volume [µl]
ddH2O, autoclaved	26
5x KAPA B	10
5x Enhancer	10
dNTPs	1
primer for/rev mix (10 µM)	1
DNA template (1:10 dilution)	1
KAPA2G Robust	1

Table 42: PCR program for KAPA2G Robust

step	duration
Heat lid to 110.0 ºC	-
Pause at 95.0 ºC	-
95 ºC	3'
Start loop, 35x	
95 ºC	15 s
50 ºC	15 s
72 ºC	2,5 – 3 min depending on amplicon length
Close loop	
72 ºC	5 min
Store forever at 8 ºC	

Table 43: Primers to amplify deletion cassettes.

oligo no	name	gene	for rev	total sequence	source
Sg911	SPAC23D3.01_KO_F	$pdp3^+$	for	GCACGAAGCCTTTCTATTTCCACA	Braun Lab
Sg912	SPAC23D3.01_KO_R	$pdp3^+$	rev	CCAGGAGAGCCATAAAACAACATG	Braun Lab
Sg1264	mst2_KO_F	$mst2^+$	for	TGCTGCTTCCTTTGCATTCTTACA	this study
Sg1265	mst2_KO_R	$mst2^+$	rev	CTATAGGAAATGAACTTCTTCCCC	this study
Sg1270	eaf6_KO_F	$eaf6^+$	for	GTCAATTGAGACGAGCTCTTTGAT	this study
Sg1271	eaf6_KO_R	$eaf6^+$	rev	GAACCGGGCCAAGCCCGATGTGGA	this study
Sg1276	nto1_KO_F	$nto1^+$	for	TAGGTAAACTCTAGAGGCCCATTT	this study
Sg1277	nto1_KO_R	$nto1^+$	rev	GCTTCCTTAGCTATCCCACTTATT	this study
Sg1282	tfg3_KO_F	$tfg3^+$	for	GTGCTCGAGGGTTTGTTTACTATA	this study
Sg1283	tfg3_KO_R	$tfg3^+$	rev	GGCAGAATACTTCTCAAAGGCTAA	this study
Sg1288	ptf1_KO_F	$ptf1^+$	for	ACGAAACTGCGTAGCTAACATTAG	this study
Sg1289	ptf1_KO_R	$ptf1^+$	rev	GGTATGGTAGTAGACAGGATACAT	this study
Sg1294	ptf2_KO_F	$ptf2^+$	for	CTTATTGACTCAAACCGGGATTGA	this study
Sg1295	ptf2_KO_R	$ptf2^+$	rev	CACAACCGAAGTGCGTTTAATGTA	this study
Sg1661	set2_KO_R	$set2^+$	for	GCTACATAAGGCGCCGAGTGTAAA	this study
Sg1662	set2_KO_R	$set2^+$	rev	GTGGAACCATTGAAGAACGGATTG	this study
Sg1826	clr3_KO_F	$clr3^+$	for	CGTTCTTCCTACATCTTGATCCTT	Braun Lab
Sg1827	clr3_KO_R	$clr3^+$	rev	GCTAACCATTACACCATACAACCA	Braun Lab

3.3.3.4 PCR to amplify fragments for homologous recombination in *S. cerevisiae*

Fragments for construct generation were generated using a KAPA HiFi PCR Kit (HiFi = high fidelity) in a peqSTAR 96X HPL (both *PEQLAB Biotechnologie GMBH*). The primers utilized are documented in Table 46. The fragments were amplified from DNA purified by Kit (see chapter 3.3.2.4) to further reduce the possibility of mutations. The *natMX6* cassette containing a resistance against nourseothricin (NAT) was amplified from pFA6a-natMX6. One µl per product was diluted in H_2O, mixed with 6x Orange G buffer and loaded a gel for testing. PCR products were purified according to sections 3.3.4.3 and 3.3.4.4.

Table 44: Reaction mix for 50 µl PCR reaction

solution	volume [µl]
ddH2O, autoclaved	31.5
5x Buffer	10
dNTPs	1.5
primer for/rev mix (10 µM)	5
DNA template (1:10 dilution)	1
KAPA2G HiFi	1

Table 45: PCR program for 1.5 kb amplicons

step	duration
Heat lid to 110.0 ºC	-
Pause at 95.0 ºC	-
95 ºC	3 min
Start loop, 35x	
98 ºC	20 s
55 ºC	15 s
72 ºC	1 min per kb
Close loop	
72 ºC	10 min
Store forever at 8 ºC	

Table 46: Fragment primers for homologous recombination in *S. cerevisiae*

oligo no	name	gene	for rev	total sequence	source
1467	pRS_mst2_F	*mst2+*	for	TTGGGTACCGGGCCCCCCCTCGAG GTCGACGGTATCGATAAGCTTGATA TCGGTTTAAACGCTGCTTCCTTTGC ATTCTT	this study
1468	mst2_FLAG_R	*mst2+*	rev	TCCATCTTCTCTTAGAACCAGAACCA ACGGAATCCAGATGATGAGAGTTA	this study
1469	mst2_FLAG_F	*mst2+*	for	TAACTCTCATCATCTGGATTCCGTTG GTTCTGGTTCTAAGAGAAGATGGA	this study
1470	FLAG_pTEF1_R	*C-terminal FLAG*	rev	GGAGGGTATTCTGGGCCTCCATGTC GCTGGCCGGGTGACCCGGCGGGG AC	this study
1471	FLAG_pTEF1_F	*C-terminal FLAG*	for	GTCCCCGCCGGGTCACCCGGCCAG CGACATGGAGGCCCAGAATACCCTC C	this study
1472	tTEF1_mst2_R	*mst2+*	rev	AGATTAAAATACTTATTTATTTGAAC AGTATAGCGACCAGCATTCACATA	this study
1473	tTEF1_mst2_F	*mst2+*	for	TATGTGAATGCTGGTCGCTATACTG TTCAAATAAATAAGTATTTTAATCT	this study
1474	mst2_pRS_R	*mst2+*	rev	ACCGCGGTGGCGGCCGCTCTAGAA CTAGTGGATCCCCCGGGCTGCAGG AATTGTTTAAACAAATGAACTTCTTC CCCTTT	this study
1478	pdp3_tTEF1_R	*pdp3+*	rev	AGAATCTTTTTATTGTCAGTACTGAT TAGGTAGTGATGACAGATGGTCTG	this study
1479	pdp3_tTEF1_F	*pdp3+*	for	CAGACCATCTGTCATCACTACCTAAT CAGTACTGACAATAAAAAGATTCT	this study
1491	pdp3_pRS_R	*pdp3+*	rev	ACCGCGGTGGCGGCCGCTCTAGAA CTAGTGGATCCCCCGGGCTGCAGG AATTGTTTAAACAGCCATAAAACAAC ATGTGA	this study
1496	Pdp3_A_mt2_R	*pdp3+*	rev	AATAGCGTAATCTCTTGAAGGAAGT GCCTGAACAAATATTCCATTGTCCA	this study
1497	Pdp3_A_mt2_F	*pdp3+*	for	TGGACAATGGAATATTTGTTCAGGC ACTTCCTTCAAGAGATTACGCTATT	this study
1863	FLAG-Pdp3_F5_F	CBP-FLAG cassette	for	TAAAGATGACGATGACAAGGGGTCA GGGTCAGTTGCTAGGACACGCAGT C	this study
1864	FLAG-Pdp3_F1_F	*pdp3+*	for	TTGGGTACCGGGCCCCCCCTCGAG GTCGACGGTATCGATAAGCTTGATA TCGGTTTAAACGTCATATTCTTCTTT TGGGT	this study
1867	FLAG-Pdp3_F2_R	natMX	rev	TATCCTTATAAAATGTTCAAAATGGC AGTATAGCGACCAGCATTCACATA	this study
1868	FLAG-Pdp3_F3_F	*pdp3+*	for	TATGTGAATGCTGGTCGCTATACTG CCATTTTGAACATTTTATAAGGATA	this study
1869	FLAG-Pdp3_F3_R	*pdp3+*	rev	AAATTCTTTTTCCATCTTCTCTTCATC GTTAATTACATTCCTTATAAGCC	this study

oligo no	name	gene	for rev	total sequence	source
1870	FLAG-Pdp3_F4_F	*pdp3*+	for	GGCTTATAAGGAATGTAATTAACGAT GAAGAGAAGATGGAAAAAGAATTT	this study
1871	FLAG-Pdp3_F4_R	*pdp3*+	rev	GACTGCGTGTCCTAGCAACTGACCC TGACCCCTTGTCATCGTCATCTTTA	this study
1972	FLAG-Pdp3_c_1_R	*pdp3*+	rev	AGGAGGGTATTCTGGGCCTCCATGT CGTTAATTACATTCCTTATAAGCCA	this study
1973	FLAG-Pdp3_c_2_F	natMX	for	TGGCTTATAAGGAATGTAATTAACGA CATGGAGGCCCAGAATACCCTCCT	this study

3.3.3.5 Quantitative PCR (qPCR)

The DNA gained from ChIP and RT experiments were quantified by PCR using 2x PowerUp™ SYBR® Green Master Mix (*Life Technologies™*) and a 7500 Fast Real-Time PCR System (*Applied Biosystems*). The reaction set-up is shown in Table 47.

Table 47: qPCR reaction set-up

components	volume
2x PowerUp™ SYBR® Green Master Mix	4 µl
FOR/REV primer mix	1 µl
cDNA	1 µl

Samples of RT experiments were diluted 1:25 for heterochromatic genes (e.g. the *ura4*+ reporter gene or the *dg repeats*); for euchromatic genes (e.g. *act1*+) they were diluted 1:2000. The qPCR primers used are listed below in Table 48.

Table 48: Primers used for RT-qPCR

oligo no	name	gene	for/rev	total sequence	source
Sg1020	cen-dg_F	*dg repeats*	for	TGCTCTGACTTGGCTTGTCTT	Braun Lab
Sg1021	cen-dg_R	*dg repeats*	rev	CCCTAACTTGGAAAGGCACA	Braun Lab
1022	cen-dh-F	*dh repeats*	for	TGAATCGTGTCACTCAACCC	Braun Lab
1023	cen-dh-R	*dh repeats*	rev	CGAAACTTTCAGATCTCGCC	Braun Lab
Sg1026	ura4_3'-F	*ura4*+	for	CAGCAATATCGTACTCCTGAA	Braun Lab
Sg1027	ura4_3'-R	*ura4*+	rev	ATGCTGAGAAAGTCTTTGCTG	Braun Lab
Sg1030	*act1*+ (V) forward	*act1*	for	AACCCTCAGCTTTGGGTCTT	this study
Sg1031	*act1*+ (V) reverse	*act1*	rev	TTTGCATACGATCGGCAATA	this study
Sg2940	tlh1-6_F (T4-1_F)	*tlh1/2*+	for	TGCCCCGTACGCTTATCTAC	this study
Sg2941	tlh1-6_R (T4-1_R)	*tlh1/2*+	rev	TTGCCTTTCTAGCCCATGAC	this study
Sg2942	T4-2_F	*SPAC212.09c*+	for	TCCTTCAGAAATGGCTTGCT	this study
Sg2943	T4-2_R	*SPAC212.09c*+	rev	GCATGTGTGTTATCCCGTTG	this study
Sg2944	T4-3_F	*SPAC212.08c*+	for	TAATGAGTTGCCCCGGGTAT	this study
Sg2945	T4-3_R	*SPAC212.08c*+	rev	CCGAATGGCAAGATGGTAAT	this study
Sg2946	T4-4_F	*SPAC212.12c*+	for	TGACAGCCAAAAGCCCTACT	this study
Sg2947	T4-4_R	*SPAC212.12c*+	rev	GTGGCAAGGCAGACTCATTT	this study
Sg2948	T4-5_F	*SPAC212.06c*+	for	GGCGAATGTGTATGTTGTGC	this study
Sg2949	T4-5_R	*SPAC212.06c*+	rev	ACTGCTACTCCCTGGCTGTG	this study

For ChIP experiments, qPCR was performed with 1:100 dilutions of both inputs and IPs. The primers used are noted in Table 49.

Table 50, and Table 51. The quantification and analysis of the readout is described in section 3.4.2.

Table 49: Tiled arrays for high resolution profiling of euchromatin

oligo no	name	gene	for/ rev	total sequence	source
Sg1742	mitoDNA_qPCR_F	mitochondrial DNA	for	ACCAGTACACGAACACGCATT	this study
Sg1743	mitoDNA_qPCR_R	mitochondrial DNA	rev	ATCCTTCAATCTCCCTCTCCA	this study
Sg2670	*ade2*+ forward	*ade2*+	for	AGGCATCTGATCCCAATGAG	Braun Lab
Sg2671	*ade2*+ reverse	*ade2*+	rev	ATTTTGGATGCCTTGGATGA	Braun Lab
Sg2736	*tef3*+ forward	*tef3*+	for	TGGCCTTCTTAGCCTTTTCA	Braun Lab
Sg2737	*tef3*+ reverse	*tef3*+	rev	CTGAGGAAGTTTGGGCTGTC	Braun Lab
Sg2864	mto1 downstream_F	*mto1*+	for	TTCCCAGAACCCGGTGTTTG	this study
Sg2865	mto1 downstream_R	*mto1*+	rev	TCCCAAGTGAATTGCTTTTTCCA	this study
Sg2866	mto1 3'-UTR_F	*mto1*+	for	CTGGATAGTTTGCGGTTGAAGT	this study
Sg2867	mto1 3'-UTR_R	*mto1*+	rev	TCAGGGAGATACAAACACCAAA	this study
Sg2868	mto1-6_F	*mto1*+	for	CAAGGGCTTCAAAACGCGTT	this study
Sg2869	mto1-6_R	*mto1*+	rev	TACGACCTTCTTGCTCAGCC	this study
Sg2870	mto1-5_F	*mto1*+	for	CCCACTGCTCGGTTAACCAT	this study
Sg2871	mto1-5_R	*mto1*+	rev	GGATCGTCTTTCCGCATCCA	this study
Sg2872	mto1-4_F	*mto1*+	for	GGACTGAAGCAGAGCGTGAA	this study
Sg2873	mto1-4_R	*mto1*+	rev	AAGTTTGCAGCCGCTTTTGT	this study
Sg2874	mto1-2/3_F	*mto1*+	for	CCACGATCAGGAGGTTCAAGA	this study
Sg2875	mto1-2/3_R	*mto1*+	rev	ATTAGGTTTGAAGGGGCCGG	this study
Sg2876	mto1-2_F	*mto1*+	for	ACATTCTCAAGATGCCCCCA	this study
Sg2877	mto1-2_R	*mto1*+	rev	AAAGTTAAGGAGGAGCCGGG	this study
Sg2878	mto1 5'-UTR_F	*mto1*+	for	GCGTCAAGTAGAGACAGCCA	this study
Sg2879	mto1 5'-UTR_R	*mto1*+	rev	AGCAAATCCAAAGCAGTAGGC	this study
Sg2880	mto1-tef3 1_F	*mto1*+ *tef3*+	for	TCCGCTACGATTATGCTTGAGT	this study
Sg2881	mto1-tef3 1_R	*mto1*+ *tef3*+	rev	CCGTTGCGATTGAAATCATCGA	this study
Sg2882	mto1-tef3 2_F	*mto1*+ *tef3*+	for	ACTTGGCATCATCACTCGCT	this study
Sg2883	mto1-tef3 2_R	*mto1*+ *tef3*+	rev	GATATTCAGCGTTGTGTATCGCA	this study
Sg2884	mto1-tef3 3_F	*mto1*+ *tef3*+	for	CGCGAATGAACTCATAAACGGA	this study
Sg2885	mto1-tef3 3_R	*mto1*+ *tef3*+	rev	AGGGTCGGCATAATCGCATT	this study
Sg2886	tef3 5'-UTR_F	*tef3*+	for	TGGCCACCACCAAGAAGAAA	this study
Sg2887	tef3 5'-UTR_R	*tef3*+	rev	GACATCCCGGGGAAATGGTT	this study
Sg2888	tef3-1_F	*tef3*+	for	TGTCGAGCCTTACTTGGTCG	this study
Sg2889	tef3-1_R	*tef3*+	rev	CCAGTGGTGTGGATGGACTC	this study
Sg2890	tef3-2_F	*tef3*+	for	GAATGAGCGTTCCACTCCCA	this study
Sg2891	tef3-2_R	*tef3*+	rev	GTGGTGATGGCACGTTGAAC	this study
Sg2892	tef3-3_F	*tef3*+	for	TGGTGCTTCTCATGCTGAGG	this study
Sg2893	tef3-3_R	*tef3*+	rev	TGGCACGCATAAGGGTAGAC	this study
Sg2894	tef3-4_F	*tef3*+	for	TGTTGCCTGGTTGGAGAACT	this study
Sg2895	tef3-4_R	*tef3*+	rev	GACTTGGCGGAAGGAACCTT	this study
Sg2896	tef3-5_F	*tef3*+	for	TATCCACAGCCGTCGTAAGC	this study

oligo no	name	gene	for/ rev	total sequence	source
Sg2897	tef3-5_R	*tef3*[+]	rev	CACTCTTCAAGGCCTCAGCA	this study
Sg2898	tef3-6_F	*tef3*[+]	for	AAGAGAAGGAGGAGGGCGAT	this study
Sg2899	tef3-6_R	*tef3*[+]	rev	ACAGCTCATCGTCACTGACC	this study
Sg2900	tef3 3'-UTR_F	*tef3*[+]	for	GGTCAGTGACGATGAGCTGT	this study
Sg2901	tef3 3'-UTR_R	*tef3*[+]	rev	ACCACATGTTAGAGTCGTATACTGG	this study
Sg2902	tef3 downstream1_F	*tef3*[+]	for	ATGAAAGGCGTTCGTCGTCC	this study
Sg2903	tef3 downstream1_R	*tef3*[+]	rev	AGCAAAGAATACCTATGCTGCA	this study
Sg2904	bub1-6_F	*bub1*[+]	for	CCACCGGCCTTGGGTTTAAT	this study
Sg2905	bub1-6_R	*bub1*[+]	rev	GCGCCCATCTTTATTGCGTG	this study
Sg2906	bub1-5_F	*bub1*[+]	for	CACTCAGAGTCTGCAACGGT	this study
Sg2907	bub1-5_R	*bub1*[+]	rev	GCGCATAATTGAAGCCCTGC	this study
Sg2908	bub1-4_F	*bub1*[+]	for	CGAACCTCCAGTGGAATGGT	this study
Sg2909	bub1-4_R	*bub1*[+]	rev	ACTTGCCAATGACGGAGGAG	this study
Sg2910	bub1-3_F	*bub1*[+]	for	ACTGCTGCTTCTTTCCCGAA	this study
Sg2911	bub1-3_R	*bub1*[+]	rev	CGGCCACAGGGTTCTTGTAA	this study
Sg2912	bub1-2_F	*bub1*[+]	for	TGCAACGTTGGAAAGAGGCT	this study
Sg2913	bub1-2_R	*bub1*[+]	rev	GAGAACTCAGCAGCGTTCCT	this study
Sg2914	bub1-1_F	*bub1*[+]	for	AACCCAGGGAGTCCAAGACT	this study
Sg2915	bub1-1_R	*bub1*[+]	rev	AAACATCCACGGGGTCATCC	this study
Sg2916	bub1-ade6 1_F	*bub1*[+] *ade6*[+]	for	TTCTGCACTTGGTTCGACGA	this study
Sg2917	bub1-ade6 1_R	*bub1*[+] *ade6*[+]	rev	ACCTTATACTGCACCAGGCTG	this study
Sg2918	ade6 5'-UTR_F	*ade6*[+]	for	TTAAGCTGAGCTGCCAAGGT	this study
Sg2919	ade6 5'-UTR_R	*ade6*[+]	rev	GACCACCTCCAAGGATCCCT	this study
Sg2920	ade6-1_F	*ade6*[+]	for	GGGCCGAATGATGGTAGAGG	this study
Sg2921	ade6-1_R	*ade6*[+]	rev	GTGCTCACGTCCTCCATCAA	this study
Sg2922	ade6-2_F	*ade6*[+]	for	ATTTTGCGATGCACCTGACC	this study
Sg2923	ade6-2_R	*ade6*[+]	rev	CGTAATTCCACGACCGTCG	this study
Sg2924	ade6-3_F	*ade6*[+]	for	CGACGGTCGTGGAAATTACG	this study
Sg2925	ade6-3_R	*ade6*[+]	rev	AAAGCGGACGATCACCAAGT	this study
Sg2926	ade6-4_F	*ade6*[+]	for	TGCAGTGATGGTAGTACGCA	this study
Sg2927	ade6-4_R	*ade6*[+]	rev	GAAGACGAGCAGGGGCATAT	this study
Sg2928	ade6-5_F	*ade6*[+]	for	CAACGAAATTGCTCCTCGGC	this study
Sg2929	ade6-5_R	*ade6*[+]	rev	ATGGCCCGTAAGTGAGCTTC	this study
Sg2930	ade6-6_F	*ade6*[+]	for	ACGTTCTCTGTCCATTCCCG	this study
Sg2931	ade6-6_R	*ade6*[+]	rev	TAACGTGTCCCATCTTGCGA	this study
Sg2932	ade6-8_F	*ade6*[+]	for	TGTCGCCACTGTTGCTATCA	this study
Sg2933	ade6-8_R	*ade6*[+]	rev	CAGCCAAAAGGGAGGGTTGA	this study
Sg2934	ade6-9_F	*ade6*[+]	for	TGGCTGCTATGGAGAGCTTT	this study
Sg2935	ade6-9_R	*ade6*[+]	rev	GTCTATGGTCGCCTATGCAGA	this study
Sg2936	ade6-vtc4 2_F	*ade6*[+] *vtc4*[+]	for	TGCTGTGAAGCAGTTGAAAGA	this study
Sg2937	ade6-vtc4 2_R	*ade6*[+] *vtc4*[+]	rev	TTGGGAACATGGTCAACGGG	this study
Sg2938	vtc4-3_F	*vtc4*[+]	for	GCCAAACATAATGCGGTCCG	this study
Sg2939	vtc4-3_R	*vtc4*[+]	rev	AACATTGGCGCTGATTGCAG	this study

Table 50: Tiled array used for profiling of constitutive HC and HC-EC boundaries

oligo no	name	gene	for/rev	total sequence	source
standard plate	sam1-3'_fwd	*sam1+*	for	CAAAACACCAGGACGAAGGT	Braun Lab
standard plate	adf1-3'_fwd	*adf1+*	for	CGGAGAAATCAGTTGCTTGG	Braun Lab
standard plate	tif51-3'_fwd	*tif51+*	for	GCGGAGACAACGGTAATGAT	Braun Lab
standard plate	sam1-3'_rev	*sam1+*	rev	ATTGCCAAATCTTTGGTTGC	Braun Lab
standard plate	adf1-3'_rev	*adf1+*	rev	CCTGAAAAGGATTGCCGTTA	Braun Lab
standard plate	tif51-3'_rev	*tif51+*	rev	CCTTCCACTCACAACATGGA	Braun Lab
HC plate	IRC-L/R_alt1	*IRC - L boundary*	for	TGTCAAGGGAAAAACCGAGA	Braun Lab
HC plate	IRC-L/R_alt2	*IRC - L boundary*	for	CCCTTGAAGTTTGCCAAAAA	Braun Lab
HC plate	ICR-L/R_alt3	*IRC - L boundary*	for	CCCGCAAAACCATAAAATGT	Braun Lab
HC plate	IRC-L4	*IRC - L boundary*	for	TCGTTAGCATTTGGCTTTGA	Braun Lab
HC plate	IRC-L2	*IRC - L boundary*	for	AACCCAAGCAGATAGACTGAAA	Braun Lab
HC plate	cen01	*cnt*	for	GCAAAGATCGAACGAGTTGTC	Braun Lab
HC plate	cen06	*cnt/imr*	for	TTACCAAATTTGTCAAACGTTAAAT	Braun Lab
HC plate	cen07	*cnt/imr*	for	TGAGGTTTTTCGTTCTTAGGG	Braun Lab
HC plate	cen08	*cnt/imr*	for	TGGACACCACTCTTGCCATA	Braun Lab
HC plate	cen10	*cnt/imr*	for	GGCATTTTGTAAGCGGAAAT	Braun Lab
HC plate	cen12	*cnt/imr*	for	CAGCTTCTTGTACTCACTCACTCA	Braun Lab
HC plate	cen16	*imr*	for	ATCACGCTTCCTTAGCATGG	Braun Lab
HC plate	cen17	*imr*	for	ACATTGCTCCGGTGATTTTC	Braun Lab
HC plate	cen18	*imr*	for	AACCACCACCATGCTCTTTT	Braun Lab
HC plate	cen19	*dg repeats/imr*	for	TGCGGTCATTTAAAGGCATA	Braun Lab
HC plate	cen20	*dg repeats*	for	CCCATGATGTCGTTGGTTAAA	Braun Lab
HC plate	cen21	*dg repeats*	for	ATTTCGCTTTGGCAAAACAT	Braun Lab
HC plate	cen22	*dg repeats*	for	TGGAACCCCTAACTTGGAAA	Braun Lab
HC plate	cen24	*dg repeats*	for	AGAAAATTTCACAACTCCGTTGAT	Braun Lab
HC plate	cen25	*dg repeats*	for	ACAACATGCAATACCGATTGT	Braun Lab
HC plate	cen26	*dg repeats*	for	GCACCGTTTTTCCAAATGTC	Braun Lab
HC plate	cen27	*dg repeats*	for	TCGGAAAATTCATCCTTCAAA	Braun Lab
HC plate	cen28	*dg repeats*	for	TGAGGTTCATGATGGGTTCA	Braun Lab
HC plate	cen29	*dg repeats*	for	CGAAGTATGACCCGAATTGC	Braun Lab
HC plate	cen30	*dg/dh repeats*	for	CGAAAATTGTGTTGTGCCAGT	Braun Lab
HC plate	cen31	*dg/dh repeats*	for	ATGCTCCGTTGCTTATCTCG	Braun Lab
HC plate	cen33	*dh repeats*	for	TTTGCATTCTTATCACTTGGATG	Braun Lab
HC plate	cen34	*dh repeats*	for	GTTTGTTTTGGGGAGACGAA	Braun Lab
HC plate	cen35	*dh repeats*	for	CCTACCGAACGTATGATTAGCA	Braun Lab
HC plate	cen36	*dh repeats*	for	CGATCGATTTCTCTTGGTTTTC	Braun Lab
HC plate	cen37	*dh repeats*	for	CCAAAGCAAATAGTCTAATGATCAAA	Braun Lab
HC plate	cen38	*dh repeats*	for	CCACCAGACCATTACAAGCA	Braun Lab
HC plate	cen39	*dh repeats*	for	CGTTGAATGTTGTTGCTTTCA	Braun Lab
HC plate	cen40	*dh repeats*	for	CATCTCGACTCGCTTGATGA	Braun Lab
HC plate	cen41	*dh repeats*	for	GTCCTGAATCTTGGCAAACAG	Braun Lab

oligo no	name	gene	for/ rev	total sequence	source
HC plate	cen42	*dh repeats*	for	GAAATGGGCAACAAGTCGAT	Braun Lab
HC plate	cen43	*dh repeats*	for	TCCACTTGGATGACAGAATCC	Braun Lab
HC plate	IRC-L/R_alt1	*IRC - R boundary*	for	TTGTCACGGTTTGGTTTTCA	Braun Lab
HC plate	IRC-L/R_alt2	*IRC - R boundary*	for	TTTTCCCTTGACAAAGCTGA	Braun Lab
HC plate	ICR-L/R_alt3	*IRC - R boundary*	for	TTGGCAAACTTCAAGGGAGT	Braun Lab
HC plate	IRC-L/R1	*IRC - R/L boundary*	for	TGCTGAATGTAACCAACATCA	Braun Lab
HC plate	IRC-R2	*IRC - R boundary*	for	GCAGTGTTTACCAACAAGCGTA	Braun Lab
Sg1787	CEN1 RB1_F (mb4719)	*IRC - R boundary*	for	ATGCGTTTGCGATTCTCTGC	Bühler Lab
HC plate	IRC-R3	*IRC - R boundary*	for	TGTGTGTCAAGCAAGAAAGC	Braun Lab
Sg1789	CEN1 RB2_F (mb4721)	*emc5+*	for	ACACTGCTTATTCTGCACATGA	Bühler Lab
Sg1791	CEN1 RB3_F (mb4509)	*rad50+*	for	AGCCAAACTACATATATTCTCTT CATCG	Bühler Lab
Sg1793	CEN1 RB4_F (mb4539)	*rad50+*	for	ACGTACATCTTCGACTAGTTTA TCCA	Bühler Lab
HC plate	IRC-L/R_alt1	*IRC - L boundary*	rev	TGAAAACCAAACCGTGACAA	Braun Lab
HC plate	IRC-L/R_alt2	*IRC - L boundary*	rev	TTTTCCCTTGACAAAGCTGA	Braun Lab
HC plate	ICR-L/R_alt3	*IRC - L boundary*	rev	TTGGCAAACTTCAAGGGAGT	Braun Lab
HC plate	IRC-L4	*IRC - L boundary*	rev	TGCCATATCGTCTTCCGTCT	Braun Lab
HC plate	IRC-L2	*IRC - L boundary*	rev	TAGGACCGAACTGCCAAAAC	Braun Lab
HC plate	cen01	*cnt*	rev	TGAAATTCCATAAACGGGCTA	Braun Lab
HC plate	cen06	*cnt/imr*	rev	TGCGTTTTCTTAGTAAAAACCT GAT	Braun Lab
HC plate	cen07	*cnt/imr*	rev	GGCAATGTCACAAAGTTTCAA	Braun Lab
HC plate	cen08	*cnt/imr*	rev	TTGCGCATCAAGTATTTTGC	Braun Lab
HC plate	cen10	*cnt/imr*	rev	TGCTTGTTTAGTGTTTGAACGA A	Braun Lab
HC plate	cen12	*cnt/imr*	rev	TCGTTCTTGCCTAGCGAAAT	Braun Lab
HC plate	cen16	*imr*	rev	TCATTCGTTGTACCAACTGCT	Braun Lab
HC plate	cen17	*imr*	rev	GGCGTGAATATTGATGTTTTGA	Braun Lab
HC plate	cen18	*imr*	rev	TCGCAACGATTTGAACTGTC	Braun Lab
HC plate	cen19	*dg repeats/imr*	rev	CTGTTGTTGAGTGCTGTGGA	Braun Lab
HC plate	cen20	*dg repeats*	rev	CATGGAGAGCGTATGTTGAAA	Braun Lab
HC plate	cen21	*dg repeats*	rev	GTTTCCCGCCCAGTAGATG	Braun Lab
HC plate	cen22	*dg repeats*	rev	TGCTCTGACTTGGCTTGTCTT	Braun Lab
HC plate	cen24	*dg repeats*	rev	AGAGTTGCCGCAATTGAAAC	Braun Lab
HC plate	cen25	*dg repeats*	rev	TCGTTATTGAAACACGAATAGG A	Braun Lab
HC plate	cen26	*dg repeats*	rev	AACCATTCGCATCCATTTTT	Braun Lab
HC plate	cen27	*dg repeats*	rev	TCAGCAATTGTTTCAGAAAATG	Braun Lab
HC plate	cen28	*dg repeats*	rev	TTCGGTCTTTGCAGGACTCT	Braun Lab
HC plate	cen29	*dg repeats*	rev	CCACGGAAAACAAATTACCG	Braun Lab
HC plate	cen30	*dg/dh repeats*	rev	CATTCATCTTGCGTGTCTGC	Braun Lab
HC plate	cen31	*dg/dh repeats*	rev	TCCTCACATTCGACATGACTG	Braun Lab
HC plate	cen33	*dh repeats*	rev	TGTCTACGTACGCCAGTTGC	Braun Lab
HC plate	cen34	*dh repeats*	rev	CGATCAAATCGGTCAGTACG	Braun Lab
HC plate	cen35	*dh repeats*	rev	TGGGATCGCAATTTTTGATT	Braun Lab
HC plate	cen36	*dh repeats*	rev	TCGCGAACATCAGCATTACT	Braun Lab
HC plate	cen37	*dh repeats*	rev	CACGGCGATAAGAAATGGA	Braun Lab

oligo no	name	gene	for/ rev	total sequence	source
HC plate	cen38	*dh repeats*	rev	CTCGCCTATTTACCGATCCA	Braun Lab
HC plate	cen39	*dh repeats*	rev	AATGACAAAGGTGCCGAATC	Braun Lab
HC plate	cen40	*dh repeats*	rev	TGGGCATTCACGAAACATAG	Braun Lab
HC plate	cen41	*dh repeats*	rev	TACAAGGACTAAGCCCAAGCA	Braun Lab
HC plate	cen42	*dh repeats*	rev	GTTGCGCAAACGAAGTTATG	Braun Lab
HC plate	cen43	*dh repeats*	rev	CAACGCATCTACCTCAGCAG	Braun Lab
HC plate	IRC-L/R_alt1	*IRC - R boundary*	rev	TGTCAAGGGAAAAACCGAGA	Braun Lab
HC plate	IRC-L/R_alt2	*IRC - R boundary*	rev	CCCTTGAAGTTTGCCAAAAA	Braun Lab
HC plate	ICR-L/R_alt3	*IRC - R boundary*	rev	CCCGCAAAACCATAAAATGT	Braun Lab
HC plate	IRC-L/R1	*IRC - R/L boundary*	rev	GCCTCAATTGCCTATTAGTGCT	Braun Lab
HC plate	IRC-R2	*IRC - R boundary*	rev	AGAGAATCGCAAACGCATCT	Braun Lab
Sg1788	CEN1 RB1_R (mb4720)	*IRC - R boundary*	rev	GTGTGAGCGCTAACTTTTGCT	Bühler Lab
HC plate	IRC-R3	*IRC - R boundary*	rev	TTCATGTGCAGAATAAGCAGTG	Braun Lab
Sg1790	CEN1 RB2_R (mb4722)	*emc5+*	rev	TGCCGCATGTGGTAAAGACA	Bühler Lab
Sg1792	CEN1 RB3_R (mb4510)	*rad50+*	rev	TTGGCAGAATGTCTAGGTGTAA ACTGTG	Bühler Lab
Sg1794	CEN1 RB4_R (mb4540)	*rad50+*	rev	CTATACTGGCTAACCAACTGAT GACATTG	Bühler Lab
TMH plate	T4-1	*tlh1/2+*	for	TTGCCTTTCTAGCCCATGAC	Braun Lab
HC plate	tel95	*tlh1/2+*	for	TCGTGGTCATAAACGCACAT	Braun Lab
HC plate	tel92	*tlh1/2+*	for	CTGCAAGGACTAAGCCCAAG	Braun Lab
HC plate	tel90	*tlh1/2+*	for	GCAACAGCCAGTCATTCATTT	Braun Lab
HC plate	tel88	subTelIIR	for	TCAAAAATGGCTTTTGTCCA	Braun Lab
TMH plate	T4-2	*SPAC212.09c+*	for	TCCTTCAGAAATGGCTTGCT	Braun Lab
HC plate	tel86	subTelIIR	for	CATACGGCAGGCTCTTTCTC	Braun Lab
TMH plate	T4-3	*SPAC212.08c+*	for	TAATGAGTTGCCCCGGGTAT	Braun Lab
TMH plate	T4-4	*SPAC212.12+*	for	TGACAGCCAAAAGCCCTACT	Braun Lab
TMH plate	T4-5	*SPAC212.06c+*	for	ACTGCTACTCCCTGGCTGTG	Braun Lab
HC plate	tel85	subTelIIR	for	GATCGAACACACACACATCG	Braun Lab
HC plate	tel83	subTelIIR(LTR)	for	CTGAGGAACGATGTTCAGTTG	Braun Lab
TMH plate	T4-6	*SPAC212.04c+*	for	AGACGTCTCCTGATGTCACAA	Braun Lab
TMH plate	T4-7	*SPAC212.01c+*	for	CACAGACGTCTCCTGGTGTC	Braun Lab
TMH plate	T5-1	*SPAC977.04+*	for	TTTTGAGGGGTCAAATGGTC	Braun Lab
TMH plate	T5-2	*SPAC977.06+*	for	TTGTAGAAGCCAATGGCAGA	Braun Lab
TMH plate	T5-3	*SPAC977.08+*	for	AAAGCAATTTCGCATTTTGG	Braun Lab
TMH plate	T4-1	*tlh1/2+*	rev	ACGTGTGGTGCAATTGTGTT	Braun Lab
HC plate	tel95	*tlh1/2+*	rev	ATACTCGGCGAAATGAATGG	Braun Lab
HC plate	tel92	*tlh1/2+*	rev	AGTCCTGAACTTTGGCAAACA	Braun Lab
HC plate	tel90	*tlh1/2+*	rev	TCACCCATGTTGAATCGAGA	Braun Lab
HC plate	tel88	subTelIIR	rev	CGCCCTTCATGTTACGAAGT	Braun Lab
TMH plate	T4-2	*SPAC212.09c+*	rev	TGCAACAGTTGGTTCTGACA	Braun Lab
HC plate	tel86	subTelIIR	rev	GGCTTTTGGCTGTCACATTT	Braun Lab
TMH plate	T4-3	*SPAC212.08c+*	rev	ATCGCTTAGCAAGGGATTTG	Braun Lab
TMH plate	T4-4	*SPAC212.12+*	rev	GGCTTTTGGCTGTCACATTT	Braun Lab
TMH plate	T4-5	*SPAC212.06c+*	rev	CGCCCTTCATGTTACGAAGT	Braun Lab
HC plate	tel85	subTelIIR	rev	ATCGCTTAGCAAGGGATTTG	Braun Lab

oligo no	name	gene	for/rev	total sequence	source
HC plate	tel83	subTelIIR(LTR)	rev	TGCAACAGTTGGTTCTGACA	Braun Lab
TMH plate	T4-6	*SPAC212.04c*[+]	rev	TCACCCATGTTGAATCGAGA	Braun Lab
TMH plate	T4-7	*SPAC212.01c*[+]	rev	AGTCCTGAACTTTGGCAAACA	Braun Lab
TMH plate	T5-1	*SPAC977.04*[+]	rev	ACGTGTGGTGCAATTGTGTT	Braun Lab
TMH plate	T5-2	*SPAC977.06*[+]	rev	TGCAACAGTTGGTTCTGACA	Braun Lab
TMH plate	T5-3	*SPAC977.08*[+]	rev	ATCGCTTAGCAAGGGATTTG	Braun Lab

HC = heterochromatin, TMH = TEL-MEI-HOOD

Table 51: Primers for mei4 array

oligo no	name	gene	for/rev	total sequence	source
Sg2222	cdk9-1_qPCR_F	*cdk9*[+]	for	GACGGGAAGGTATATGCGCT	this study
Sg2223	cdk9-1_qPCR_R	*cdk9*[+]	rev	GCAATCAAGTCGATGCGTCC	this study
Sg2224	cdk9-2_qPCR_F	*cdk9*[+]	for	TTCCGGTTCATGACTCGTGG	this study
Sg2225	cdk9-2_qPCR_R	*cdk9*[+]	rev	TTTGCTGACGCTTAGGCTGA	this study
Sg2226	cdk9 3'U_qPCR_F	*cdk9*[+]	for	TAATGGCCTTTCCGCGTGAT	this study
Sg2227	cdk9 3'U_qPCR_R	*cdk9*[+]	rev	CCGTGCTCAATTTGCTAAGGT	this study
Sg2228	mei4-1_qPCR_F	*mei4*[+]	for	AATGGCGGGCTTTGTGGATA	this study
Sg2229	mei4-1_qPCR_R	*mei4*[+]	rev	AAACGTGTTGCGAATCCACG	this study
Sg2230	mei4-2_qPCR_F	*mei4*[+]	for	CCACTACGTCCATCATCCCG	this study
Sg2231	mei4-2_qPCR_R	*mei4*[+]	rev	AGCGTAGGACTTGAAGGTGC	this study
Sg2232	mei4 3'U_qPCR_F	*mei4*[+]	for	GCCATGCATTCAACATCCCT	this study
Sg2233	mei4 3'U_qPCR_R	*mei4*[+]	rev	TGCCTGAACTCGTGACAGAG	this study
Sg2234	act1 3'U_qPCR_F	*act1*[+]	for	TGTTTCTTCTCGAGTCCGGC	this study
Sg2235	act1 3'U_qPCR_R	*act1*[+]	rev	TACATTGCACCACTTCCGCT	this study
Sg1030	act1_3'(5)-F	*act1*[+]	for	AACCCTCAGCTTTGGGTCTT	Braun Lab
Sg1031	act1_3'(5)-R	*act1*[+]	rev	TTTGCATACGATCGGCAATA	Braun Lab
Sg1028	act1_mid(4)-F	*act1*[+]	for	GATTCTCATGGAGCGTGGTT	Braun Lab
Sg1029	act1_mid(4)-R	*act1*[+]	rev	CGCTCGTTTCCGATAGTGAT	Braun Lab
Sg1878	act1-5P_F	*act1*[+]	for	AAGAAATCGCAGCGTTGGTT	this study
Sg1879	act1-5P_R	*act1*[+]	rev	AGCTTCATCACCAACGTAGGA	this study
Sg1872	act1-P1_F	*act1*[+]	for	CGTGAAGTGCTAACGCTGTG	this study
Sg1873	act1-P1_R	*act1*[+]	rev	CTGAGGTGGTATGAAGCCGT	this study

3.3.4 Molecular cloning methods

3.3.4.1 Restriction digest of plasmids

pRS416 plasmids and plasmid constructs using the pRS416 as a backbone were digested in different phases of the mutant generation process. Plasmid constructs were tested by digestion with one to two restriction enzymes that produce 3-4 fragments, which can be easily differentiated on an agarose gel (see section 3.3.4.2). The digestion reactions were set up according to Table 52.

Table 52: Set-up of plasmid digestions with restriction enzymes

compound	25 µl control digest	50 µl reaction for linearization or insert removal
enzyme	0.5 µl per enzyme!	3 µl for linearization, 1 µl PmeI for insert removal
5x Buffer	5 µl	10 µl
plasmid DNA	5 µl	5 µg
ddH2O, autoclaved	14.5 µl	37 µl-x ml plasmid for linearization, 39 µl -x µl plasmid for insert removal

The success of the linearization or insert removal was tested using 1 µl of reaction. For plasmid constructs 5 µl were used.

3.3.4.2 Agarose gel electrophoresis

PCR products and restriction digests were visualized on 0.8% agarose gels containing 0.5 µg/ml EtBr (25 ml gel, 90 V; 50 ml gels, 100 V; 200 ml gel, 125 V). The gels were prepared and run with TAE buffer (see Table 53). Unless noted otherwise the PCR products were stored at -20 C in 10 mM Tris, pH 7.5. Except for diagnostic PCR, 6x Orange (Table 54) was used as a loading buffer.

Table 53: 50x TAE buffer (5 l)

compound	amount	final concentration
Tris Acetate	1800.38 g	2 M
EDTA	93.06 g	50 mM
ddH$_2$O	up to 5 l	-

Autoclave and store at RT

Table 54: 6x Orange DNA loading buffer (50 ml)

compound	amount	final concentration
SDS	150 mg	3 mg/ml
orange G	75 mg	1.5 mg/ml
glycerol	75 µl	0,15 % (v/v)
0.5 M EDTA, autoclaved	1,500 µl	15 mM
ddH$_2$O	up to 50m l	-

Store at 4 °C

3.3.4.3 Purification of DNA fragments from gels

For samples with more than one PCR product, the relevant band was cut out with a scalpel under UV light and purified according to instructions using a *mi*-Gel Extraction Kit (*metabion international AG*). The samples were eluted to 10 mM Tris, pH 7.5 and stored at -20 °C.

3.3.4.4 Purification of PCR samples and linearized plasmid

Samples and for use in homologous recombination in *S. cerevisiae* (section 3.1.2.4) were purified using a *mi*-PCR Purification Kit (*metabion international AG*). The samples were eluted to 10 mM Tris, pH 7.5 and stored at -20 °C. This method was also used to purify linearized plasmid as loss of sample is less extensive compared to gel purification.

3.3.4.5 Sequencing

Plasmid constructs with the correct restriction pattern were sent for sequencing to GATC (https://www.eurofinsgenomics.eu/en/custom-dna-sequencing/gatc-services/) with the respective primers to check for point mutations, deletions and insertions. The sequencing results were analyzed as described in section 3.4.3. The sequencing primers are listed in Table 55. In addition, cassette-specific internal primers such as Sg781 were used to sequence starting from a resistance cassette.

Table 55: Sequencing primers

oligo no	name	gene	for rev	total sequence	source
1555	pdp3_SEQ_1	*pdp3*⁺	for	GTTGATGGCGAAGAAATGCT	this study
1556	pdp3_SEQ_2	*pdp3*⁺	for	GTTGCTAGGACACGCAGTCA	this study
1557	pdp3_SEQ_3	*pdp3*⁺	for	ACTTCAAAAGCCCATCGAGA	this study
1558	pdp3_SEQ_4	*pdp3*⁺	for	TTGAGAATTTCAGCGCAATAAA	this study
1559	pdp3_SEQ_5	*pdp3*⁺	for	GGTCAGGTTGCTTTCTCAGG	this study
1560	pdp3_SEQ_6	*pdp3*⁺	for	TGGGTACCACTCTTGACGAC	this study
1561	pdp3_SEQ_7	*pdp3*⁺	for	TGGGTACCACTCTTGACGAC	this study
1562	pdp3_SEQ_8	*pdp3*⁺	for	AAGAAAACGGAGCAGGAAGC	this study
1842	mst2_SEQ_1	*mst2*⁺	for	GCTGCTTCCTTTGCATTCTT	this study
1843	mst2_SEQ_2	*mst2*	for	CCAGAGGAGTATAGCTGTGCA	this study
1844	mst2_SEQ_3	*mst2*	for	GCTTGGATCACCTGAAAAGCC	this study
1845	tTEF1_SEQ	*tTEF1*	for	TTGTTTTCAAGAACTTGTCA	this study
1846	mst2_SEQ_4	*mst2*	for	GGCTTTTGGCTTGGAAGTGG	this study
1955	pRS416-5'_SEQ	pRS416 plasmid	for	CCCTCGAGGTCGACGGTATC	this study

3.4 Computer-based methods

3.4.1 Primer design

3.4.1.1 Primers designed with Perl

Primers for knockout generation and confirming successful integration were designed using the script KOprim_ver13.5.7 written by S. Braun in *ActivePerl V5.16.3 Build 1603* (*ActiveState Software Inc*) (48ºC as annealing temperature). The program has the purpose to automatically calculate the optimal annealing temperature and binding positions for these primers while avoiding polyA stretches. It outputs the sequences of three primer pairs, which consist of (1) a gene internal set to determine the presence of an ORF (~500 bp amplicon), (2) a set to amplify a locus-specific deletion cassette with 500 bp homology on each side of the cassette, and (3) flanking (Chk) primers that anneal to a region 600 bp up- or downstream of the cassette. The chromosome sequences used for primer design were taken from *PomBase*.

3.4.1.2 Primers for plasmid construction via homologous recombination in *S. cerevisiae*

Tagged Pdp3 and Mst2 were inserted into *S. pombe* by replacing a deletion cassette. A selection marker was included either upstream of an N-terminal tag or downstream of a C-terminal tag. The constructs were devised as inserts with 500 bp of homology to the locus on each side for homologous recombination.

Primers with overlap for recombination with the plasmid were designed with a total length of 80 bp of which were 20 bp homologous to the neighboring insert followed by a PmeI restriction site and homology to a backbone linearized with EcoRI. Primers between insert fragments were designed with 50 bp of total length with the forward primer complimentary to the reverse primer of the previous fragment. To insert point mutations the homologous primer pairs were designed with the mutation at the center. The plasmids and primers were designed using *SeqBuilder*, *Lasergene 10* (*DNA Star Inc.*).

3.4.1.3 Sequencing primers

Sequencing primers for the Pdp3 and Mst2 constructs were designed as forward primers with a length of 20 bp and a spacing interval of 600 bp using *Primer3Plus V2.4.0* [251]. In addition, a general sequencing primer was designed for the 5' insertion site of pRS416.

3.4.1.4 Tiled arrays for qPCR

Four sets of tiled array primers were designed for this study. Two arrays were designed to profile the binding pattern of Pdp3 and Mst2 via ChIP-qPCR. The loci were chosen based on gene length and clear separation by a long intergenic region. Additionally, the gene sets were of differing directionality to each other to examine the influence of gene orientation on the binding pattern of Pdp3 and Mst2 on neighboring genes. The coverage was defined as one amplicon to every 500 bp between the centers of the amplicons using *SeqBuilder*, *Lasergene 10* (*DNA Star Inc.*). The primers were designed by inputting 1000 bp of target region from the end of the last primer set into Primer3Plus and adjusting the general parameters to an amplicon length of 150-200 bp and a primer length of 20-25 bp length. The resulting primers were then narrowed down to one primer pair based on GC content (50-60%). Each primer pair was tested by running a 6-point standard curve with 1:10 dilutions using a 1:20 dilution of a WT input ChIP as starting solution.

3.4.2 Analysis of qPCR data

Using the cloud-based data analysis app *Standard Curve* (*Thermo Fisher Cloud*) the measured sample data was assigned relative values based previously generated triplicates of standard curves of a 1:10 dilution series. For further analysis, the data was imported into *Excel 365* (*Microsoft Corp.*).

For RT-qPCR experiments, the resulting relative values were analyzed as ratio of the respective heterochromatin PCR product over actin.

For ChIPs, data sets from each independent experiment (n=3-4) were standardized using an experimental normalization by defining a global mean value for ChIP efficiency. This global mean value includes all qPCR amplicons (used for each tiling array) from the entire sample pool of strains (wild-type and mutant strains used in each experiment). For ChIP experiments with FLAG-tagged Mst2 and Pdp3, the raw values were first normalized against mitochondrial DNA as an internal control before applying the same calculations as above. The background signal for each amplicon was subtracted. Here, the signal is defined as the mean value of the untagged strain and the *pdp3Δ* (or pdp3-F109A) for each amplicon as opposed to using only the untagged control as this significantly reduces the noise level in the background-corrected data. For ChIP with H3K14ac and H3, the raw values were also normalized against mitochondrial DNA and input; these normalized data were then put in relation to the mean value of the wild type for each amplicon. For ChIPs with H2K9me2, the raw value of each amplicon was normalized normalized to the mean value of three differentially expressed euchromatic loci: *adf1*[+], *sam1*[+], and *tif1*[+].

The qPCR data was visualized using *Prism V6-V8* (*GraphPad Software, Inc*).

3.4.3 Analysis of sequencing data

Finished sequencings were compared to the expected DNA sequence of the construct or tagged region using *SeqMan*, *Lasergene 10* (*DNA Star Inc.*). Constructs with point mutations, except silent mutations, or deletions in the sequence were discarded. The first 20 bp of the sequencing data were discounted for analysis as empirically these are prone to being misread by the polymerase.

3.4.4 Analysis of SGA data

The ratio of the growth of in FOA presence on day 4 to the growth EMM on day 2 was used to discern possible synthetic and epistatic interactions.

To this end, the colony sizes were processed with the software programs *HT Colony Grid Analyzer V1.1.7* [252]. The conversion of the ratio of +FOA /–FOA into $\log_2$ values and the normalization to the median were achieved using R and RStudio with the R script *screen_analyzer V1.8* written by S. Braun and exported to text files [253], [254]. All text files were imported into *Excel 365* (*Microsoft Corp.*) and unrelated files added to the analysis to act as additional controls. The $\log_2$ values of the double mutants were compared to the values of the single mutants from an SGA with the library and the background of PSB582 as well as the unrelated array. To assess the genetic interaction, the averaged $\log_2$ value for each query mutant crossed with PSB582 ($W_{x[MED]}$) was subtracted from the corrected median normalized value of each double mutant ($W_{xy[MED]}$) (see section 4.2). $\log_2$ values specific to the Mst2C subunits were collected and exported. For visualization in *Java TreeView V1.1.6r4,* the data was transcribed into a *.cdt file in *Cluster V3.0* [255], [256].

3.4.5 Quantification of western blot data

Quantification was done using *ImageJ V1.47* [257]. To this end, the signal intensity of the protein band was divided by the signal of the cross-reactive band above it, which is present in all samples. The ratio of the mutant was then put into relation to that of the respective wild-type to measure changes in protein expression.

3.4.6 Data research

For database searches (sequence search, literature search) services were used that were provided by *PomBase* (http://www.pombase.org/) and *National Center for Biotechnology Information* (http://www.ncbi.nlm.nih.gov/pubmed).

3.4.7 Thesis composition

The thesis text and tables were composed in *Word 365* (*Microsoft Corp.*). The figures were designed with *Photoshop* and *Illustrator* of *Creative Suite V5.1* (*Adobe Systems Inc.*). Citations were added using *Mendeley Desktop V1.19.4* (*Mendeley Ltd.*).

4 Results

4.1 Loss of the PWWP domain protein Pdp3 causes a silencing defect

The PWWP domain protein Pdp3 (Figure 6A) was isolated as a potential silencing factor in multiple independent genetic screens for mutants with silencing defects in the fission yeast *Schizosaccharomyces pombe* (*S. pombe*). However, its function has not yet been elucidated. The first screen entailed a small collection of deletion mutants of genes encoding either proteins with similar nuclear localization of the HP1 protein Swi6 or proteins that contained motifs known to associate with chromatin [231]. The second screen employed a genome-wide library of deletions of all non-essential genes [18]. The readout of these screens was a growth-based reporter assay utilizing the auxotrophic *ura4*+ gene that encodes orotidine 5'-phosphate decarboxylase, which metabolizes the nucleotide analog 5-fluorootidine (5-FOA) into cytotoxic 5-fluorouracil (Figure 6C) [258]. To monitor the silent state of heterochromatin *in vivo, ura4*+ was inserted into a heterochromatic region, thus allowing cells to grow on 5-FOA-containing medium when heterochromatin is intact, and the locus is transcriptionally repressed. Conversely, perturbation of heterochromatin causes expression of *ura4*+ and results in impaired growth on 5-FOA. In previous studies, as well as here, *ura4*+ is integrated at the left innermost repeat located adjacent to the centromere on chromosome 1 (*imr1L*). Due to its position at the boundary between heterochromatin and euchromatin, the *imr1L::ura4* reporter is highly sensitive towards perturbation of heterochromatin.

Lack of Pdp3 results in reduced growth when plated onto 5-FOA containing medium whereas no difference to wild-type (WT) is observed on non-selective medium (Figure 6B) [18], [231]. On the other hand, no silencing defect was detected when *ura4*+ was inserted into the silenced mating type locus, suggesting that silencing at this domain is not affected by the loss of Pdp3 [231]. To test whether the silencing defect results from deletion of *pdp3*+ or is caused by a secondary mutation in the strain background of the deletion library, I generated a re-knockout mutant (re-KO). For this, I amplified the *pdp3Δ* deletion cassette by PCR from genomic DNA of the library *pdp3Δ* mutant and transformed it into a WT strain that harbors the same reporter as the original mutant. Unlike the previous KO strain, which comes from a genetic cross and has a mixed genetic background, the WT strain used for the re-knockout has a clearly defined genotype. I isolated several transformants and compared them with the

deletion strain from the previous screen [18]. Analogous to the library mutant, two representative re-KO mutants displayed a reproducible silencing defect in presence of 5-FOA, while displaying WT growth phenotypes on non-selective media (Figure 6B). The silencing defect of *pdp3Δ* is moderate when compared to a deletion of *clr4⁺*, the sole H3K9 methyltransferase in *S. pombe.* This suggests that Pdp3 is not a critical component of the core silencing machinery (H3K9me or RNAi).
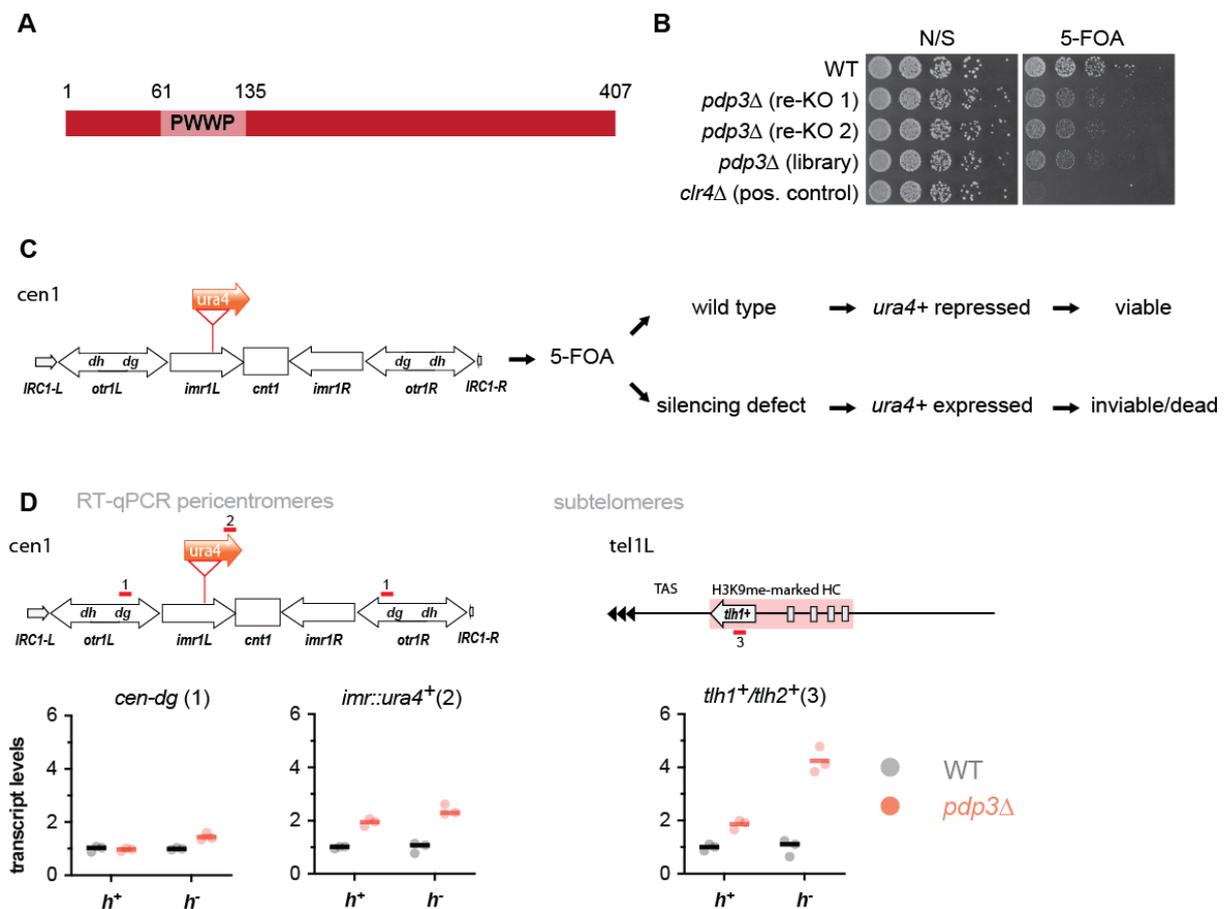
Figure 6- Loss of Pdp3 causes a silencing defect: (A) domain organization of Pdp3; (B) silencing assay utilizing an *imr::ura4⁺* reporter strain; 5-fold dilution series of wild-type (WT), two independent *pdp3⁺* knockout strains (re-KO 1 and 2), the commercial Bioneer strains of *pdp3Δ* (library) and *clr4Δ* (positive control) crossed with the reporter background; (N/S) non-selective, (5-FOA) medium containing 5-fluroorotic acid; (C) flow diagram of the *imr::ura4⁺* reporter assay employed for this study. (D) RT-qPCR analysis; displayed are transcript levels relative to wild-type after normalization to *act1⁺*; *imr::ura4⁺* represents transcription of the *ura4⁺* gene inserted into the *imr* region of the left arm of chromosome 1, *tlh1⁺* is the first gene of the subtelomeric region on the left arm of chromosome 1; *h⁺* and *h⁻* refer to the mating types; data are presented as individual data (circles) and median (horizontal line) from 3 independent experiments.

Since growth-based assays are an indirect and semi-quantitative method for assessing heterochromatin silencing, I used a more quantitative and direct approach to study levels of heterochromatic transcripts. To this end, I employed a reverse transcription assay coupled to quantitative PCR (RT-qPCR). cDNA is generated by 1st strand

63

synthesis from poly-adenylated mRNA and quantified by qPCR. For normalization, I used the euchromatic housekeeping gene $act1^+$ as an internal control. $act1^+$-normalized transcript levels were displayed relative to the mean value of all biological replicates of the WT strain (i.e. set to 1) for the respective heterochromatic loci. The *dg* repeats, which are located further inside the silenced pericentromeric region, were mostly unaffected (Figure 6D, left panel). In contrast, the $ura4^+$ reporter at the pericentromeric *imr1L* displayed 2-2.3 higher transcript levels in *pdp3Δ* mutant cells compared to WT (Figure 6D, middle panel). Conversely, silencing of the homologous $tlh1^+$ and $tlh2^+$ genes, which are located subtelomeric gene ~10 kb downstream of the telomeric repeats of chromosome 1 and 2, was perturbed as well (Figure 6D, right panel).

Interestingly, I noticed that heterochromatic transcripts in the h^- WT strain are stronger repressed than in the corresponding h^+ WT strain (data not shown), suggesting that this strain is more sensitive to perturbations in heterochromatic transcription. In support of this notion, the silencing defects in *pdp3Δ* were more pronounced in strains with the h^- mating type at all loci tested. Together, the results suggest that lack of Pdp3 impairs silencing. However, the influence of Pdp3 loss appears to vary depending on the heterochromatic region.

4.2 Pdp3 acts as a negative regulator of the histone acetyltransferase Mst2C

I found that loss of Pdp3 causes a silencing defect, but the actual function of Pdp3 with Mst2C was unknown (Figure 7A). To elucidate if the silencing defect of Pdp3 was connected to a specific silencing mechanism, I tested genetic interactions on a genomic scale using the synthetic genetic array (SGA) approach. To that end, I crossed a query *pdp3Δ* strain that harbors the $imr::ura4^+$ reporter with a genome-wide library of non-essential mutants (y). To calculate quantitative genetic interactions, which require assessing the silencing defects in *pdp3Δ*, the other library single mutants and the resulting double mutants, I additionally performed a cross with the WT reporter (Figure 7B). Upon mating, germinated spores were selected for the presence of both, the selection markers of the mutations (*natMX* for the query strain, *kanMX* for the library mutation) and the reporter gene (a *hphMX* cassette 2 kb adjacent of $imr::ura4^+$). The quantitative readout of each SGA was calculated as log_2 value of the ratio of growth (colony size) on 5-FOA containing medium versus growth on non-selective

medium (Figure 7B) and normalized the data to the median of each plate using the programs described in section 3.4.4. The level of genetic interaction ε, I calculated as difference of colony growth in the double mutant ($W_{x,y\ [MED]}$) and growth of the query mutation (x) in a WT background ($W_{x\ [x]}$):

$$\varepsilon = W_{x,y[MED]} - W_{x[MED]}$$

Following the readout, I organized the data by similarities of the silencing phenotype of the single mutants and the respective double mutants with *pdp3Δ* between the different crosses.
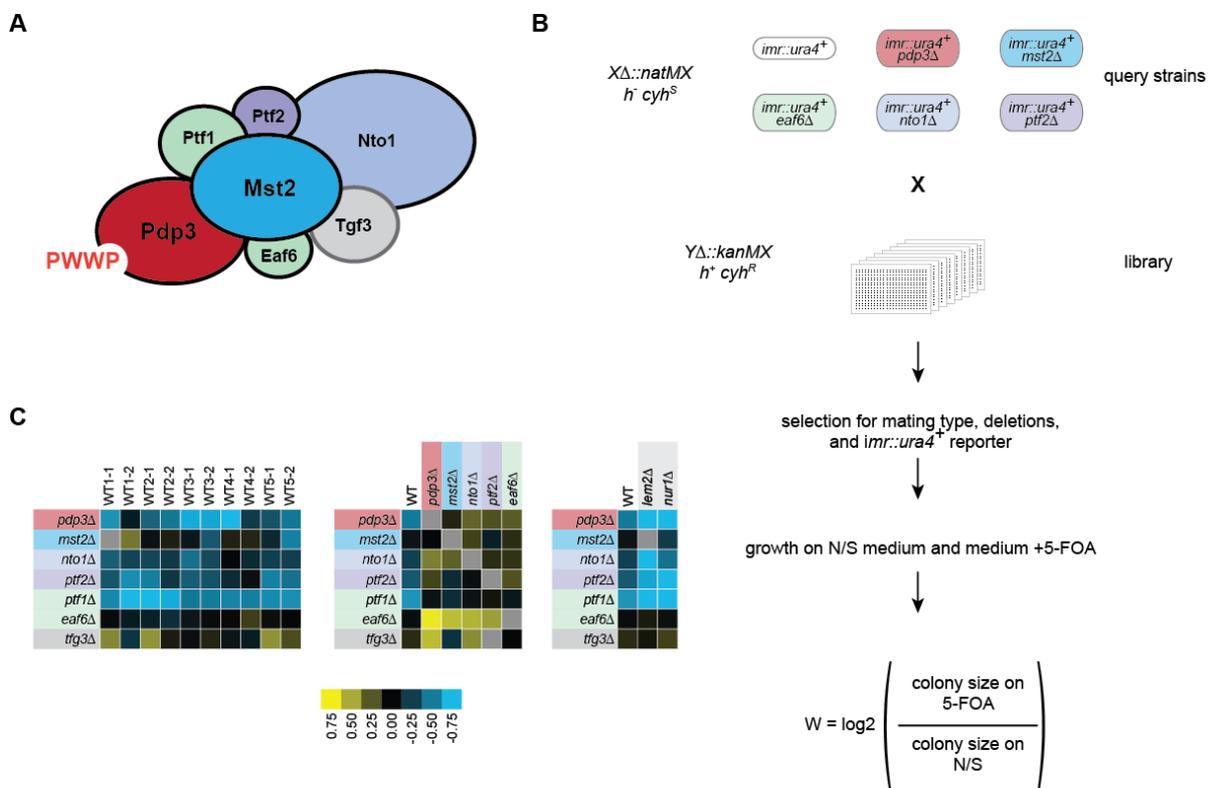
Figure 7 - Pdp3 is a negative regulator of the Mst2 complex: (A) Composition of the Mst2 complex, color key: red – Pdp3, blue – integral subunits; green – complex-specific non-essential subunits, grey – multi complex subunit; the color code of the subunits applies for all subfigures; (B) flow diagram depicting an overview of the synthetic genetics array (SGA) performed in this study; the query strains containing the *imr::ura4⁺* marker in a wild type background or a deletion of the gene of interest (*XΔ::natMX*) were crossed with a commercial library containing all null-mutants of non-essential genes (Bioneer; *YΔ::kanMX*), the ratio of colony sizes on 5-FOA over non-selective medium (N/S) was used as a readout; (C) Pdp3 is a negative regulator of the Mst2 complex: heatmap visualizing log2 values compiled of the readout of crosses of the Mst2C subunits with: left – wild-types, middle - subunits of Mst2C complex, right - query strains from an unrelated study as non-specific control; columns – arrays, rows – cross with the library mutant; each data point represents the average of crosses performed with the same query strain; color key: yellow – suppression or epistatic interaction, black – no interaction, blue – synthetic interaction, grey – synthetic lethal.

Since the readouts were comparable between technical and biological replicates (see Figure 7C - left panel), I took the average of the log$_2$ values from all replicates per single and double mutant SGAs with the same query strain (e.g. WT or *pdp3Δ*). These values are visualized in a heat map with columns representing the query strains and the rows representing the cross with the library strain. This I then used to determine whether the silencing defect of a single mutant could be suppressed or even reversed by additional deletion of another gene. The log$_2$ values are represented in the heat-map ranging from blue ($\varepsilon < 0$) over black ($\varepsilon = 0$) to yellow ($\varepsilon > 0$). The respective readout appears blue-colored if the additional deletion added through a mating with the library mutant either causes a growth defect on its own and/or it exacerbates the genetic defect of the queried mutant and is synthetic. In the latter case, the gene products work in parallel pathways that are part of the silencing machinery. The square is black if lack of the gene does not result in any growth difference in general or the queried genetic defect is not influenced by concomitant deletion of the gene targeted in the library mutant. The gene products can be part of unrelated molecular pathways or are part of the same step of a pathway, i.e. as subunits of the same complex. If the readout is represented by yellow coloring, the lacking gene product may antagonize silencing on its own and/or the additional deletion alleviates the silencing defect in the queried strain.

In accordance with the silencing assay and RT-qPCR data at *imr::ura4$^+$* (see Figure 6), deletion of *pdp3$^+$* caused a silencing defect at pericentromeric heterochromatin (Figure 7C - left panel, first lane). When I analyzed the cross of *pdp3Δ* with the deletion library, I discovered that the silencing defect of *pdp3Δ* was suppressed by several mutants (Figure 7C - middle panel first and second column). Intriguingly, all mutants belonged to the MYST histone acetyltransferase complex Mst2 (Mst2C) of which Pdp3 is a subunit. A study of the Jia group has previously demonstrated that Mst2C consists of seven subunits, of which five have homologs in the *S. cerevisiae* histone acetyltransferase NuA3 complex [245]. The conserved subunits comprise Mst2, Nto1, Eaf6, Tfg3, and Pdp3 (Figure 2A). The remaining two subunits are Ptf1 and Ptf2 (Pdp three- interacting factor 1 and 2). Among the subunits, only Mst2, Nto1 and Ptf2 are critical for the integrity and catalytic activity of the complex.

Mst2 antagonizes telomeric silencing, and *mst2Δ* mutant cells are able to bypass the need for RNAi in the silencing of pericentromeric heterochromatin [238], [242]. Considering that Pdp3 contributes to heterochromatic silencing, it is tempting to

speculate that Pdp3 negatively regulates Mst2C. To test this hypothesis, I repeated the first SGAs with two more biological replicates. Moreover, in parallel to pdp3Δ, I tested the deletions of two more subunits of Mst2C in the *imr::ura4⁺* reporter strain (*mst2⁺*, *eaf6⁺*, *nto1⁺*, *ptf2⁺*) per assay replicate (Figure 7C – middle panel) to analyze genetic interactions of Mst2C at a genome-wide scale. As a negative control, I compared my genetic interaction data to data from an unrelated study in the lab (Figure 7C – right panel, *lem2Δ* and *nur1Δ*).

As single mutants, all Mst2C subunits displayed silencing defects whose extent was close to or less pronounced than that of *pdp3Δ* (Figure 7C – left panel). The average of all $\log_2$ values for the single mutants is shown in the first columns in the middle panel of Figure 7C. Double mutants with Mst2C subunits on the other hand consistently displayed complete suppression of the silencing defect of *pdp3Δ* both when *pdp3Δ* was used as a query strain (Figure 7C – middle panel, column 2) as well when the *pdp3⁺* deletion was crossed in (Figure 7C – middle panel, lane 1). Contrarily, disrupting *lem2⁺* or *nur1⁺* did not suppress the silencing defect of *pdp3Δ* or other Mst2C mutants (like *ptf1Δ* and *ptf2Δ*; Figure 7C, right panel, columns two and three). The suppression of the silencing defect of *pdp3Δ* by additional deletion of *mst2⁺*, *nto1⁺*, or *ptf2⁺* suggests that Pdp3 is a negative regulator of the anti-silencing activity of Mst2C.

To verify the suppression phenotype for the *mst2Δ pdp3Δ* double mutant and rule out secondary effects through crossing with the library strain, I deleted both *pdp3⁺* and *mst2⁺* in same the background (*imr::ura4⁺, h⁻*) I used for SGA query strain. I then compared this strain with both query strain mutants by individual silencing assays and quantification of transcript levels.

When plated on non-selective medium, the three tested mutants displayed no growth defect compared to WT, suggesting that none of them affect cell proliferation (Figure 8B, left panel). On 5-FOA-containing media, loss of Pdp3 led to a moderate silencing defect as previously observed, whereas lack of Mst2 (Figure 8A) did not perturb pericentromeric heterochromatin (Figure 8B, right panel, compare to Figure 6B). However, when *mst2⁺* was deleted in the *pdp3Δ* strain silencing was rescued, supporting the hypothesis that the silencing defect of *pdp3Δ* depends on Mst2C.
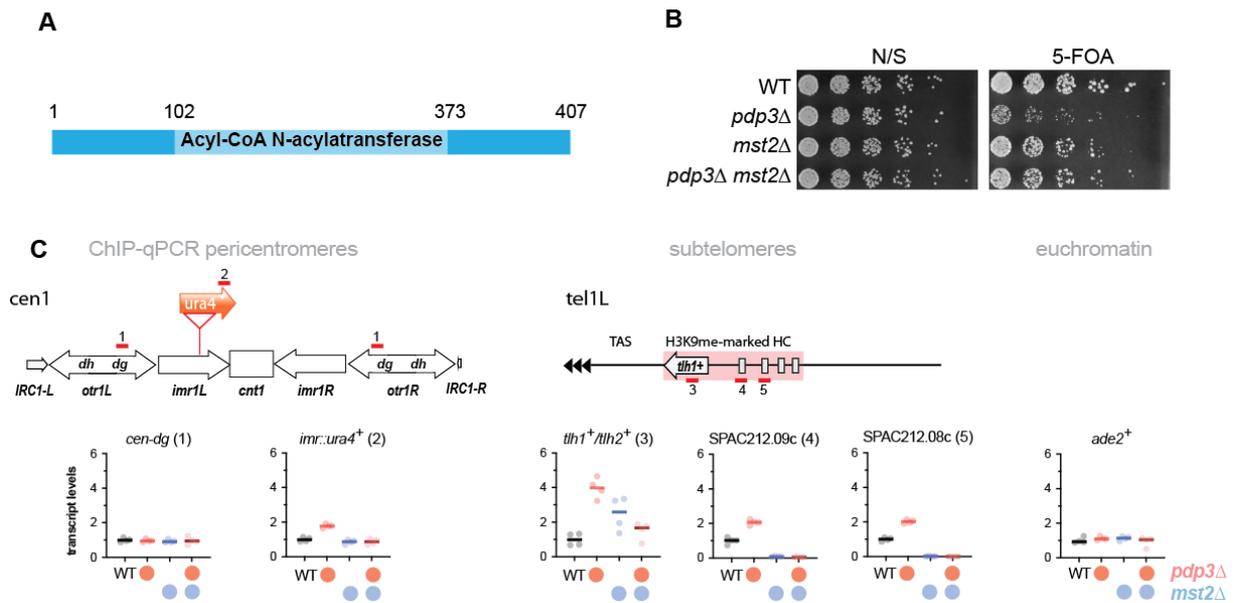
Figure 8 - The silencing defect of *pdp3Δ* can be suppressed by concomitant deletion of Mst2: (A) domain organization of the HAT Mst2; (B) *imr::ura4+* silencing reporter assay for verification of the SGA; a 5-fold serial dilutions of wild type (WT), *pdp3+* and *mst2+* single knockouts as well as a *pdp3+ mst2+* double knockout, N/S – non-selective.(C) RT-qPCR analysis at pericentromeric and subtelomeric heterochromatin as well as *ade2+* as control for euchromatin, experiments were performed with the same mutants as the silencing reporter assay, data is shown relative to WT after normalization to *act1+*, circles represent individual data of 3 independent experiments and the horizontal their median**.**

To quantitatively analyze the suppression of the silencing defect, I compared levels of heterochromatic transcripts in the *pdp3Δ* and *mst2Δ* single mutants and the corresponding double mutant by RT-qPCR (Figure 8C). At pericentromeric heterochromatin, I tested *imr::ura4+* and the *dg* repeats. At the subtelomeric heterochromatin domain, I analyzed *tlh1+/tlh2+* at the left arm of chromosome 1 (TEL1L) and chromosome 2 as it is affected by loss of Pdp3 (see Figure 6D). However, not only *tlh1+/tlh2+* but also the following four genes (*SPAC212.08c*, *SPAC212.09c+*, *SPAC212.12*, and *SPAC212.06c*) have robust H3K9me2 levels that are comparable to heterochromatin at pericentromeres [18]. To test if this region is similarly sensitive towards loss of Pdp3, I analyzed heterochromatic transcripts at *tlh1+/tlh2+*, *SPAC212.08c+*, and *SPAC212.09c+*, at which H3K9me2 enrichment peaks. At both *imr::ura4+* (Figure 8C - 2nd panel) and TEL1L (Figure 8C - 3rd to 5th panel) concomitant deletion of *mst2+* suppressed the silencing defect of *pdp3Δ.* At *imr::ura4+* the transcript level of *mst2Δ pdp3Δ* was comparable to that of the WT, at *SPAC212.08c* and *SPAC212.09c* transcription was significantly lower in the double mutant than in WT. At the flanking gene *tlh1+/tlh2+*, the silencing defect of *pdp3Δ* was also suppressed nearly to WT levels in *mst2Δ pdp3Δ*.

Regions whose transcript levels were not perturbed by loss of Pdp3, like the pericentromeric *dg* repeats or euchromatic genes such as *ade2*+ (Figure 8C – last panel), were equally unaltered in the *mst2Δ* single mutant or the *mst2Δ pdp3Δ* double mutant.

At nearly all loci tested, the *mst2Δ* single mutant reflected the phenotype of the *mst2Δ pdp3Δ* double mutant. As an exception, at *tlh1*+*/tlh2*+ the *mst2Δ* single mutant itself displayed a silencing defect.

In summary, loss of Mst2 suppresses the silencing defect of *pdp3Δ* to the transcription level found in the *mst2Δ* single mutant, suggesting the catalytic activity and possibly presence of Mst2 as a likely cause. The silencing defect of *mst2Δ* at *tlh1*+*/tlh2*+ implies that acetylation by Mst2 may indirectly promote heterochromatin maintenance.

4.3 Pdp3 recruits Mst2C to gene bodies and prevents its encroachment into heterochromatin

Given that loss of Pdp3 causes a silencing defect that is suppressed by additional removal of the anti-silencing factor Mst2, I postulated that Pdp3 might prevent Mst2 from invading heterochromatin. Therefore, I studied the binding pattern of Mst2 and Pdp3 each other.

In order to study chromatin association of Mst2 at a genome-wide scale, I collaborated with Valentin Flury (VF), a member of the group of Marc Buehler at the Friedrich Miescher Institute in Basel. His group is experienced in the use of DamID, a technique that allows the detection of even transient protein-chromatin interactions on a global scale by DNA methylation in *S. pombe* and higher eukaryotes [259]–[261]. To this end, the protein of interest is expressed as a fusion with the prokaryotic DNA methyltransferase Dam, which modifies adenine bases at GATC sites. Methylated DNA sites are digested by the DNA methylation-sensitive restriction enzyme *DpnI*. Blunt ends generated by *DpnI* digestion are ligated with direction-specific adapters; the remaining unmethylated GATC are digested with *DpnII* to remove fragments of regions that were not targeted by the Dam-fused protein. Specific ligation products are amplified with adapter-complementary primers and then analyzed by DNA micro-arrays or next-generation sequencing. DamID data generated by Dam-fusion proteins are corrected by analysis of the non-fused enzyme (Dam-only) to factor in the propensity of Dam to bind to DNA. The readout of DamID is calculated as the ratio of Dam-fused proteins to Dam-only.

Using this method to study the localization pattern of Dam-Mst2 via DNA microarrays, we found that Mst2 is distributed across all chromosomes but depleted from centromeric and telomeric regions (Figure 9A – bottom). When the DamID data were compared with H3K9me2-specific ChIP sequencing data, we found that Mst2 is specifically depleted from constitutive heterochromatin; this becomes most evident for the centromeres and (sub)telomeric regions (Figure 9A – top, H3K9me data from [262]; Figure 9B). This suggests a mechanism that sequesters Mst2C to euchromatin and limits its access to heterochromatin. Since my findings imply that Pdp3 is a negative regulator for Mst2C, VF tested whether the deletion of Pdp3 influences the global distribution of Mst2. Indeed, when performing DamID with a strain lacking Pdp3, we found that Mst2 encroached on heterochromatin, suggesting that Pdp3 prevents unrestricted access of Mst2 to heterochromatin (Figure 9C).

The advantage of DamID is the visualization of the global distribution of a Dam-fused protein across different chromatin domains and even within large genes [259]. Furthermore, it is very sensitive due to the high procession rate of Dam and allows the detection of transient interactions via stable DNA methylation of regions in the vicinity of the Dam-fused protein. Thus, based on the Mst2-DamID results, we hypothesized that Mst2 is restricted to specific regions in euchromatin and that recruitment of Mst2C depends on Pdp3. This is likely mediated by its PWWP domain, since these domains often interact with methylated histones [200]. However, it was not clear whether Mst2 is recruited to a specific euchromatic posttranscriptional modification or region, such as enhancers, promoters, intergenic regions, or a specific end of the open reading frame. DamID is a stochastic process and thus does not reflect the quantity of Mst2 present at a specific domain. This is generally the case with Dam-fused proteins, as Dam recognizes GATC sites, which occur every 265 nucleotides, and DamID empirically has maximum resolution of one kilobase [259]. To validate the DamID results and clarify the manner of Mst2C recruitment and its location on chromatin, I applied an alternative method. The first priority was to assess where Pdp3 is located on euchromatin, followed by studying whether Mst2 binds to euchromatic regions but is no longer recruited in absence of Pdp3. To address these questions, I employed chromatin immunoprecipitation coupled to qPCR (ChIP-qPCR).

For this purpose, I generated strains with C-terminally FLAG-tagged Mst2 and Pdp3; this type of epitope-tagging has been successfully used in a previous study in pull-down experiments to determine the subunits of the Mst2 complex [245].

First, I examined the association of Pdp3 with euchromatin (Figure 9D). Euchromatin comprises transcriptionally active regions including genes that encode proteins and non-coding RNAs. To better understand the function of Pdp3 and Mst2 at chromatin I needed an approach that allows me to differentiate whether Pdp3 preferentially associates with specific chromatin regions (e.g. parts of a gene). To achieve a higher resolution than 1 kb as observed for DamID, I designed and generated tiled primer pairs in approximately 500 bp intervals for genes with large intergenic regions that ideally span more than a kilobase. One of the arrays includes the genes $mto1^+$ and $tef3^+$, which are in divergent orientation (Figure 9D - first panel). These two genes also differ significantly in the cellular mRNA level during vegetative growth (1.7 and 160 mRNA molecules per cell for $mto1^+$ and $tef3^+$, respectively) [263]. When examining FLAG-Pdp3, I found that Pdp3 was preferentially enriched at the $mto1^+$ and $tef3^+$ gene bodies while being depleted from the intergenic region. I detected no difference in the level of Pdp3 enrichment for $mto1^+$ and $tef3^+$. I observed a similar enrichment for $sam1^+$ and $pgk1^+$, which are present in a head-to-tail orientation, and a small gene for a non-coding RNA present in their intergenic region (160 and 250 mRNA molecules per cell, for $sam1^+$ and $pgk1^+$ respectively, Figure 9D - second panel). Thus, Pdp3 binds to genes and is not found in intergenic regions. Further, Pdp3 association is not correlated with the transcription rate of the gene.

Next, I assessed the distribution of Mst2-FLAG. Like with Pdp3, I observed that Mst2 was enriched over gene bodies at $mto1^+$ and $tef3^+$ (Figure 9E, left panel). Analogously, I detected comparable results for the $ade6^+$ gene and its neighboring genes $bub1^+$ and $vtc4^+$ (Figure 9E – right panel). Notably, in absence of Pdp3 all Mst2 association was lost in both regions.

One possibility is that Pdp3 binds to a specific histone mark that gene bodies are decorated with. The other option is that loss of Pdp3 results in nucleosome reduction. To rule out nucleosome loss as a cause for reduced Mst2 binding, I performed H3 ChIP as a proxy for the nucleosome levels in $mst2$-FLAG and the $pdp3\Delta$ strains. I chose this approach to monitor nucleosome density as H3, besides H2A, H2B, and H4, is one of the four core histones that form the canonical nucleosome present in transcribed regions [2], [5]. H3 density remained unchanged, suggesting that epitope-tagging of Mst2 or deleting $pdp3^+$ does not interfere with nucleosome levels and chromatin integrity (Figure 9F). Thus, Mst2 recruitment to gene bodies depends on the presence of Pdp3. Taken together, the DamID and ChIP data suggest that Pdp3 acts as a factor

that recruits Mst2 to gene bodies and thereby prevents Mst2 from encroaching on heterochromatin.
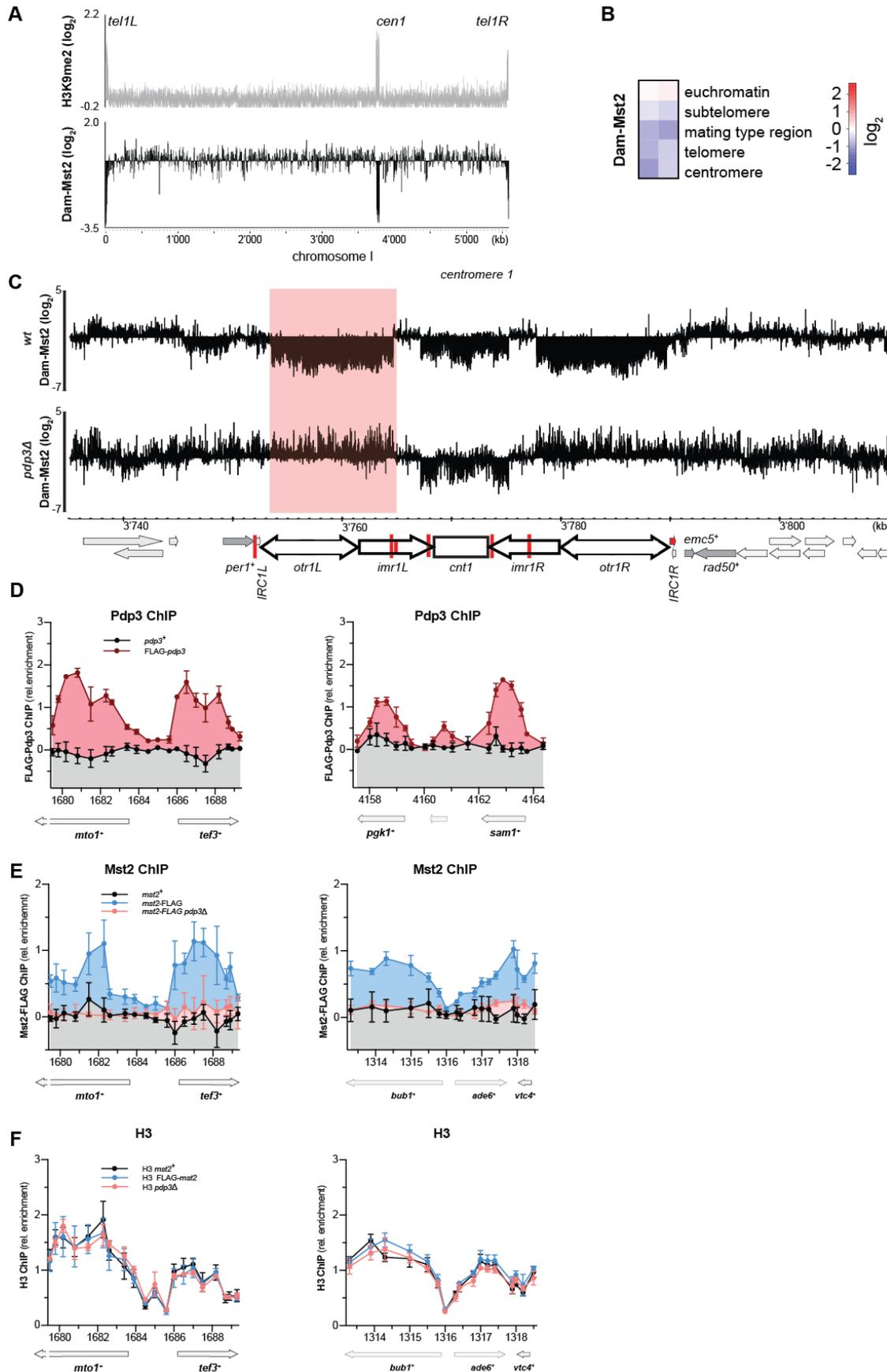
Figure 9 - Mst2 requires Pdp3 for recruitment to gene bodies: (A) Mst2 is depleted from heterochromatin: shown is an overview of chromosome 1 with annotated heterochromatin domains; top – H3K9me2 ChIP-seq to denote the location of the heterochromatic domains; bottom – DamID of Dam-Mst2 over Dam-only; data is represented in log2 scale; (B) Mst2 is excluded from all heterochromatic loci: Mst2 DamID heatmap representing the average of all enrichment values of primers binding in the regions annotated as the respective chromatin domain; blue – depleted, red – enriched relative to Dam-only. (C) Mst2 encroaches on heterochromatin in absence of Pdp3; depicted are Dam-Mst2 enrichment values in relation to Dam-only (log2 scale) for oligos covering the pericentromeric region of chromosome 1; top – wild-type, bottom – *pdp3Δ* background. (D) ChIP enrichment of FLAG-Pdp3 at *mto1+/tef3+* and *sam1+/pgk1+*, data presented with background subtracted, $n = 3 \pm$ SEM; (E) first and second panel - ChIP enrichment of Mst2-FLAG at *mto1+/tef3+* and *bub1+/ade6+/vtc4+*, data presented with background subtracted, $n = 4 \pm$ SEM; (F) H3 ChIP enrichment at *mto1+/tef3+* and *bub1+/ade6+/vtc4+*; data is presented relative to *FLAG-mst2*; $n = 3$; subfigures (A to C) adapted from Valentin Flury, who performed the experiments.

4.4 Pdp3-dependent recruitment of Mst2 requires H3K36me3

Our previous data showed that Pdp3 is essential for the recruitment of Mst2 to gene bodies. This suggests that Pdp3 interacts with chromatin through a histone modification that is found in actively transcribed chromatin. Pdp3 is a PWWP domain protein and a member of the Tudor family of histone readers [195]. Tudor family members are known to recognize histone proteins methylated at lysine or arginine residues. The prevalent histone mark recognized by PWWP domains is trimethylated H3K36 (H3K36me3) [200]. H3K36me3 is conserved across a variety of species and considered as one of the hallmarks of transcribed chromatin [168]. Indeed, probing the *mto1+* and *tef3+* loci for H3K36me3 by ChIP revealed that the methylation pattern overlapped with the regions enriched for Pdp3 and Mst2 (compare the WT sample of Figure 10A with 10C). A similar result was observed when probing the *sam1+* and *pgk1+* loci (data not shown).

In *S. pombe,* methylation of H3K36 is mediated by a sole histone methyltransferase, Set2 [168]. To test whether methylation of H3K36 is crucial for the recruitment of Pdp3, I performed Pdp3-ChIP in a strain lacking Set2. Recruitment of Pdp3 was completely abolished at all tested loci (Figure 10A). Similarly, Mst2-FLAG was absent at gene bodies in a strain deleted for *set2+*. This suggests that methylation of H3K36 by Set2 is essential for the recruitment of Pdp3 and Mst2. However, it remained elusive, which specific modification state (i.e. di- or trimethylation) is recognized by Pdp3. For example, in *S. cerevisiae,* Pdp3 preferentially interacts with H3K36me3 but also binds to H3K36me2, though with lower specificity [140], [141]. *In vitro* assays in *S. cerevisiae*

revealed that H3K36me2 is sufficient to recruit the histone deacetylase (HDAC) Rdp3p (the *S. cerevisiae* homolog of Clr6) via the chromodomain protein Eaf3, suggesting that H3K36me3 may have a different function [184], [185]. In that vein, in *S. pombe*, genes with a high H3K36me2 display lower levels of H3K27ac, likely due to recruitment of the HDAC Clr6 by Alp13, the *S. pombe* homolog of Eaf3 [128], [264].

To determine the binding specificity of Pdp3, I took advantage of a property that is unique to fission yeast Set2: All Set2 homologs contain a SET domain and a Set2 Rpb1 interacting domain (SRI), which are both critical for methylation activity [176]. The SRI domain binds the S2-S5-biphosphorylated C-terminal repeats of RNA polymerase II during the elongation step of transcription. However, in contrast to *S. cerevisiae* Set2, which is inactive in absence of the SRI domain, the fission yeast SRI truncation mutant is defective in trimethylation but still mediates dimethylation of H3K36 [177], [265]. To discern the specificity of Pdp3 binding, I analyzed the binding profiles of Pdp3 and Mst2 in strains expressing the Set2 mutant lacking the SRI domain (*set2-SRI*Δ). H3K36me3 was lost at all tested loci in the *set2-SRI*Δ mutant, apart from *tef3*+ where it was partially retained (Figure 10C – left and middle panels). Mirroring the pattern of H3K36me3, Pdp3 and Mst2 binding was completely abolished from all tested genes lacking H3K36me3 in the Set2-SRIΔ strain (Figure 10A and 10B, respectively). On the other hand, at the *tef3*+ locus where H3K36me3 was partially retained, both Pdp3 and in part Mst2 remained bound. To ensure that loss of H3K36 methylation did not affect nucleosome abundance at the analyzed loci, I performed ChIP for non-modified histone H3 in H3K36me-deficient mutants (*set2*Δ, *set2-SRI*Δ) and in the isogenic WT strain (Figure 10C - right panel). H3 levels in both mutants were comparable to the WT, indicating that loss of H3K36me3 is not indirectly caused by loss of nucleosome density but rather a direct consequence of the lack of Set2 activity. However, it was not clear if the recruitment of Pdp3 proceeded via its PWWP domain. In *S. pombe,* three PWWP domain proteins are present but only the Set9 complex subunit Pdp1 has been studied in detail [197], [266]. Pdp1 recruits the H3K20-specific histone methyltransferase to monomethylated H3K20 as part of a positive feedback loop [266]. The binding pocket of the Pdp1 PWWP domain consists of three aromatic residues (Y63, W66, and F94) of which W66 and F94 are essential for maintaining the binding function. To test whether PWWP domain of Pdp3 had a similar role, I mutated phenylalanine F109 to alanine, this residue putatively corresponding to the essential residue F94 in the Pdp1 PWWP domain (Figure 10D). This F109A mutation is

expected to prevent binding. By ChIP experiments, I found that the F109A mutation abolished chromatin binding of FLAG-Pdp3 to all tested loci (Figure 10E).

To exclude potential secondary effects by fusion with the FLAG-tag and the introduction of an additional mutation, I examined the transcript levels of *pdp3⁺* and *mst2⁺* mRNA in all strains used for ChIP and compared them to the respective untagged strain (Figure 11). Further, I interrogated the protein levels of tagged Mst2 and Pdp3.

Transcription of *mst2⁺-FLAG* was unaltered compared to *mst2⁺* and unaffected by concomitant deletion of *pdp3⁺* but slightly increased in the *set2Δ* strain and *set2-SRIΔ* mutant (Figure 11A - left panel). This observation was mirrored in strains, I used to profile Pdp3 binding (Figure 11A - middle panel). Additionally, I analyzed the protein level of Mst2-FLAG in the wild-type and the *pdp3Δ* strain (Figure 11A - right panel). Mst2 levels were increase by 30 % in *pdp3Δ* compared to WT. Thus, a reduction in mRNA transcription or in protein level can be excluded as a cause for reduced Mst2 binding in the pdp3Δ and the *set2* mutants (Figure 9E and Figure 10B, respectively).

Transcription of *pdp3⁺* was slightly increased in both the wild-type and the *set2Δ* mutant of the *mst2-FLAG* strain, when compared to the untagged strain (Figure 11B – left panel). Transcription of *pdp3⁺* in the *set2-SRIΔ* mutant was comparable to that of the untagged strain. When I tested the transcript levels of the epitope-tagged versions of the WT and mutant alleles of *pdp3⁺*, both strains displayed increased transcription compared to the untagged WT (Figure 11B - middle panel). However, transcription was not altered between WT and point mutant. Complete loss of Set2 did not reduce FLAG-*pdp3⁺* expression but rather led to heightened transcription. mRNA transcription of *FLAG-pdp3⁺* in the *set2-SRIΔ* mutant equaled that of the WT. Thus, lack of Pdp3 binding in all tested mutants (Figure 10A and 10E) is not the result of reduced mRNA transcription at the *pdp3* locus. At the protein level, I assessed the FLAG-tagged WT and the F109A mutant. The amount of point mutant detected was 0.6-fold less than that of Pdp3-FLAG. However, rather than a reduction, I observed a complete loss of binding in the point mutant. Therefore, the loss of Pdp3 binding for the F109A point mutant and in the Set2 mutants is based purely on the mutation of the PWWP domain and lack of its target, respectively.
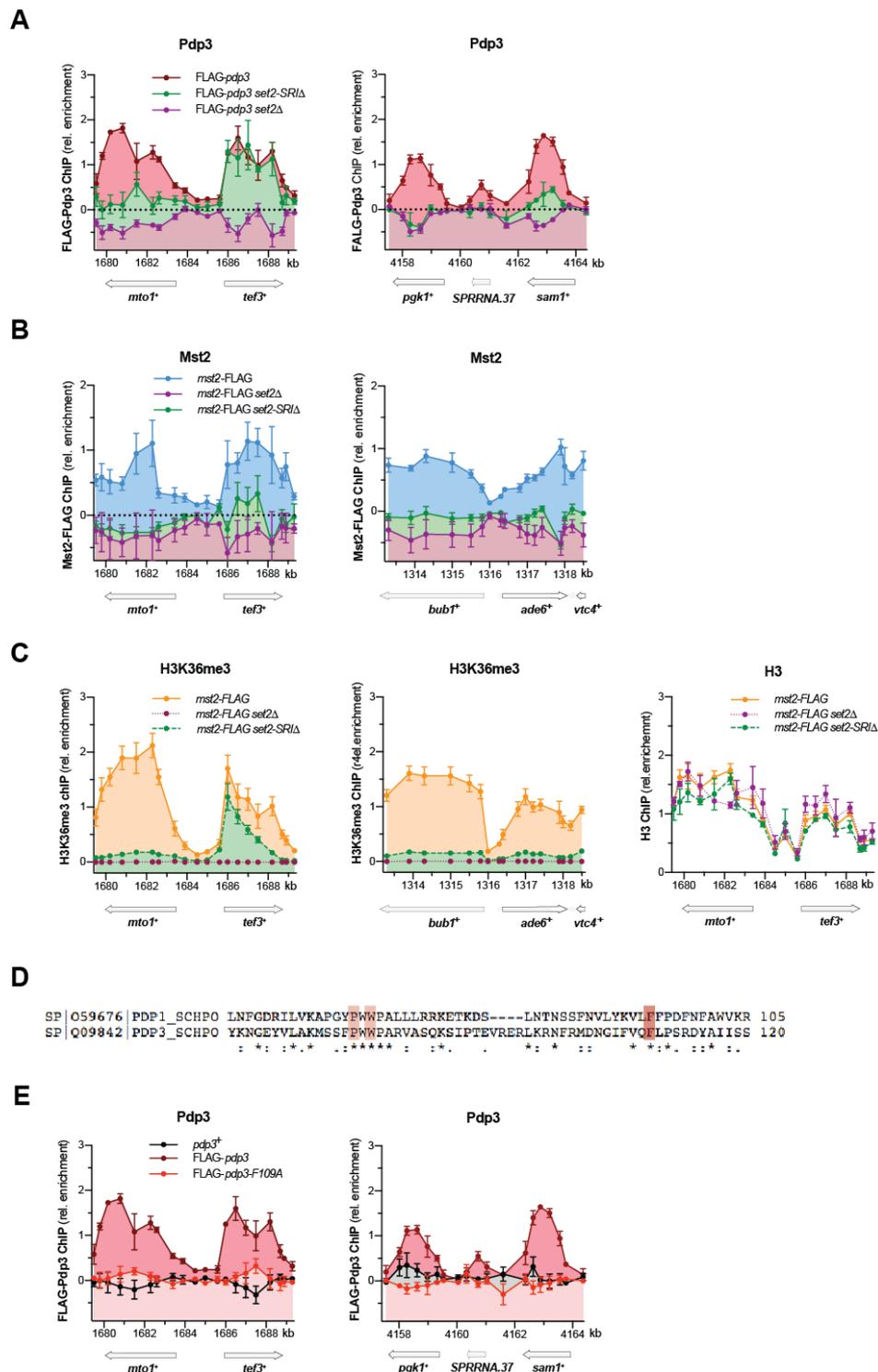
Figure 10 - The PWWP domain of Pdp3 and H3K36me3 mediate the recruitment of Mst2: (A) + (E) binding of Pdp3 is abolished in a PWWP domain mutant and in strains lacking H3K36me3: ChIP enrichment of FLAG-Pdp3 at *mto1⁺*/*tef3⁺* and *sam1⁺*/*pgk1⁺*, data is depicted with background subtracted, *n* = 3 ± SEM; (B) ChIP enrichment of Mst2-FLAG over untagged at *mto1⁺*/*tef3⁺* and *mto1⁺*/*pgk1⁺*/*vtc4⁺*, data is depicted with background subtracted, n=4 ± SEM, zero enrichment represented by dotted line; (C) first and second panel - H3K36me3 enrichment over gene and third panel – H3 enrichment at the loci tested in (B), data is shown relative to *mst2-FLAG*; *n* = 3 ± SEM (for H3, *mst2-FLAG set2Δ n* = 2 ± range); (D) sequence alignment of the PWWP domains of Pdp1 and Pdp3, residues forming the binding pocket are marked in red with the point mutant shown in a darker shade.

In addition to testing transcription of the *mst2* and *pdp3* loci and the corresponding protein levels, I interrogated whether epitope tagging of either Mst2 or Pdp3 in its wild-type or point mutant form compromise silencing (Figure 11C). To this end, I examined transcription at *tlh1+/tlh2+* as these loci displayed de-repression in both *pdp3Δ* and *mst2Δ* (see Figure 8C – 3rd panel). I detected no de-repression of heterochromatin when either Mst2 or Pdp3 was fused to a FLAG tag (left and right panels, respectively). Rather in both cases less *tlh1+/tlh2+* was transcribed less than in the corresponding untagged strain. In contrast, mutating F109 in Pdp3 did resulted in 6-fold more mRNA expression than in the untagged strain, mirroring the silencing defect of *pdp3Δ*. In conclusion, the epitope tagging with FLAG as used in the ChIP experiments has no negative influence the function of either Pdp3 or Mst2. However, mutating F109 in the PWWP domain of Pdp3 results in a silencing defect. Based on these results and in agreement with previous findings [140], I conclude that Ppd3 recruits the Mst2 complex to gene bodies via specific interaction with H3K36me3 likely involving its PWWP domain.

A Influence of tagging and deletions on *mst2*[+] RNA expression and Mst2 protein levels
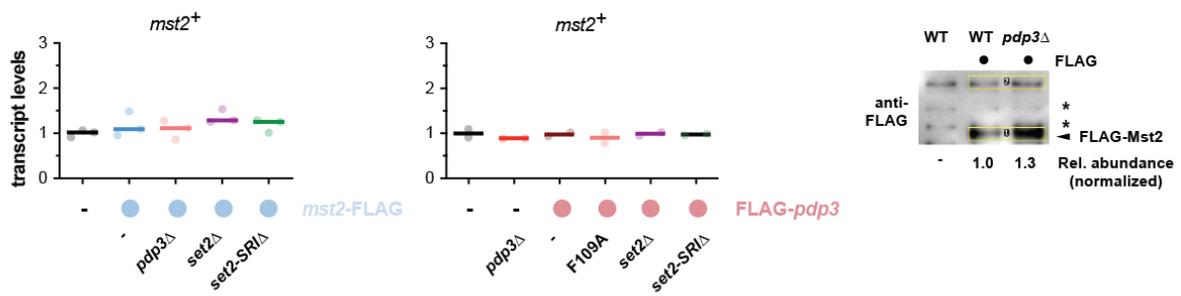
B Influence of tagging and deletions on *pdp3*[+] RNA expression and Pdp3 protein levels
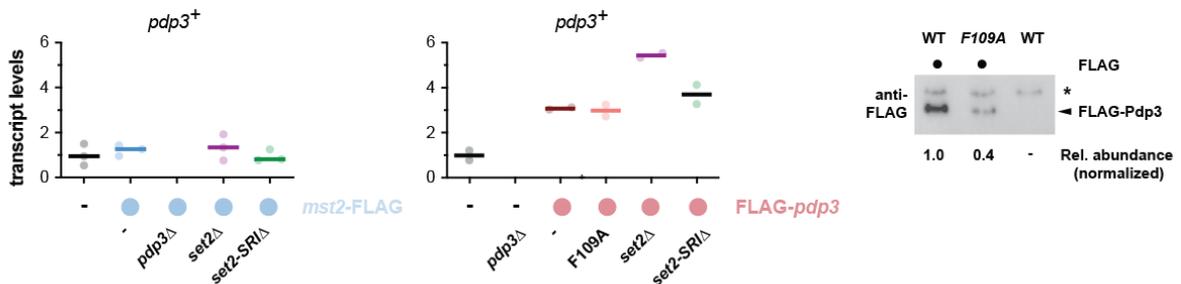
C Influence of tagging on silencing

tel1L
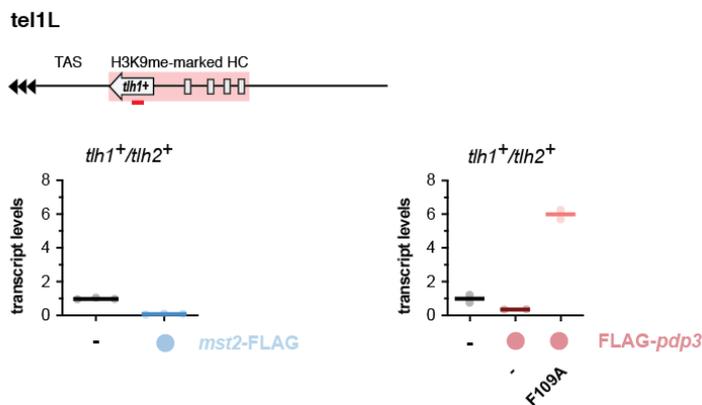
Figure 11- Control experiments for the strains used in Figures 9 and 10: (A) first and second panel - RT-qPCR at the *mst2*[+] locus, data has been normalized to *act1*[+] and is presented relative to wild-type, shown are individual data of 3 and 2 independent experiments (circles) and median (horizontal lines) for the Mst2-FLAG and FLAG-Pdp3 strains, respectively, last panel - immunodetection of Mst2-FLAG, lysate equating 1 OD was loaded per lane, numbers below represent protein enrichment relative to enrichment in Mst2-FLAG after normalization to uppermost unspecific band as loading control; (B) first and second panel - RT-qPCR at the *pdp3*[+] locus, data was normalized and is presented similar to (A), last panel - immunodetection of FLAG-Pdp3; experiment and normalization performed as in (A), except for presentation relative to FLAG-Pdp3; (C) RT-qPCR at subtelomeric *tlh1*[+]*/tlh2*[+], data has been normalized and is presented as in (A).

4.5   The silencing defect in *set2Δ* cells is caused by Mst2

Distribution of H3K36me2 and H3K36me3 within active genes differs among eukaryotes. For example, in chicken and budding yeast, H3K36me2 peaks towards the 3' end of genes, while it is enriched at promoters and the 5' region of genes in *Drosophila melanogaster* and *S. pombe* [128], [145], [186], [267]. In *S. cerevisiae*, H3K36me3 (but not H2K26me2) correlates with the rate of transcription [128], [146], [267]. However, my data implies that in *S. pombe* H3K36me3 is saturated on gene bodies regardless of the gene's transcription rate (see Figure 10C). This raises the question whether there is a specific function of H3K36me3 beyond transcriptional regulation.

In *S. pombe*, H3K36me3 can be sometimes detected within silenced chromatin, which seems counterintuitive as it is considered a euchromatic mark [177]. One possibility is that the detected H3K36me3 is a remnant of reestablishing heterochromatin during S phase [268]. However, H3K36 methylation is required for maintaining the 'knobs', a silenced region lacking histone marks that is found next to the subtelomeric region and constitutes a very condensed form of chromatin in the interphase nucleus [269]. Furthermore, loss of H3K36me, either by deletion of *set2+* or a mutation in histone H3 (H3K36R), has been associated with transcriptional de-repression at centromeres and telomeres [177], [233], [269]. Since I demonstrated that presence of Pdp3 and H3K36me3 ensures specific recruitment of Mst2 to gene bodies, I hypothesized that the silencing defect of *set2Δ* could be attributed to the delocalization of Mst2, resulting in the encroachment on heterochromatin. To test this hypothesis, *mst2+* in a *set2Δ* strain and analyzed the outcome by heterochromatic transcription at pericentromeric and subtelomeric heterochromatin.

At all tested loci, loss of *set2+* resulted in a silencing defect. At pericentromeric HC (Figure 12A - left side), I detected for *set2Δ* cells an upregulation of 2–4-fold at the *dg* and *dh* repeats as well as for the *imr::ura4+* reporter gene. In contrast, *mst2Δ set2Δ* displayed a suppression phenotype with silencing being completely restored at *imr::ura4+* and the *dg* repeats, and partially rescued at the *dh* repeats. As shown before (see Figure 3), loss of *mst2+* had no effect on pericentromeric heterochromatin. At subtelomeric heterochromatin (Figure 12A – right side) the silencing defect of *set2Δ* was more pronounced than at pericentromeric heterochromatin with a 10-fold, 14-fold, and a more than 60-fold increase in heterochromatic transcripts at *tlh1+/tlh2+*, *SPAC212.09c*, and *SPAC212.08c*, respectively. When I concomitantly deleted *mst2+*

in the *set2Δ* strain background, heterochromatic transcription was completely suppressed to the level seen in the *mst2Δ* mutant at all three loci.

Since de-repression of heterochromatin in *set2Δ* depends on *mst2+*, I tested whether a lack of Pdp3, which directly interacts with H3K36me3, would cause a similar phenotype, thus putting Pdp3 into the same pathway as Set2. As in the experiments before (compare to Figure 6 and Figure 8) I detected a moderate silencing defect with a 2-fold increase in transcripts at pericentromeric *imr::ura4+* in a *pdp3Δ* strain. Similarly, loss of Set2 caused de-repression of pericentromeric heterochromatin, albeit the de-repression was stronger than in *pdp3Δ*. De-repression in the *pdp3Δ set2Δ* double mutants was 3-fold and thus lower than the transcript level of *set2Δ* cells but higher than in *pdp3Δ*. I also tested silencing in these three mutants at subtelomeric heterochromatin domain of TEL1L using the *tlh1+/tlh2+* and *SPAC212.09c* loci (Figure 12B – right side). Transcriptional de-repression was more pronounced for the subtelomeric region than for pericentromeric heterochromatin, with a 3- and 6-fold increase and a 2- and 9-fold increase in the *pdp3Δ* and *pdp3Δ set2Δ* strains, respectively. This is in accordance with previous findings that indicate this region as more sensitive to chromatin perturbations [233]. Nonetheless, the behavior at subtelomeres was comparable to pericentromeric heterochromatin. Deletions of either *pdp3+* or *set2+* led to heterochromatin de-repression, with the *set2Δ* mutant displaying a stronger silencing defect than *pdp3Δ*, while the *pdp3Δ set2Δ* double mutant displayed partial suppression compared to the *set2Δ* single mutant.

Apart from Mst2 and Pdp3, Mst2C contains 5 other subunits: Eaf6, Nto1, Ptf1, Ptf2, and Tfg3, though not much is known about their functions within chromatin [245]. Of these, I excluded Tfg3 from further investigation as it is also a subunit of Ino80, TFIID, TFIIF, and SWI/SNF, thus any mutation would have a widespread effect [270]–[272]. Of the remaining four subunits, neither Eaf6 nor Ptf1 have been shown as vital for Mst2C, whereas Nto1 and Ptf2 have been revealed as critical for complex integrity and function [245]. Based on these previous observations, I investigated whether lack of either Nto1 or Ptf2 affects silencing in *set2Δ* deletion mutants (Figure 12B - second panels). The *set2Δ nto1Δ* and *set2Δ pft2Δ* double mutants resembled the *mst2Δ set2Δ* strain in that silencing of heterochromatin was fully restored at all tested loci. Likewise, neither loss of *nto1+* nor of *ptf2+* caused heterochromatic de-repression; rather, akin to *mst2Δ*, transcript levels remained comparable to WT at *imr::ura4+* and were decreased

at subtelomeric heterochromatin. This implies that the silencing defect of *set2Δ* depends on the integrity of Mst2C.
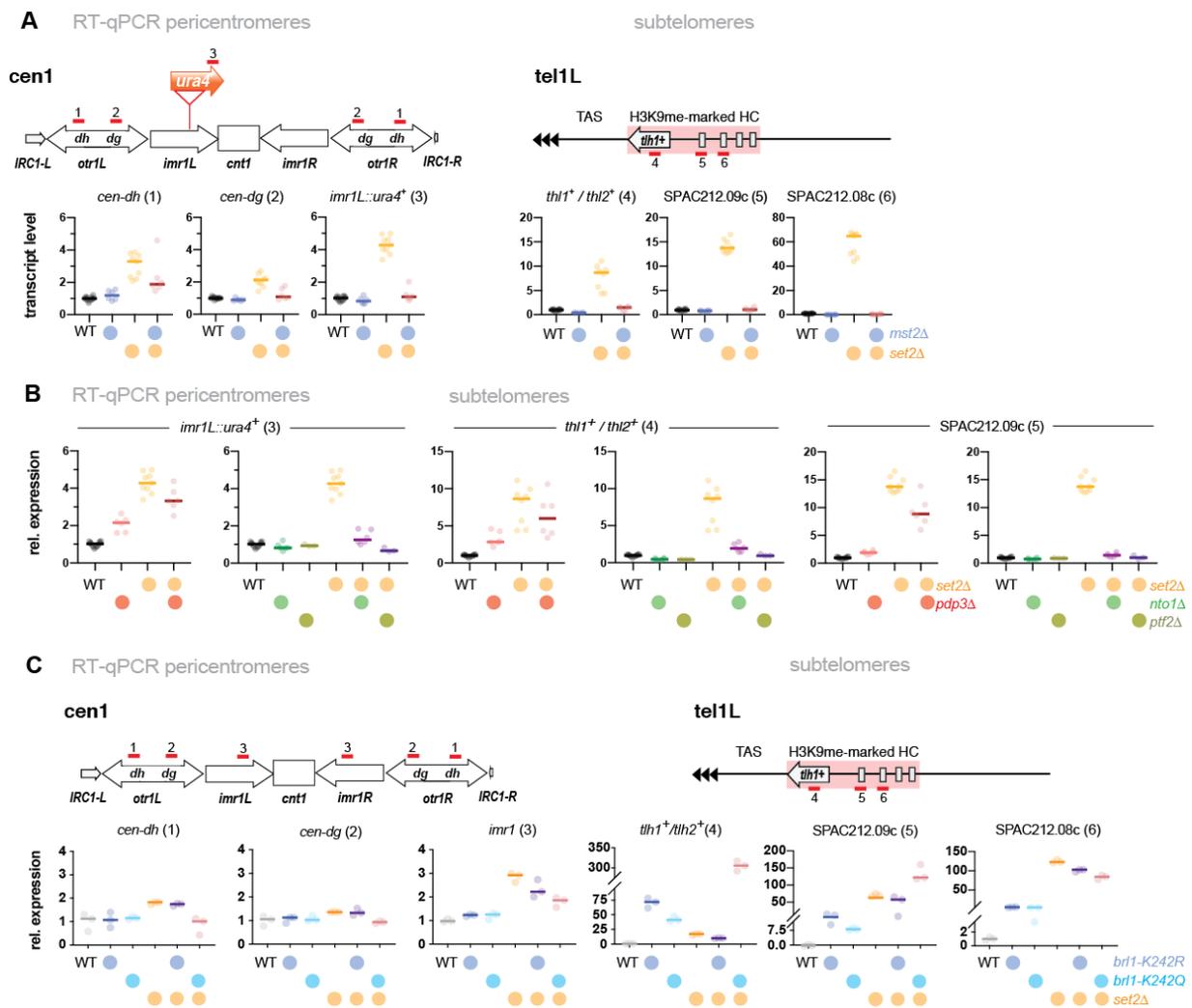
Figure 12 - The silencing defect of *set2Δ* is caused by encroachment of Mst2C on heterochromatin but Brl1-independent: shown are RT-qPCR experiments at pericentromeric and subtelomeric heterochromatin, (A) *set2+* and *mst2+* single knockouts as well as a *set2+ mst2+* double knockout, n = 6-12; (B) each 1st panel - *set2+* and *pdp3+* single knockouts as well as a *set2+ pdp3+* double knockout, each 2nd panel - *set2+ nto1+*, and *ptf2+* single knockouts as well as a *set2+ nto1+* and *set2+ ptf2+* double knockouts, *n* = 6, except *n* = 3 for *ptf2Δ* and *ptf2Δ set2Δ*, and *n* = 12 for WT; (C) *set2+*, *brl1-K242R*, *brl1-K242Q* single knockouts as well as *set2Δ brl1-K242R* and *set2Δ brl1-K242R* double mutants, *n* = 3; all data has been normalized to *act1+* and is depicted in relation to wild-type (WT), circles represent individual data and horizontal lines the median from n independent experiments.

As part of our collaborative work, we showed recently that Mst2 acetylates K242 of Brl1, a non-histone substrate [273]. Brl1 forms with Rhp6, a homolog of *S. cerevisiae* Rad6, the histone H2B ubiquitin ligase complex (HULC) [152], which mediates ubiquitylation of histone H2Bub at K119, thereby promoting H3K4 methylation and transcription [152], [274]. To interrogate whether Mst2C-dependent acetylation of Brl1

is responsible for the silencing defect of *set2Δ* in heterochromatin, I employed two previously used Brl1 mutants: *brl1-K242R* and *brl1-K242Q* [273]. Brl1-K242R cannot be acetylated, whereas Brl1-K242Q mimics the acetylated state. However, in contrast to deletion of *mst2⁺*, silencing in the absence of Set2 was not rescued in the *brl1-K242R set2Δ* double mutant. Rather, compared to *set2Δ* there was no detectable suppression at the outer centromeric repeats and only a partial suppression from 3- to 2.3-fold over WT at *imr::ura4⁺* (Figure 12C- 1st to 3rd panel). Furthermore, unlike in *mst2Δ* cells, silencing at subtelomeric heterochromatin in the *brl1-K242R* single mutant was reduced rather than enhanced, resulting in a 70-, 14- and 6-fold increase over WT at *tlh1⁺/tlh2⁺ SPAC212.09c*, and *SPAC212.08c*, respectively (Figure 12C – 4th to last panels). Since Brl1-K242Q mimics constitutively acetylated Brl1, its phenotype should be independent of Mst2 but epistatic with *set2Δ* [273]. Though the *brl1-K242Q* single mutant indeed showed de-repression for some of the heterochromatic transcripts examined, it was much less than seen for *set2Δ*. Even more surprisingly, when examining the *brl1-K242Q set2Δ* double mutant, I found that silencing was restored at pericentromeres, whereas I observed a synthetic de-repression at the subtelomeric *tlh1⁺/tlh2⁺* and *SPAC212.09c* loci, increasing transcription substantially compared to the *set2Δ* single mutant. Taken together, these observations for *brl1-K242R* and *brl1-K242Q* suggest that Brl1 is not the primary target of delocalized Mst2C in heterochromatin.

In summary, I found that *pdp3Δ set2Δ* exhibits a non-additive phenotype that is partially suppressed compared to *set2Δ*, whereas lack of Mst2, Nto1 or Ptf2 suppresses the silencing defect of *set2Δ* at all tested loci. This corroborates the notion that Pdp3 acts downstream of Set2, but upstream of the other Mst2C subunits. These results further imply that the silencing defect of *set2Δ* mutants is caused by encroachment of Mst2 on heterochromatin and underline the importance of H3K36me3 for the global regulation of Mst2C localization. However, the results of the experiments with the Brl1 mutants indicate that Mst2C has a different target in heterochromatin as compared to euchromatin.

4.6 Acetylation of H3K14 remains unaffected in the absence of Mst2

Mst2 is an anti-silencing factor that prevents the ectopic assembly of heterochromatin, as shown by our collaborative study [273]. Moreover, we found that Mst2C invades heterochromatin and causes a silencing defect when not anchored to gene bodies by

Pdp3 and H3K36m3. However, so far it remains elusive how Mst2 functions in the prevention of silencing. Mst2 belongs to the MYST family of histone acetyltransferases and acts redundantly with Gcn5 *in vivo* in acetylation of H3K14 (H3K14ac). Yet contrary to lack of Mst2, loss of Gcn5 does not perturb silencing, suggesting that Mst2C functions in a separate pathway to Gcn5 [242], [245]. To gain more insight into the role of Mst2C in chromatin regulation, I examined whether H3K14ac levels in euchromatin and heterochromatin are affected by delocalization or loss of Mst2. For this, I interrogated the levels of H3K14ac in a *pdp3Δ*, an *mst2Δ*, and in a WT strain at the *mto1+/tef3+* locus for euchromatin as well as pericentromeric and subtelomeric heterochromatin. As a gauge for the maximum accumulation of H3K14ac, I employed a null mutant of *clr3+* (*clr3Δ*), the H3K14ac-specific histone deacetylase [99]. Furthermore, to exclude indirect effects, I normalized the H3K14ac enrichments to H3 ChIP experiments I performed in parallel using the same lysates since loss of Clr3 has been associated with decreased nucleosome occupancy [101], [233]. By examining the *mto1+/tef3+* locus (Figure 13A), to which Pdp3 and Mst2 bind (left panel of Figure 4D and 4E), I found that neither loss of Pdp3 nor Mst2 significantly affected H3K14ac levels. except for a slight increase in H3K14ac over *tef3+* in *pdp3Δ* (right panel). In conformance with earlier studies, the *clr3Δ* mutant displayed a 25 to 50% loss of nucleosome occupancy and notable increase in H3K14ac enrichment, due to its role in counteracting histone turnover by global regulation of H3K14ac levels [43]. Similarly, I did not detect a significant difference in H3K14ac enrichment at any of the tested pericentromeric and subtelomeric loci in either *pdp3Δ* or *mst2Δ* (Figure 13B - bottom row)

The lack in net change of euchromatic H3K14ac levels in *pdp3Δ* and in *mst2Δ* suggests that Gcn5 likely compensates the loss of Mst2. However, these results also imply that Mst2 acts on another substrate that is not targeted by Gcn5.
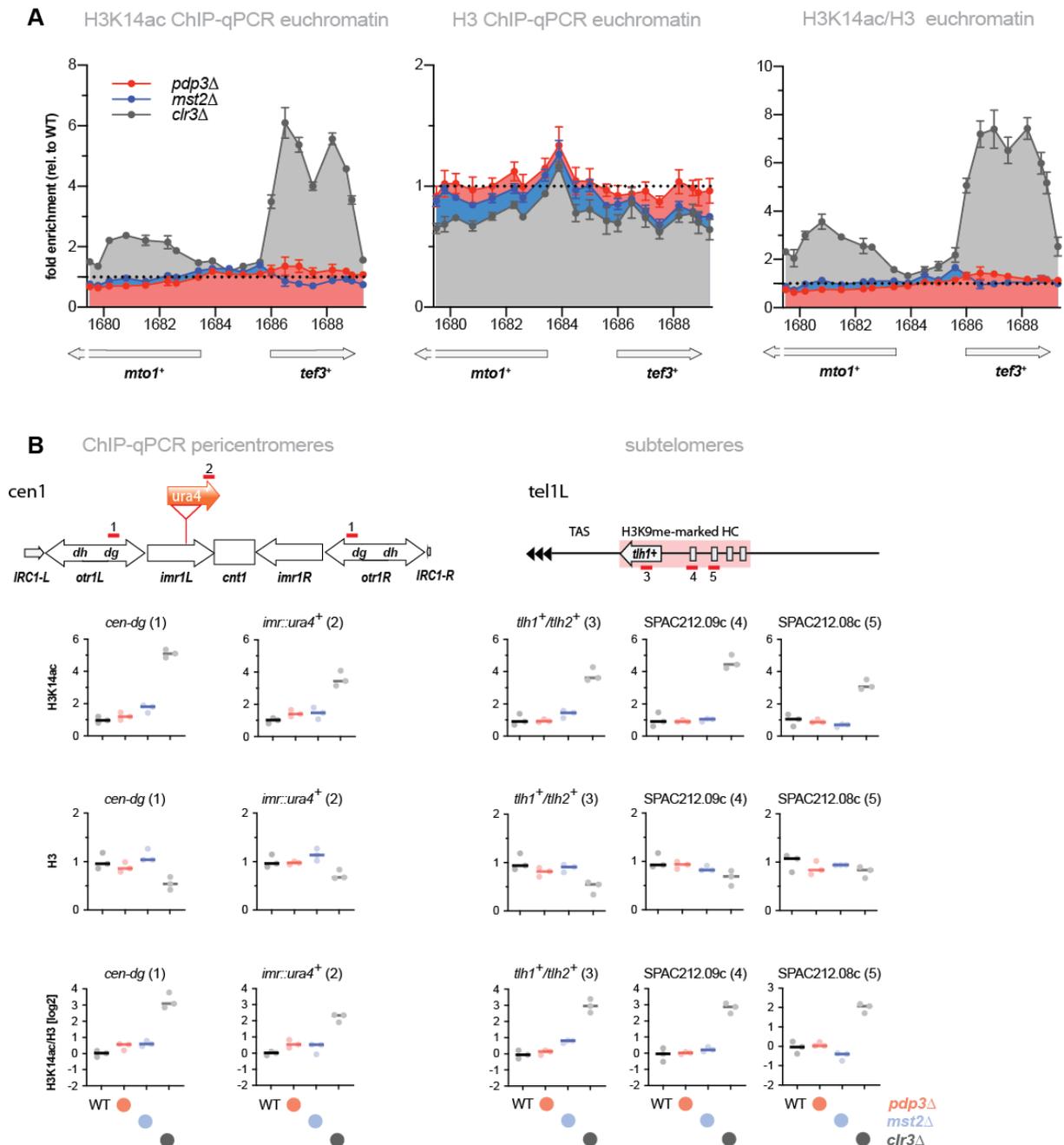
Figure 13 - Encroachment of Mst2C on heterochromatin does not affect acetylation of H3K14: ChIP-qPCR of H3K14ac and H3 enrichments in *pdp3*[+] and *mst2*[+] single knockouts with a *clr3*[+] knockout as positive control (A) enrichments at euchromatic *mto1*[+]/*tef3*[+], data for H3K14ac and H3 is shown relative to WT with n = 3 ± SEM; H3K14ac/H3 is shown as is (B) enrichments at pericentromeric and subtelomeric heterochromatin; enrichments for H3K14ac and H3 are shown relative to wild-type, The ratio of H3K14acc 7H3 is shown at log2 scale; represented is individual data (circles) of same experiments as in (A) with their median as horizontal line.

4.7 Mst2, but not Pdp3, prevents spreading of H3K9me2

My results showed that loss of Mst2 anchoring and invasion into heterochromatin induces de-repression of silenced regions, resulting in increased levels of heterochromatic transcripts (see Figure 8C and Figure 12C). On the other hand, loss

of Mst2 results in increased silencing compared to WT at subtelomeric heterochromatin (see Figure 8C- 4th and 5th panel, and Figure 12A). Thus, within subtelomeric heterochromatin, Mst2 appears to maintain basal levels of transcription. At euchromatic regions, neither Pdp3 nor Mst2 influence transcription (Figure 8C - last panel) but prevent the initiation of silencing [273]. However, none of these Mst2-dependent mechanisms involves acetylation of H3K14 (Figure 13). Methylation of H3K9 (here dimethylation, H3K9me2) is the hallmark of heterochromatin in *S. pombe* and higher eukaryotes [52], [275]. An earlier study showed that Mst2, like the ant-silencing factor Epe1, prevents spreading of H3K9me2 across heterochromatin boundaries [247]. Thus, I asked whether Pdp3 influences methylation of H3K9 as well. To analyze the influence of Pdp3 and Mst2 on H3K9 methylation, I performed H3K9me2-specific ChIP experiments at pericentromeric and subtelomeric heterochromatin and their boundaries in WT and the respective single mutant strains as well as the *mst2Δ pdp3Δ* double mutant.

When testing the pericentromeric region, I found that H3K9me2 levels in *pdp3Δ* were reduced by ~20% compared to WT (Figure 14A). Conversely, H3K9me2 outside the pericentromeric boundaries (inverted repeats at centromeres, IRC; Figure 14B) was not affected. Subtelomeric heterochromatin displayed an opposing behavior: While the first 18 kb of TEL1 of subtelomeric heterochromatin, H3K9me2 was not affected, the region beyond showed reduced H3K9me2 levels, reaching a minimum of ~50% compared to WT.

Next, I examined the strain lacking *mst2+*. Here, H3K9me2 levels remained unaffected inside the heterochromatic domain of the tested CEN1 region (Figure 14D). However, in agreement with the earlier study [247], H3K9me2 spread outside of heterochromatin at the pericentromeric boundary (IRC; Figure 14E). Similarly, I observed for the subtelomeres an increase in H3K9me2 starting from approximately the 18 kb with a maximum level at ~32 kb (Figure 14F).

The *mst2Δ pdp3Δ* double mutant exhibited a similar phenotype as the *pdp3Δ* single mutant inside pericentromeric heterochromatin but presented the phenotype of *mst2Δ* with H3K9me2 spreading outside of the heterochromatin boundaries (Figure 14G and 14H). Similarly, at telomere-proximal subtelomeres, H3K9me2 in the *mst2Δ pdp3Δ* double mutant resembled the *pdp3Δ* single mutant, while telomere-distal ~18 kb the double mutant phenocopied *mst2Δ* (Figure 14I). In summary, *pdp3Δ* and *mst2Δ* displayed differing phenotypes with the *mst2Δ pdp3Δ* acting like *pdp3Δ* inside

heterochromatin but like *mst2Δ* at heterochromatin boundaries and heterochromatin-adjacent regions. The reduction in pericentromeric H3K9me2 levels in *pdp3Δ* and at pericentromeres in the double mutant suggests that Pdp3 indirectly influences heterochromatin levels. The fact that I detected spreading of heterochromatin in the *mst2Δ* single and double mutant but not the *pdp3Δ* single mutant suggests that transient presence of Mst2 is sufficient to prevent spreading of H3K9me2 at heterochromatin boundaries.
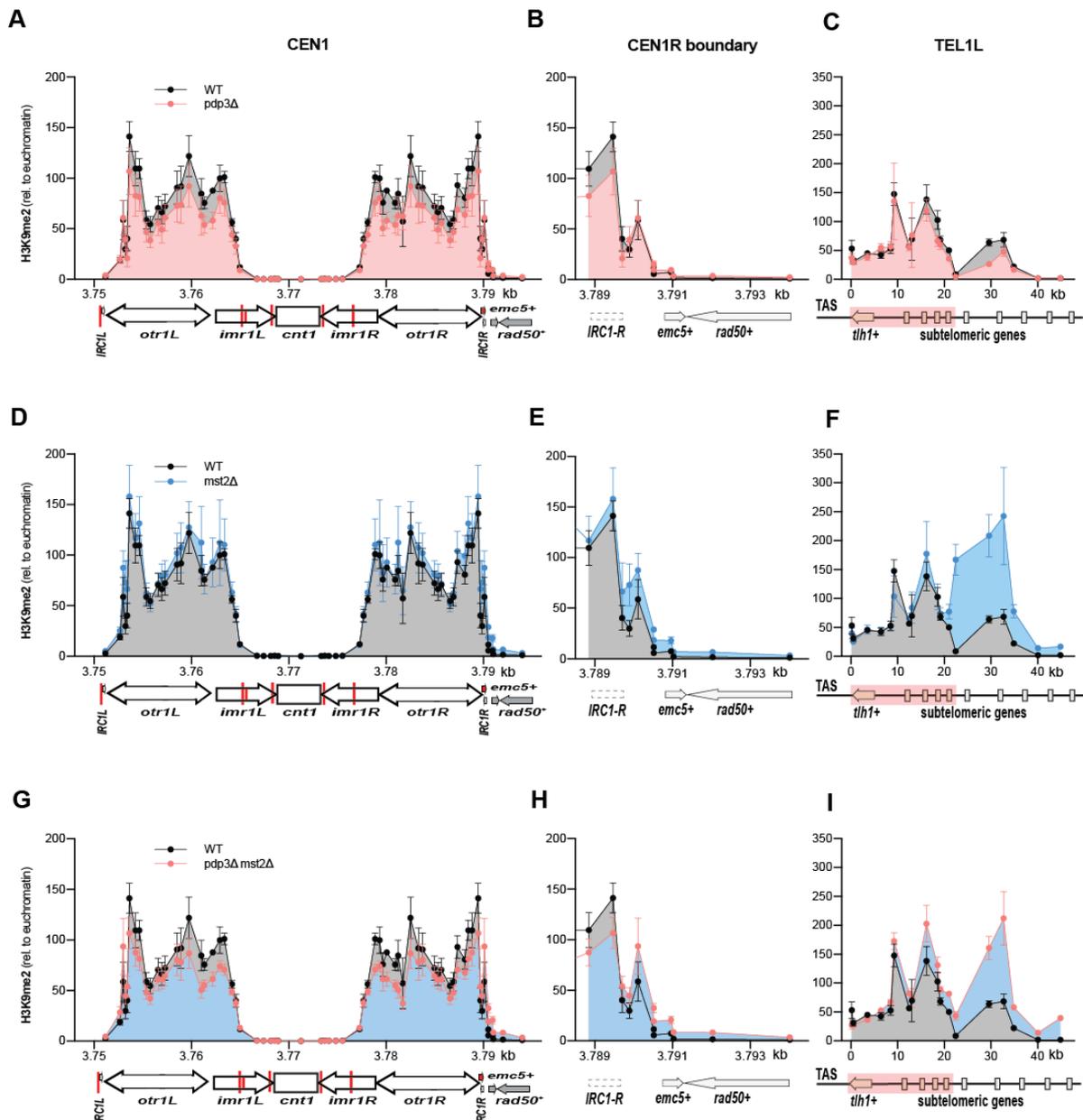

Figure 14 - Mst2 prevents spreading of H3K9me2 over heterochromatin boundaries independent of Pdp3: Shown is enrichment of H3K9me2 over different heterochromatic regions with (A, D, G) pericentromeric heterochromatin of centromere 1, (B, E, H) righthand boundary of centromere 1, and (C, F, I) TEL1L; (A - C) enrichment in *pdp3Δ*, (D-F) enrichment in *mst2Δ*, and (G-I) enrichment in *mst2Δ pdp3Δ*; all data have been normalized to the average of three euchromatic genes (*adf1⁺*, *sam1⁺*, *tif51⁺*); *n* = 3 ± SEM.

4.8 The *mei4*⁺ locus presents a special case with regards to the function of Mst2C

When performing H3K9me2 ChIP, I first used the housekeeping gene *act1*⁺, a commonly used reference for both RT-qPCR and ChIP experiments, as a control for normalization. However, while usually euchromatic genes display no notable H3K9me2 levels and remain unaffected by the deletion of heterochromatin factors, I noticed an increase in H3K9me2 for *act1*⁺, when *pdp3*⁺ was deleted (compare Figure 10F). Interestingly, the *act1*⁺ locus is situated next to *mei4*⁺, a meiotic gene.

Meiotic genes belong to the class of facultative heterochromatin [276]. These genes are transcriptionally and post-transcriptionally silenced during vegetative growth, and form small 'heterochromatic islands' within a euchromatic domain [221]. Intriguingly, while heterochromatin islands, like the *mei4*⁺ gene, are decorated with H3K9me2 during cell growth, the levels of this modification are very low compared to constitutive heterochromatin. [221]. H3K9me2 at heterochromatin islands is established via the exosome pathway through the RNA elimination factor Red1 that recruits Clr4. Thus, H3K9me2 at heterochromatin islands may be a byproduct. Interestingly, ChIP-chip data revealed that H3K9me2 levels are further enriched at *mei4*⁺ in *mst2Δ* [247]. My H3K9me2 data for *act1*⁺ raised the question whether Mst2 and Pdp3 are involved in the regulation of silencing at heterochromatin islands modified with H3K9me2. To test this hypothesis, I conducted H3K9me2 ChIP experiments on the *mei4*⁺ locus, and its two flanking genes *cdk9*⁺ and *act1*⁺.

Consistent with other euchromatic genes (compare Figure 9D and 9E), Mst2 and Pdp3 are present at all three loci (Figure 15A and 15B). Their recruitment depends on Pdp3 or its PWWP domain, respectively. Interestingly, Mst2 recruitment was stronger at the highly expressed *act1*⁺, compared to the other two genes (Figure 15B). In *set2Δ* and *set2-SRIΔ* mutants, which completely lack H3K36me or only H3K36me3, respectively, I detected neither Pdp3 nor Mst2 at the gene bodies of *cdk9*⁺ and *mei4*⁺ (Figure 15D and 15E). However, like the highly expressed *tef3*⁺ (Figure 10A and 10B), *act1*⁺ also retained binding of Pdp3 in the absence of the Set2-SRI domain, supporting the notion of an alternative mechanism apart from interaction of Set2-SRI domain with the RNAP II CTD. As seen for the other loci tested (see Figure 10C), enrichment of Pdp3 and Mst2 overlapped with H3K36me3, with nucleosome density remaining unaffected in the *set2-SRIΔ* (Figure 15G). Thus, the *mei4* locus does not differ from other euchromatic regions tested in terms of Pdp3 and Mst2 binding.
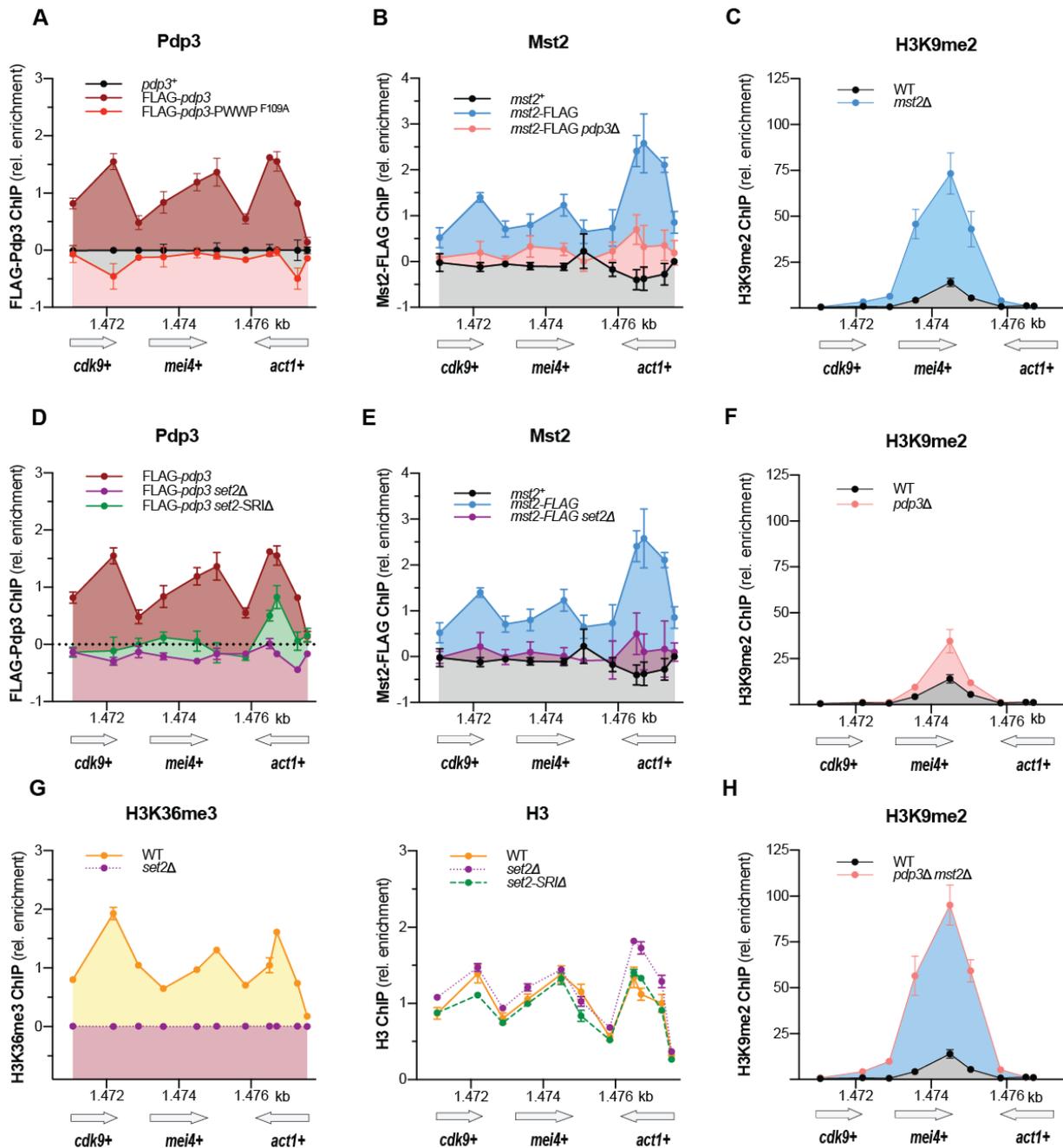
Figure 15 - The *mei4* locus displays similar behavior to the previously tested loci for recruitment of Pdp3 and Mst2 as well as for H3K36me3 but peculiar behavior in terms of H3K9me2 enrichment: (A and D) ChIP-qPCR of FLAG-Pdp3 with (A) Pdp3_F109A, and (D) Set2 mutants, data shown with background subtracted; (B and E) ChIP-qPCR of Mst2-FLAG in (B) *pdp3*Δ, and (E) Set2 mutants; data shown with background subtracted; (C, F, H) ChIP-qPCR of H3K9me2 in *pdp3*Δ (C), *mst2*Δ (F) and *mst2*Δ *pdp3*Δ (H), data relative to three euchromatic loci (*adf1*+, *sam1*+, *tif51*+); (G) ChIP-qPCR of left – H3K36me3, right – H3; data shown relative to respective enrichments in Mst2-FLAG; *n* = 3 ± SEM for all experiments.

However, since *mei4*+ is also decorated with H3K9me2, I tested whether H3K9me2 levels are altered in *mst2*Δ, a *pdp3*Δ, or the *mst2*Δ *pdp3*Δ strain. I discovered a substantial increase in H3K9me2 in *mst2*Δ at *mei4*+ (14-fold to 73-fold over the average of 3 euchromatic loci) coupled to spreading of this mark into *cdk9*+ and *act1*+ (Figure

15C). Interestingly, I noted a similar affect for *pdp3Δ*, although at lower level (14 – 35-fold) (Figure 15F). Furthermore, whereas *mst2Δ pdp3Δ* behaved like a *pdp3Δ* single mutant inside constitutive heterochromatin (compare Figure 14), at *mei4*+ the double mutant looked rather like the *mst2Δ* strain (Figure 15H), though H3K9me2 was more enriched (up to ~95-fold over the average of 3 euchromatic loci).

In summary, the *mei4*+ locus displayed the characteristics of other euchromatic loci for binding of Mst2 and Pdp3 as well as for H3K36me3 but showed behavior reminiscent of heterochromatin boundaries for H3K9me2. However, this data also suggests that H3K9me2 spreading at this and similarly regulated heterochromatin islands is completely suppressed by direct recruitment of Mst2 to the locus via Pdp3 and partially suppressed in absence of Pdp3.

5 Discussion

Mst2 and Gcn5 are H3K14-acetylating histone acetyl transferases. However, whereas Gcn5 has no influence on heterochromatin silencing, Mst2C promotes transcription of pericentromeric heterochromatin in the absence of a functional RNAi machinery [242]. Paradoxically, the Mst2C subunit and PWWP domain protein Pdp3 displays opposing behavior as deletion of *pdp3+* leads to increased heterochromatic transcription of pericentromeric heterochromatin [231], [277]. Earlier studies indicate that a variety of specification factors contribute to the maintenance of HC via positive feedback loops [278], [279]. Here, I will discuss how the silencing defect of Pdp3 and Set2 are connected to their functions in a positive feedback loop that promotes transcription and suppresses HC formation.

5.1 Pdp3 contributes to heterochromatin maintenance

RT-qPCR experiments revealed that the silencing defect caused by the loss of Pdp3 not only compromises silencing of pericentromeric HC, as reported in a previous study [231], but affects HC at a global scale. This came to light when I examined transcript levels in *pdp3Δ* strains with primers specific to pericentromeric HC and a primer set that is annealing to the telomere proximal 3'-end of the *tlh1/tlh2+* gene. In contrast to Pdp3, Mst2 has been described as an anti-silencing factor that counteracts RNAi, a prerequisite to HC formation. Using functionally genetics I found through SGA that the silencing defect of *pdp3Δ* was suppressed by additionally deleting any other Mst2C subunit (see Figure 2). This gave rise to the notion that Pdp3 may act as a negative regulator for Mst2C with regard to antagonizing heterochromatin

Similar behavior of *mst2Δ* to catalytically inactive Mst2 point mutants in a previous study indicated that any influence of Mst2C on heterochromatin is coupled to its catalytic activity [242].

Corroborating this notion, concomitant deletion of *mst2+* completely suppressed the silencing defect of *pdp3Δ* at both pericentromeric *imr::ura4+* and several subtelomeric genes (see Figure 6), which suggests that the silencing defect is caused by the catalytic activity of Mst2C.

5.2 Pdp3 acts as a specification factor for Mst2C localization

In *S. cerevisiae,* the remodeler Isw1b is recruited to actively transcribed regions via the PWWP subunit Ioc4p that interacts with H3K36me3 [280]. Similarly, the Mst2C homolog NuA3b is recruited to H3K36me3 via its PWWP domain subunit Pdp3p [140]. In *S. pombe*, Pdp3 is one of three PWWP domain proteins [266]. While the function of Pdp2 has not been determined, Pdp1 forms a heterodimer with the H4K20-methylating KMT Set9 and recruits this enzyme to H4K20me1 where it mediates the addition of further methyl groups to H4K20me1 [266]. This study further revealed that mutating the binding site of Pdp1-PWWP caused diminished Set9 recruitment to chromatin. However, only H4K20me3 levels were reduced, while H4K20me1 and H3K20me2 was increased or unaltered, respectively, suggesting that delocalized Set9 is still active, though not fully processive.

Mst2C is able to acetylate H3K14, and potential other targets, in the absence of Pdp3 [245]. In addition, my results showed that loss of Pdp3 causes transcriptional de-repression that is suppressed when $mst2^+$ is deleted. Therefore, we tested the hypothesis whether Pdp3 localizes Mst2C to specific chromatin regions to restrain its activity and prevent aberrant acetylation of silent chromatin. Indeed, our collaborators at the FMI showed using DamID that Mst2 is usually depleted from heterochromatin but invades repressed pericentromeres and subtelomeres in the absence of Pdp3. Thus, Pdp3 was critical to keep Mst2C from encroaching on HC. By determining the binding pattern of Pdp3 and Mst2 on EC by ChIP, I discovered that both proteins preferentially localize to gene bodies, while being depleted from the intergenic regions. Furthermore, Mst2 recruitment was lost in absence of Pdp3. This implies that, similar to the PWWP protein Ioc4p for *S. cerevisiae* remodeler Isw1b, Pdp3 is responsible for keeping the Mst2 complex to euchromatin [280].

Additional evidence was provided by mutagenesis studies with other PWWP domain proteins such as Pdp1 [266]. To test whether Pdp3 is directly interacting with chromatin, I first mutated one of the three binding residues comprising the PWWP domain (F109A). This led to a loss of Pdp3 binding to chromatin. While protein levels of Pdp3_F109A were also partially reduced, probably due instability, the complete loss of binding of Pdp3_F109A suggested that this was largely due to a loss of function of the PWWP domain. Although mass spectrometry data from previous studies indicates that Pdp3 is more than 100-fold higher translated than Mst2 [281], steady state levels examined by immunoblot experiments using the same epitope tag show comparable

amounts of Mst2 and Pdp3 , suggesting that stability of Pdp3 might require interaction with Mst2C (Figure 6A and 6B). To test this further end, interaction of Pdp3 and Mst2 could be examined by co-immunoprecipitation experiments with Pdp3 and Pdp3_F109A, as well as when Mst2 is overexpressed.

To identify the binding site on chromatin for Pdp3 we focused on H3K4me and H3K36me, as both residues are targeted by NuA3 the, *S. cerevisiae* homolog of Mst2C, and are reportedly recognized by PWWP domains [141], reviewed in [200]. To this end, our collaboration partner studied genome-wide localization of Mst2 in *set1Δ* and *set2Δ* strains by DamID. This revealed that loss of Set2, but not Set1, caused delocalization of Mst2 (see Figure 4C and data not shown). Therefore, unlike the NuA3a subcomplex, which is recruited to H3K4me3 via its PHD finger subunit Yng1 [139], Mst2C is exclusively targeted to H3K36me. In both *S. cerevisiae* and S. pombe, H3K36me2 is sufficient to mediate HDAC recruitment, suggesting a different function for trimethylated H3K36 [184], [185], [264]. In *S. cerevisiae* H3K36me3 is recognized by Ioc4 and Pdp3p. Moreover, in *S. pombe,* H3K36me3 was recently shown to be critical for heterochromatic silencing and the suppression of cryptic transcripts [177]. Consistent with previous reports, I found that H3K36me3 was distributed across the gene body. To elucidate whether Pdp3 discriminates between di- and trimethylated H3K36 I took advantage of truncated mutant lacking the Set2– Rpb1 interaction (SRI) domain, which can convey mono- and dimethylation of H3K36 but not H3K36me3 [177]. This revealed that binding of Pdp3 and recruitment of Mst2, respectively, were lost in absence of H3K36me3 at gene bodies, though H3 levels remained the same. Therefore, the PWWP domain of Pdp3 is specific for H3K36me3.

5.3 The interaction of Pdp3 with H3K36me3 contributes to a positive feedback loop promoting transcription

Results from our collaboration partner suggest that Mst2C is part of a regulatory circuit that prevents ectopic silencing of euchromatic genes by RNAi. In a previous study, they uncovered that mutation of *paf1+* or other subunits of Paf1C results in the local production of siRNAs and accumulation of H3K9me at a locus targeted by an RNA hairpin [282]. In our collaborative study, genetic experiments with a *paf1* mutant and *mst2Δ* revealed that the corresponding double mutant was more prone to ectopic silencing compared to the *paf1* mutant alone [273]. Therefore, in the absence of Mst2, Paf1 likely acts as a buffer to prevent ectopic silencing and allows for normal

progression of transcription in euchromatin. Mst2C is a known acetyltransferase for H3K14 whose acetylation has been shown to promote DNA damage response but also histone turnover in HC domains [101], [245]. However, several lines of evidence suggest that Mst2 has additional targets besides H3K14. Loss of Pdp3 causes neither a decrease in this modification at euchromatic genes not does this induce increased H3K14ac across pericentromeric and subtelomeric HC, i.e. under conditions when Mst2 encroaches heterochromatin. Similarly, loss of Mst2 did not affect euchromatic or heterochromatic H3K14ac enrichment. Likely Gcn5, which acts redundant in acetylating H3K14, compensates for the loss of Mst2 [283], [284]. Furthermore, *mst2Δ* but not *gcn5Δ* is capable of bypassing RNAi [242]. Conversely, the silencing defect of HDAC mutants cannot be suppressed by concomitant deletion of *mst2+* [242]. Put into context with the present H3K14ac data, I conclude that Mst2 has an additional target besides H3K14, whose acetylation affects heterochromatin initiation. Through a combination of pan-acetylation ChIP and mass spectrometry in *mst2Δ* and *gcn5Δ* strains, our collaborators identified a new Mst2 target involved in preventing ectopic heterochromatin, the E3 ubiquitin ligase Brl1. Brl1 is a subunit of the H2B ubiquitin ligase complex (HULC) that monoubiquitylates histone H2B at lysine 119 (H2Bub), a mark that is associated with positive regulation of transcriptional elongation [152], [285]. In our collaborative study, we showed that acetylation of Brl1 promotes HULC activity and di- and trimethylation of H3K4me [273], which is consistent with the findings that this modification requires the presence of H2Bub on gene bodies (see chapter 2.1.4.4). Set2 is recruited to transcribed genes via its SRI domain that interacts with the phosphorylated C-terminus of elongating RNAPII. In addition, H3K36me3 deposition also requires the Paf1 complex [176]. Thus, the recruitment of Mst2C to H3K36me3 participates in a positive feedback loop promoting transcription.

Taking the findings into account (i) that the *mst2Δ paf1* double mutant displays higher rates of ectopic silencing, (ii) that Pdp3 target Mst2C to H3K36me3 and (iii) that Mst2C acetylates Brl1, the following working model for the prevention of ectopic silencing by Mst2C emerges. Concomitant deletion of *mst2+* in the *paf1* mutant may result in slower transcription compared to the *paf1* single mutant, which may result in prolonged presence of nascent RNA at the locus. Furthermore, these cells expressed an RNA hairpin, that caused the production of reporter gene-specific siRNAs loaded onto RITS. The nascent reporter gene RNA is targeted by RITS and acts as nucleation site for HC formation via RNAi [67], which shuts down transcription of the reporter gene. In

contrast, slowed down transcription in the *paf1* mutant is suppressed when Mst2C is recruited to H3K36me3 by Pdp3 and acetylates Brl1, as the succeeding increase in H2Bub promotes the positive feedback loop described in Figure 2 .

5.4   The silencing defect of *set2Δ* is caused by the delocalization of Mst2C

The Mst2C functions not only in the prevention of ectopic silencing euchromatin but is also required to maintain a basal level of transcription in subtelomeric heterochromatin [238]. This is further supported by my observation that the levels of several subtelomeric transcripts were reduced below WT level in yeast strains lacking Mst2 (Figure 6D). As mentioned above, Mst2C encroaches on heterochromatin when not anchored to euchromatin by its subunit Pdp3. Similarly, Mst2C was delocalized from euchromatin in the absence of Set2 or when a Set2-SRIΔ truncation mutant was expressed (Figure 10B). In addition, earlier studies reported that heterochromatic transcription at pericentromeres and subtelomeres is elevated in the absence of Set2 [177], [233], [269]. Given these observations, it seems likely that the silencing defect not only of *pdp3Δ* but also of *set2Δ* is based on the delocalization of Mst2C to heterochromatin. To test this hypothesis, I analyzed how heterochromatic transcription in a *set2Δ* strain is affected by concomitant deletion of *pdp3+* or *mst2+*. Akin to *pdp3Δ*, loss of *set2+* caused a silencing defect at pericentromeric and subtelomeric HC, suggesting Set2 and Pdp3 work in the same pathway. Heterochromatin silencing was more affected in the *set2Δ* than in *pdp3Δ*, however, the *pdp3Δ set2Δ* double mutant showed a non-additive phenotype, which is in line with Set2 working upstream of Pdp3 (Figure 12B). This is underlined by the revelation that, as seen for *pdp3Δ*, heterochromatic transcription in *set2Δ* was completely suppressed when *mst2+* deleted (Figure 8B - 8D and Figure 12A). Similarly, silencing was restored when *nto1+* or *ptf2+*, two other subunits that are critical for Mst2C integrity and function [245] were deleted (Figure 12B). From these observations I conclude that the silencing defect in strains lacking Set2 is solely caused by Mst2C encroaching on heterochromatin.

The requirement of Mst2C for basal heterochromatic transcription as well as the silencing defect caused by its delocalization raise the hypothesis that Mst2C has acetylates a substrate within heterochromatin as well. To test whether Mst2C targets Brl1 in heterochromatin, I employed two mutants we generated in our collaborative study [273], Brl1-K242R, which cannot be acetylated, and Brl1-K242Q, which mimics constitutive acetylation (Figure 12C). However, contrary to our prediction that Brl1-

K242R would act like *mst2Δ* and rescue silencing in *set2Δ*, heterochromatin transcription in the *set2Δ* double mutant was unaffected or only partially suppressed. Even more unexpectedly, the *brl1-K242Q set2Δ* displayed synthetic phenotype at several subtelomeric loci. Thus, I conclude from this observation that Mst2C does not acetylate Brl1 within heterochromatin, or at least that Brl1 is not the relevant target. Indeed, this result is in accordance with a previous study on Set2 in *S. cerevisiae*, where the authors discovered that a silencing defect due to lack of Set2 is exacerbated by concomitant deletion of Paf1 complex subunits and Bre1, the homolog of Brl1 [286]. If Bre1 were also acetylated by NuA3B in heterochromatin, then deletion of *bre1⁺* should have suppressed the silencing defect of *set2Δ*. However, as de-repression was enhanced instead, this did not seem to be the case. These results further suggest that acetylation of Brl1, and likely Bre1, require the respective KAT to be anchored to euchromatin.

In addition, Mst2C does not seem to regulate heterochromatic transcription by acetylation of H3K14 as neither eu- nor heterochromatin showed altered H3K14ac in *pdp3Δ* or *mst2Δ* (Figure 8). Likely, H3K14ac is maintained by Gcn5, with which Mst2C acts redundantly [284].

In conclusion, I propose that Mst2C has another target in heterochromatin that is required for maintaining basal transcription but that can be modified — in contrast to Brl1 — also by transiently bound Mst2C. This observation underlines the critical role of Pdp3 sequestering Mst2C to EC.

5.5 Pdp3 is likely not the only anchoring factor in Mst2C

Although Pdp3 acts downstream of Set2, the phenotypes of *pdp3Δ* and *set2Δ* mutants differ from each other with respect to heterochromatic transcription. De-repression in *pdp3Δ* is significantly weaker that in the *set2Δ* mutant (Figure 12B). This discrepancy between the silencing defects in *pdp3Δ* and *set2Δ* might be linked to a putative role of Pdp3 in stabilizing the complex and thereby enhancing acetylation even though it is not required for catalytic activity. This hypothesis would need to be tested by performing RT-qPCR in a Set-SRIΔ strain in the absence and presence of Pdp3, as HC transcript levels should drop in that case in a *pdp3Δ* strain. However, there might also be other factors involved. According to recently published data on Set2 and H3K36me3 by the Murakami group, both the pericentromeric and subtelomeric region display a low amount of this mark with the amount in the subtelomeric region

decreasing towards the chromosome ends in chromosome 1 and 2 [177], [269]. Moreover, *SPAC212.08c*, which is found to be most repressed among the tested subtelomeric heterochromatin loci, was much more affected in *set2Δ* than in *pdp3Δ* (compare Figure 8C, and Figure 12A). This suggests while Mst2C cannot stably interact with H3K36me3 in the absence of Pdp3, it only moves freely when H3K36 methylation has been abolished through the deletion of *set2+*. Thus, even though Pdp3 is required to for stable binding of Mst2C to gene bodies, a second Pdp3-independent mechanism involving H3K36 methylation might exist to prevent Mst2C encroachment on silent chromatin. Among the other subunits of Mst2C, the PHD domain protein Nto1 poses a likely candidate. The *S. cerevisiae* homolog of Nto1, a subunit of the Mst2C homolog NuA3, contains two PHD domains, and one of these domains displays binding affinity for H3K36me3 [244]. Therefore, Nto1 could have a similar binding affinity. However, testing this hypothesis would require mutating the PHD domain, since Nto1 is essential for the integrity and function of Mst2C [245].

5.6 Mst2C activity and localization influence the maintenance of the EC-HC boundary and ectopic silencing

Mst2C fulfils multiple functions in chromatin regulation. Acetylation of H3K14 by Mst2C and Gcn5 acts as a signal for the remodeler RSC in DNA damage response and reduces nucleosome density by promoting histone turnover [245]. In our collaborative study, we showed that Mst2C also targets the HULC subunit Brl1, thereby promoting H2Bub and transcription, and prevents ectopic silencing [273] Lastly, I showed that Mst2C is part of a Pdp3-independent pathway that promotes a basal level of transcription in heterochromatin, but becomes hyperactivated when Mst2C is no longer bound to transcribed chromatin in *pdp3Δ* and Set2 mutants. However, loss of Pdp3 and Mst2C may also affect the distribution of silencing factors on chromatin. For euchromatin, this is corroborated by my observations for the *mei4+* locus, which is surrounded by *cdk9+* and *act1+*. The *mei4+* locus is a heterochromatic island marked by H3K9me2 [221]. Here, loss of both Mst2 and of Pdp3 appear to promote silencing. In wild-type cells, all three loci are decorated with H3K36me3 to which Pdp3 and Mst2 are recruited Figure 15A, 15B, and 15G). Similar to other euchromatic domains, the recruitment of Mst2 is lost in the absence of either Pdp3 or H3K36me3. An exception of this observation is the residual binding of Pdp3 to the genes *act1+* and *tef3+* in the Set2-SRI mutant (Figure 10A and Figure 15D), suggesting a different mechanism in

H2K36me3 establishment (Figure 10C). H3K9me2 enrichment at the *mei4+* locus was increased in the absence of Mst2 (Figure 15C). This was also the case for H3K9me2 in *pdp3Δ*, though to a much lower degree (Figure 14F). The *mst2Δ pdp3Δ* double mutant essentially displayed a similar enrichment compared to the single *mst2Δ* mutant. Likewise, I detected H3K9me2 spreading at the pericentromeric boundary region of CEN1R and the region adjacent to TEL1L in *mst2Δ* and *mst2Δ pdp3Δ* (Figure 14E, 14F, 14H, and 14I). Based on their role in preventing ectopic silencing, the loss of Pdp3 and Mst2C is predicted to make euchromatin more prone to silencing, resulting in increased accumulation of heterochromatin.

Loss of Mst2C may also affect distribution of silencing factors indirectly. In contrast to the other loci tested at subtelomeres, loss of Mst2 did not suppress silencing at the *tlh1+/2+* loci but caused de-repression instead. In addition, the silencing defects in *pdp3Δ* and *set2Δ* at this locus were only partially rescued in the *mst2Δ pdp3Δ* and *mst2Δ set2Δ* double mutants (Figure 8C and Figure 12A, respectively). Yet, while H3K9me2 in pericentromeric and subtelomeric HC, was moderately reduced in *pdp3Δ*, it was unaltered in the absence of Mst2 (Figure 14A-14F). This suggests that the cause the heterochromatin derepression at *tlh1+/tlh2+* acts downstream of H3K9me2. The HP1 protein Swi6 binds to H3K9me2 and H3K9me3 via its chromodomain and acts as binding partner for other proteins involved in heterochromatin regulation, e.g. Epe1 [80], [230]. Furthermore, Swi6 proteins can oligomerize, thereby aiding in the spreading of heterochromatin [229]. Swi6 is also highly mobile [287] but its cellular population is limited [288]. Therefore, if ectopic silencing of a region is initiated and H3K9me2/3 starts to accumulate, then Swi6 will be likely redistributed to other domains. As subtelomeric HC has negotiable boundaries that are less rigid (see section 2.4), Swi6 is more likely to be relocated from the HC bordering regions. Thus, the silencing defect in *mst2Δ* at the TEL1L boundary genes may stem from the redistribution of Swi6 to ectopically silenced euchromatin. It is also plausible that this reorganization is partially responsible for the silencing defect in *pdp3Δ*.

In summary, the activity of Mst2C and the localization of the complex influence heterochromatin maintenance not only directly but also indirectly.

5.7 Concluding remarks

The findings from this study have provided new insights into how euchromatin maintenance is regulated by a positive feedback loop involving the acetyltransferase

Mst2C, H3K36me3 and H2Bub. Particularly, the study revealed that the PWWP domain protein Pdp3 is not just a recruitment factor but also required to maintain the identity of chromatin domains, i.e. euchromatin and heterochromatin. This function is achieved through regulating the localization of Mst2C by Pdp3. The study demonstrated that Mst2C promotes transcription at its target location on gene bodies and prevents spreading of H3K9me2 over HC boundaries through an H3K14ac-independent mechanism involving the HULC subunit Brl1.

In addition, I have uncovered a Pdp3-independent activity of Mst2C that contributes to maintaining a basal transcription level at subtelomeric HC, which does not involve Brl1 or H3K14ac. When Mst2C is delocalized from actively transcribed chromatin and gains increased access to HC in the absence of Pdp3, this mechanism becomes hyperactive, resulting in the silencing defects seen in *pdp3Δ* and *set2Δ*. Thus, the study showed that Pdp3 not only targets Mst2C but also prevents the aberrant activity of the complex (Figure 16).

Set2, which deposits the target of Pdp3, H3K36me3, is highly conserved, and many enzymes contain PWWP domains or interact with PWWP domain proteins [200]. Thus, it seems likely that other H3K36me3-bound enzymes are similarly anchored to not only specify the targeted region but also to avoid promiscuous modification of their interaction partners.
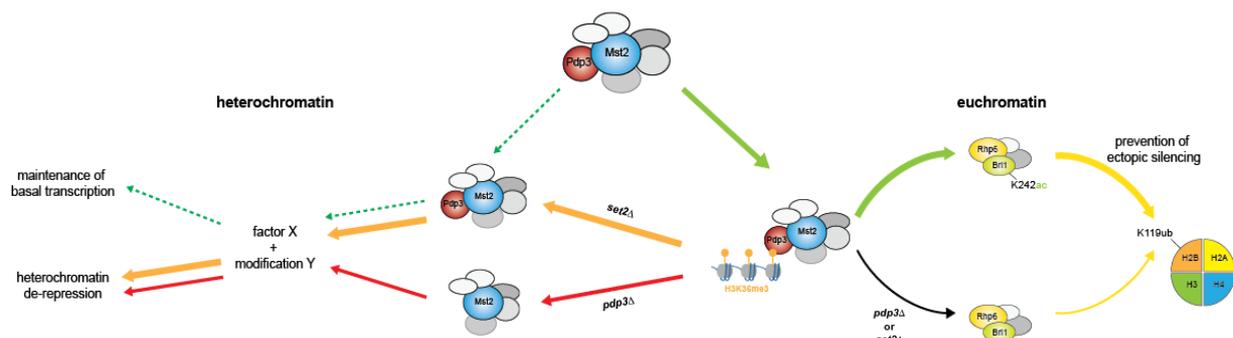
Figure 16 - Model for regulation of transcription by Mst2C In euchromatin Mst2C is recruited to H3K36me3 by Pdp3 where it acetylates the Brl1 subunit of HULC; this stimulates H2B ubiquitylation, resulting in increased transcription that prevents ectopic silencing; in addition, Mst2C is required for maintaining basal transcription through a pathway that acts in a Pdp3/H3K36me3-independent manner; in absence of Pdp3 or Set2 Mst2C is delocalized and encroaches on heterochromatin, which results in hyperactivation of this pathway and de-repression of pericentromeric and subtelomeric heterochromatin.

6 Tables and Figures

6.1 List of Tables

6.2 List of Figures

7 Abbreviations

ac	acetylated residue
ARC	Argonaute RNA chaperone
bp	basepair(s)
CEN	centromeric region
ChIP	chromatin immunoprecipitation
CLRC	Clr4 complex, mediates H3K9me
Clr6CII	Clr6 complex II
cnt	transcribed core region of centromeres
CTD	C-terminal domain (of the RNAPII subunit Rpb1)
DNA	deoxyribonucleic acid
dsRNA	double-stranded RNA
EC	euchromatin
E. coli	*Escherichia coli*
5-FOA	5-fluoroorotic acid
for	forward (in context of primers)
Gcn5	general control of amino-acid synthesis 5
H2A/2B/3/4	histone 2A/2B/3/4
H2BK119	H2B lysine 119
H2Bub(1)	monoubiquitylated H2B (in S. pombe at K119)
H3KX	H3 lysine X
H3KXac	H3 acetylated at lysine X
H3KXme1/2/3	H3 mono-, di-, or trimethylated at lysine X
H4K16ac	H4 acetylated at lysine 16
H4K20me1/2/3	H4 mono-, di-, or trimethylated at lysine 20
H4KX	H4 lysine X
HAT	histone acetyl transferase
HDAC	histone deacetylase
HMT	histone methyl transferase
Hox	homeobox
HC	heterochromatin
HP1	heterochromatin protein 1
HULC	histone ubiquitin ligase complex

imr	innermost repeats
IR	inverted repeat element at the mating type locus
IRC	inverted repeat element at centromeres
K242R/Q	substitution of lysine 242 with arginine (R) or glutamine (Q)
KAT	lysine acetyl transferase
KMT	lysine methyl transferase
KO	knockout
LTR	long terminal repeat
MAT	mating type locus
mRNA	messenger RNA
me1/2/3	mono-/di-/trimethylated residue
Mst2C	Mst2 complex
ncRNA	noncoding RNA
N/S	non-selective
ORF	open reading frame
otr	outermost repeats
Nto1	NuA three orf 1, subunit of Mst2C
NuA3/4	nucleosome acetylation at histone ¾
PCR	polymerase chain reaction
Pdp3	PWWP domain protein 3, subunit of Mst2C
Ptf1/2	Pdp three-interacting factor 1/2, subunits of Mst2C
PWWP	proline-tryptophan-tryptophan-proline
qPCR	quantitative PCR
Paf1C	polymerase II-associated factor 1 complex
PRC	Polycomb-repressive complex
PRE	Polycomb group response element
PTM	post-translational modification
RDRC	RNA-directed RNA polymerase
RITS	RNA-induced transcriptional silencing complex
RNA	ribonucleic acid
RNAi	RNA interference
RNAPII	RNA polymerase II
rpm	rounds per minute
RT-qPCR	reverse transcription coupled with qPCR

S. cerevisiae	*Saccharomyces cerevisiae*
S. pombe	*Schizosaccharomyces pombe*
SAGA	Spt-Ada-Gcn5 acetyltransferase
SHREC	Snf2/HDAC-containing repressor complex
siRNA	small interfering RNA
SRI	Set2 Rpb1 interacting domain
Su(var)	suppressor of variegation
TEL	telomeric region
TF	transcription factor
ub	ubiquitylated residue
3'/5'-UTR	3'/5'-untranslated region

8 References

[1]   A. L. Olins and D. E. Olins, "Spheroid chromatin units (ν bodies).," *Science*, vol. 183, no. 4122, pp. 330–2, Jan. 1974.

[2]   R. D. Kornberg and J. O. Thonmas, "Chromatin Structure: Oligomers of the Histones," *Science (80-.).*, vol. 184, no. 4139, pp. 865 LP – 868, May 1974.

[3]   G. Arents, R. W. Burlingame, B. C. Wang, W. E. Love, and E. N. Moudrianakis, "The nucleosomal core histone octamer at 3.1 A resolution: a tripartite protein assembly and a left-handed superhelix.," *Proc. Natl. Acad. Sci.*, vol. 88, no. 22, pp. 10148–10152, 1991.

[4]   G. Arents and E. N. Moudrianakis, "The histone fold: a ubiquitous architectural motif utilized in DNA compaction and protein dimerization.," *Proc. Natl. Acad. Sci.*, vol. 92, no. 24, pp. 11170–11174, 1995.

[5]   R. D. Kornberg, "Chromatin Structure: A Repeating Unit of Histones and DNA," *Science (80-.).*, vol. 184, no. 4139, pp. 868 LP – 871, May 1974.

[6]   K. Luger, A. W. Mäder, R. K. Richmond, D. F. Sargent, and T. J. Richmond, "Crystal structure of the nucleosome core particle at 2.8 Å resolution," *Nature*, vol. 389, p. 251, Sep. 1997.

[7]   D. V. Fyodorov, B.-R. Zhou, A. I. Skoultchi, and Y. Bai, "Emerging roles of linker histones in regulating chromatin structure and function," *Nat. Rev. Mol. Cell Biol.*, 2017.

[8]   J. C. Hansen, "Conformational Dynamics of the Chromatin Fiber in Solution: Determinants, Mechanisms, and Functions," *Annu. Rev. Biophys. Biomol. Struct.*, vol. 31, no. 1, pp. 361–392, Jun. 2002.

[9]   A. R. Cutter and J. J. Hayes, "A brief review of nucleosome structure," *FEBS Letters*, vol. 589, no. 20. pp. 2914–2922, 07-Oct-2015.

[10]   I. Solovei, K. Thanisch, and Y. Feodorova, "How to rule the nucleus: divide et impera," *Curr. Opin. Cell Biol.*, vol. 40, pp. 47–59, Jun. 2016.

[11]   A. D. Ewing and H. H. Kazazian, "Whole-genome resequencing allows detection of many rare LINE-1 insertion alleles in humans," *Genome Res.*, vol. 21, no. 6, pp. 985–990, Jun. 2011.

[12]   P. J. Thompson, T. S. Macfarlan, and M. C. Lorincz, "Long Terminal Repeats: From Parasitic Elements to Building Blocks of the Transcriptional Regulatory Repertoire," *Mol. Cell*, vol. 62, no. 5, pp. 766–776, Jun. 2016.

[13]   C. Guetg and R. Santoro, "Formation of nuclear heterochromatin the nucleolar point of view," *Epigenetics*, vol. 7, no. 8, pp. 811–814, 2012.

[14]   C. Guetg *et al.*, "The NoRC complex mediates the heterochromatin formation and stability of silent rRNA genes and centromeric repeats," *EMBO J.*, vol. 29, no. 13, pp. 2135–2146, Sep. 2010.

[15]   L. J. Barton, A. A. Soshnev, and P. K. Geyer, "Networking in the nucleus: a spotlight on LEM-domain proteins," *Curr. Opin. Cell Biol.*, vol. 34, pp. 1–8, Jun. 2015.

[16]   R. de Leeuw, Y. Gruenbaum, and O. Medalia, "Nuclear Lamins: Thin Filaments with Major Functions," *Trends in Cell Biology*, vol. 28, no. 1. Elsevier Current Trends, pp. 34–45, 01-Jan-2018.

[17] R. A. Katz, "Specifying peripheral heterochromatin during nuclear lamina reassembly," *Nucleus*, vol. 5, no. 1, pp. 32–39, 2014.

[18] R. R. Barrales, M. Forn, P. R. Georgescu, Z. Sarkadi, and S. Braun, "Control of heterochromatin localization and silencing by the nuclear membrane protein Lem2," *Genes Dev.*, vol. 30, no. 2, 2016.

[19] R. Burla, M. La Torre, and I. Saggio, "Mammalian telomeres and their partnership with lamins," *Nucleus*, vol. 7, no. 2. Taylor & Francis, pp. 187–202, 25-Apr-2016.

[20] V. Dileep, J. C. Rivera-Mulia, J. Sima, and D. M. Gilbert, "Large-Scale Chromatin Structure-Function Relationships during the Cell Cycle and Development: Insights from Replication Timing.," *Cold Spring Harb. Symp. Quant. Biol.*, vol. 80, pp. 53–63, Jan. 2015.

[21] J. Zeng *et al.*, "Identification and analysis of house-keeping and tissue-specific genes based on RNA-seq data sets across 15 mouse tissues," *Gene*, vol. 576, no. 1, Part 3, pp. 560–570, 2016.

[22] J. Zhu, F. He, S. Hu, and J. Yu, "On the nature of human housekeeping genes," *Trends Genet.*, vol. 24, no. 10, pp. 481–484, 2008.

[23] P. R. Cook, "A Model for all Genomes: The Role of Transcription Factories," *J. Mol. Biol.*, vol. 395, no. 1, pp. 1–10, Jan. 2010.

[24] A. Ghamari *et al.*, "In vivo live imaging of RNA polymerase II transcription factories in primary cells.," *Genes Dev.*, vol. 27, no. 7, pp. 767–77, Apr. 2013.

[25] C. S. Osborne *et al.*, "Active genes dynamically colocalize to shared sites of ongoing transcription," *Nat. Genet.*, vol. 36, no. 10, pp. 1065–1071, Oct. 2004.

[26] J. A. Mitchell and P. Fraser, "Transcription factories are nuclear subcompartments that remain in the absence of transcription," *Genes Dev.*, vol. 22, no. 1, pp. 20–25, Jan. 2008.

[27] C. S. Osborne *et al.*, "Myc dynamically and preferentially relocates to a transcription factory occupied by Igh," *PLoS Biol.*, vol. 5, no. 8, pp. 1763–1772, Jul. 2007.

[28] K. Weipoltshammer and C. Schöfer, "Morphology of nuclear transcription," *Histochemistry and Cell Biology*, vol. 145, no. 4. Springer Berlin Heidelberg, pp. 343–358, 04-Apr-2016.

[29] C. H. Eskiw, P. Fraser, D. A. Jackson, and P. R. Cook, "Ultrastructural study of transcription factories in mouse erythroblasts.," *J. Cell Sci.*, vol. 124, no. Pt 21, pp. 3676–83, Nov. 2011.

[30] L. Herzel, D. S. M Ottoz, T. Alpert, and K. M. Neugebauer, "Splicing and transcription touch base: co-transcriptional spliceosome assembly and function," *Nat. Publ. Gr.*, vol. 18, 2017.

[31] J. Katahira, "Nuclear export of messenger RNA," *Genes (Basel).*, vol. 6, no. 2, pp. 163–184, 2015.

[32] C. E. Murry and G. Keller, "Differentiation of Embryonic Stem Cells to Clinically Relevant Populations: Lessons from Embryonic Development," *Cell*, vol. 132, no. 4. Elsevier, pp. 661–680, 22-Feb-2008.

[33] M. Y. Fessing *et al.*, "p63 regulates Satb1 to control tissue-specific chromatin remodeling during development of the epidermis," *J. Cell Biol.*, vol. 194, no. 6, pp. 825 LP – 839, Sep. 2011.

[34] U. Grossniklaus and R. Paro, "Transcriptional Silencing by Polycomb-Group Proteins," *Cold Spring Harb. Perspect. Biol.*, vol. 6, no. 11, pp. 1–26, Nov. 2014.

[35] S. J. Geisler and R. Paro, "Trithorax and Polycomb group-dependent regulation: a tale of

opposing activities," *Development*, vol. 142, no. 17, pp. 2876–2887, Sep. 2015.

[36]   L. Ringrose and R. Paro, "E PIGENETIC R EGULATION OF C ELLULAR M EMORY BY THE P OLYCOMB AND T RITHORAX G ROUP," 2004.

[37]   J. Müller and P. Verrijzer, "Biochemical mechanisms of gene regulation by polycomb group protein complexes," *Curr. Opin. Genet. Dev.*, vol. 19, no. 2, pp. 150–158, Apr. 2009.

[38]   A. R. Pengelly, R. Kalb, K. Finkl, and J. Müller, "Transcriptional repression by PRC1 in the absence of H2A monoubiquitylation," *Genes Dev.*, vol. 29, no. 14, pp. 1487–1492, Jul. 2015.

[39]   R. S. Illingworth *et al.*, "The E3 ubiquitin ligase activity of RING1B is not essential for early mouse development," *Genes Dev.*, vol. 29, no. 18, pp. 1897–1902, Sep. 2015.

[40]   M. S. Lau *et al.*, "Mutation of a nucleosome compaction region disrupts Polycomb-mediated axial patterning," *Science (80-.)*., vol. 355, no. 6329, pp. 1081–1084, 2017.

[41]   S. Kundu *et al.*, "Polycomb Repressive Complex 1 Generates Discrete Compacted Domains that Change during Differentiation," *Mol. Cell*, vol. 65, no. 3, pp. 432-446.e5, Feb. 2017.

[42]   J. W. Tamkun *et al.*, "brahma: A Regulator of Drosophila Homeotic Genes Structurally Related to the Yeast Transcriptional Activator SNF2BWl2," *Cell*, vol. 66, pp. 561–572, 1992.

[43]   M. Wirén *et al.*, "Genomewide analysis of nucleosome density histone acetylation and HDAC function in fission yeast," *EMBO J.*, vol. 24, no. 16, pp. 2906–18, Aug. 2005.

[44]   L. Cai *et al.*, "An H3K36 methylation-engaging Tudor motif of polycomb-like proteins mediates PRC2 complex targeting.," *Mol. Cell*, vol. 49, no. 3, pp. 571–82, Feb. 2013.

[45]   N. Brockdorff, "Polycomb complexes in X chromosome inactivation.," *Philos. Trans. R. Soc. Lond. B. Biol. Sci.*, vol. 372, no. 1733, p. 20170021, Nov. 2017.

[46]   M. A. Biscotti, A. Canapa, M. Forconi, E. Olmo, and M. Barucca, "Transcription of tandemly repetitive DNA: functional roles," *Chromosom. Res.*, vol. 23, no. 3, pp. 463–477, 2015.

[47]   S. I. S. S. Grewal and S. Jia, "Heterochromatin revisited," *Nat. Rev. Genet.*, vol. 8, no. 1, pp. 35–46, Jan. 2007.

[48]   P. Mita and J. D. Boeke, "How retrotransposons shape genome regulation," *Curr. Opin. Genet. Dev.*, vol. 37, pp. 90–100, Apr. 2016.

[49]   I. Pinheiro *et al.*, "Prdm3 and Prdm16 are H3K9me1 Methyltransferases Required for Mammalian Heterochromatin Integrity," *Cell*, vol. 150, no. 5, pp. 948–960, Aug. 2012.

[50]   M. Tachibana *et al.*, "Histone methyltransferases G9a and GLP form heteromeric complexes and are both crucial for methylation of euchromatin at H3-K9.," *Genes Dev.*, vol. 19, no. 7, pp. 815–26, Apr. 2005.

[51]   H. E. Covington *et al.*, "A role for repressive histone methylation in cocaine-induced vulnerability to stress.," *Neuron*, vol. 71, no. 4, pp. 656–70, Aug. 2011.

[52]   S. Rea *et al.*, "Regulation of chromatin structure by site-specific histone H3 methyltransferases," *Nature*, vol. 406, no. 6796, pp. 593–599, Aug. 2000.

[53]   A. V Ivanova, M. J. Bonaduce, S. V Ivanov, and A. J. S. Klar, "The chromo and SET domains of the Clr4 protein are essential for silencing in fission yeast," *Nat. Genet.*, vol. 19, no. 2, pp. 192–195, 1998.

[54]   M. Melcher, M. Schmid, L. Aagaard, P. Selenko, G. Laible, and T. Jenuwein, "Structure-Function Analysis of SUV39H1 Reveals a Dominant Role in Heterochromatin Organization, Chromosome

Segregation, and Mitotic Progression," *Mol. Cell. Biol.* , vol. 20, no. 10, pp. 3728–3741, May 2000.

[55]   N. R. Rose and R. J. Klose, "Understanding the relationship between DNA methylation and histone lysine methylation," *Biochimica et Biophysica Acta - Gene Regulatory Mechanisms*, vol. 1839, no. 12. pp. 1362–1372, 2014.

[56]   J. Sharif *et al.*, "The SRA protein Np95 mediates epigenetic inheritance by recruiting Dnmt1 to methylated DNA," *Nature*, vol. 450, no. 7171, pp. 908–912, Dec. 2007.

[57]   K. Arita, M. Ariyoshi, H. Tochio, Y. Nakamura, and M. Shirakawa, "Recognition of hemi-methylated DNA by the SRA protein UHRF1 by a base-flipping mechanism," *Nature*, vol. 455, no. 7214, pp. 818–821, Oct. 2008.

[58]   T. Chen, N. Tsujimoto, and E. Li, "The PWWP domain of Dnmt3a and Dnmt3b is required for directing DNA methylation to the major satellite repeats at pericentric heterochromatin.," *Mol. Cell. Biol.*, vol. 24, no. 20, pp. 9048–58, Oct. 2004.

[59]   G. Rondelet, T. Dal Maso, L. Willems, and J. Wouters, "Structural basis for recognition of histone H3K36me3 nucleosome by human de novo DNA methyltransferases 3A and 3B," *J. Struct. Biol.*, vol. 194, no. 3, pp. 357–367, Jun. 2016.

[60]   A. Dhayalan *et al.*, "The ATRX-ADD domain binds to H3 tail peptides and reads the combined methylation state of K4 and K9.," *Hum. Mol. Genet.*, vol. 20, no. 11, pp. 2195–203, Jun. 2011.

[61]   X. Guo *et al.*, "Structural insight into autoinhibition and histone H3-induced activation of DNMT3A," *Nature*, vol. 517, no. 7536, pp. 640–644, Jan. 2015.

[62]   J. P. Thomson *et al.*, "CpG islands influence chromatin structure via the CpG-binding protein Cfp1," *Nature*, vol. 464, no. 7291, pp. 1082–1086, Apr. 2010.

[63]   B. A. Sullivan and G. H. Karpen, "Centromeric chromatin exhibits a histone modification pattern that is distinct from both euchromatin and heterochromatin," *Nat. Struct. Mol. Biol.*, vol. 11, no. 11, pp. 1076–1083, Nov. 2004.

[64]   F. Fuks, P. J. Hurd, R. Deplus, and T. Kouzarides, "The DNA methyltransferases associate with HP1 and the SUV39H1 histone methyltransferase," *Nucleic Acids Res.*, vol. 31, no. 9, pp. 2305–2312, May 2003.

[65]   H. Li, T. Rauch, Z. X. Chen, P. E. Szabó, A. D. Riggs, and G. P. Pfeifer, "The histone methyltransferase SETDB1 and the DNA methyltransferase DNMT3A interact directly and localize to promoters silenced in cancer cells," *J. Biol. Chem.*, vol. 281, no. 28, pp. 19489–19500, 2006.

[66]   F. Fuks, P. J. Hurd, D. Wolf, X. Nan, A. P. Bird, and T. Kouzarides, "The methyl-CpG-binding protein MeCP2 links DNA methylation to histone methylation.," *J. Biol. Chem.*, vol. 278, no. 6, pp. 4035–40, Feb. 2003.

[67]   R. Martienssen and D. Moazed, "RNAi and heterochromatin assembly," *Cold Spring Harb. Perspect. Biol.*, vol. 7, no. 8, p. a019323, Aug. 2015.

[68]   W. Filipowicz, L. Jaskiewicz, F. A. Kolb, and R. S. Pillai, "Post-transcriptional gene silencing by siRNAs and miRNAs," *Current Opinion in Structural Biology*, vol. 15, no. 3 SPEC. ISS. Elsevier Current Trends, pp. 331–341, 01-Jun-2005.

[69]   D. P. Bartel, "MicroRNAs: Genomics, Biogenesis, Mechanism, and Function," *Cell*, vol. 116, no.

2. Elsevier, pp. 281–297, 23-Jan-2004.

[70]   T. Sijen *et al.*, "On the role of RNA amplification in dsRNA-triggered gene silencing.," *Cell*, vol. 107, no. 4, pp. 465–76, Nov. 2001.

[71]   A. Verdel, "RNAi-Mediated Targeting of Heterochromatin by the RITS Complex," *Science (80-.).*, vol. 303, no. 5658, pp. 672–676, 2004.

[72]   H. Zhang, F. A. Kolb, L. Jaskiewicz, E. Westhof, and W. Filipowicz, "Single processing center models for human Dicer and bacterial RNase III.," *Cell*, vol. 118, no. 1, pp. 57–68, Jul. 2004.

[73]   S. M. Buker *et al.*, "Two different Argonaute complexes are required for siRNA generation and heterochromatin assembly in fission yeast.," *Nat. Struct. Mol. Biol.*, vol. 14, no. 3, pp. 200–207, Mar. 2007.

[74]   I. M. Hall, G. D. Shankaranarayana, K. Noma, N. Ayoub, A. Cohen, and S. I. Grewal, "Establishment and maintenance of a heterochromatin domain.[see comment]," *Science (80-.).*, vol. 297, no. 5590, pp. 2232–2237, 2002.

[75]   A. Sigova, N. Rhind, and P. D. Zamore, "A single Argonaute protein mediates both transcriptional and posttranscriptional silencing in Schizosaccharomyces pombe.," *Genes Dev.*, vol. 18, no. 19, pp. 2359–67, Oct. 2004.

[76]   K. M. Creamer and J. F. Partridge, "RITS-connecting transcription, RNA interference, and heterochromatin assembly in fission yeast," *Wiley Interdiscip. Rev. RNA*, vol. 2, no. 5, pp. 632–646, Sep. 2011.

[77]   H. Li *et al.*, "An Alpha Motif at Tas3 C Terminus Mediates RITS cis Spreading and Promotes Heterochromatic Gene Silencing," *Mol. Cell*, vol. 34, no. 2, pp. 155–167, 2009.

[78]   M. Ishida *et al.*, "Intrinsic Nucleic Acid-Binding Activity of Chp1 Chromodomain Is Required for Heterochromatic Gene Silencing," *Mol. Cell*, vol. 47, no. 2, pp. 228–241, 2012.

[79]   E. H. Bayne *et al.*, "Stc1: A Critical Link between RNAi and Chromatin Modification Required for Heterochromatin Integrity," *Cell*, vol. 140, no. 5, pp. 666–677, 2010.

[80]   J. Nakayama, J. C. Rice, B. D. Strahl, C. D. Allis, and S. I. S. Grewal, "Role of Histone H3 Lysine 9 Methylation in Epigenetic Control of Heterochromatin Assembly," *Science (80-.).*, vol. 292, no. 2001, pp. 110–113, 2001.

[81]   C. He *et al.*, "Structural analysis of Stc1 provides insights into the coupling of RNAi and chromatin modification," *Proc. Natl. Acad. Sci.*, vol. 110, no. 21, pp. E1879–E1888, May 2013.

[82]   M. P. Longhese, D. Bonetti, N. Manfrini, and M. Clerici, "Mechanisms and regulation of DNA end resection," *EMBO Journal*, vol. 29, no. 17. European Molecular Biology Organization, pp. 2864–2874, 01-Sep-2010.

[83]   C. W. Greider and E. H. Blackburn, "Identification of a specific telomere terminal transferase activity in tetrahymena extracts," *Cell*, vol. 43, no. 2, pp. 405–413, Dec. 1985.

[84]   F. L. Zhong, L. F. Z. Batista, A. Freund, M. F. Pech, A. S. Venteicher, and S. E. Artandi, "TPP1 OB-fold domain controls telomere maintenance by recruiting telomerase to chromosome ends.," *Cell*, vol. 150, no. 3, pp. 481–94, Aug. 2012.

[85]   H. Xin *et al.*, "TPP1 is a homologue of ciliate TEBP-β and interacts with POT1 to recruit telomerase," *Nature*, vol. 445, no. 7127, pp. 559–562, Feb. 2007.

[86]   J. Nandakumar and T. R. Cech, "Finding the end: recruitment of telomerase to telomeres.," *Nat.*

Rev. Mol. Cell Biol., vol. 14, no. 2, pp. 69–82, Feb. 2013.

[87]　J. D. Griffith *et al.*, "Mammalian telomeres end in a large duplex loop.," *Cell*, vol. 97, no. 4, pp. 503–14, May 1999.

[88]　T. Sugiyama *et al.*, "SHREC, an Effector Complex for Heterochromatic Transcriptional Silencing," *Cell*, vol. 128, no. 3, pp. 491–504, 2007.

[89]　B. A. Moser, O. N. Raguimova, and T. M. Nakamura, "Ccq1-Tpz1 [TPP1] interaction facilitates telomerase and SHREC association with telomeres in fission yeast," *Mol. Biol. Cell*, vol. 26, no. 21, pp. 3857–3866, Nov. 2015.

[90]　J. Wang *et al.*, "The proper connection between shelterin components is required for telomeric heterochromatin assembly," *Genes Dev.*, vol. 30, no. 7, pp. 827–839, 2016.

[91]　T. S. van Emden *et al.*, "Shelterin and subtelomeric DNA sequences control nucleosome maintenance and genome stability," *EMBO Rep.*, vol. 20, no. 1, p. e47181, Jan. 2019.

[92]　C. A. Armstrong *et al.*, "Fission yeast Ccq1 is a modulator of telomerase activity," *Nucleic Acids Res.*, vol. 46, no. 2, pp. 704–716, Jan. 2018.

[93]　M. García-Cao, R. O'Sullivan, A. H. F. M. Peters, T. Jenuwein, and M. A. Blasco, "Epigenetic regulation of telomere length in mammalian cells by the Suv39h1 and Suv39h2 histone methyltransferases," *Nat. Genet.*, vol. 36, no. 1, pp. 94–99, Jan. 2004.

[94]　M. Udugama *et al.*, "Histone variant H3.3 provides the heterochromatic H3 lysine 9 tri-methylation mark at telomeres.," *Nucleic Acids Res.*, vol. 43, no. 21, pp. 10227–37, Dec. 2015.

[95]　M. A. Blasco, "The epigenetic regulation of mammalian telomeres," *Nature Reviews Genetics*, vol. 8, no. 4. Nature Publishing Group, pp. 299–309, 01-Apr-2007.

[96]　S. Gonzalo *et al.*, "DNA methyltransferases control telomere length and telomere recombination in mammalian cells," *Nat. Cell Biol.*, vol. 8, no. 4, pp. 416–424, Apr. 2006.

[97]　W. Deng *et al.*, "Fission yeast telomere-binding protein Taz1 is a functional but not a structural counterpart of human TRF1 and TRF2.," *Cell Res.*, vol. 25, no. 7, pp. 881–4, Jul. 2015.

[98]　Y. Chikashige *et al.*, "Membrane proteins Bqt3 and -4 anchor telomeres to the nuclear envelope to ensure chromosomal bouquet formation," *J. Cell Biol.*, vol. 187, no. 3, pp. 413–427, Nov. 2009.

[99]　P. Bjerling, R. A. Silverstein, G. Thon, A. Caudy, S. Grewal, and K. Ekwall, "Functional divergence between histone deacetylases in fission yeast by distinct cellular localization and in vivo specificity.," *Mol. Cell. Biol.*, vol. 22, no. 7, pp. 2170–81, 2002.

[100]　J. Demmerle, A. J. Koch, and J. M. Holaska, "The nuclear envelope protein emerin binds directly to histone deacetylase 3 (HDAC3) and activates HDAC3 activity.," *J. Biol. Chem.*, vol. 287, no. 26, pp. 22080–8, Jun. 2012.

[101]　O. Aygün, S. Mehta, and S. I. S. Grewal, "HDAC-mediated suppression of histone turnover promotes epigenetic stability of heterochromatin," *Nat. Struct. Mol. Biol.*, vol. 20, no. 5, pp. 547–554, 2013.

[102]　M. Braunstein, A. B. Rose, S. J. Holmes, C. D. Allis, and J. R. Broach, "Transcriptional silencing in yeast is associated with reduced histone acetylation," *Genes Dev.*, vol. 7, pp. 592–604, 1993.

[103]　E. Birney *et al.*, "Identification and analysis of functional elements in 1% of the human genome by the ENCODE pilot project," *Nature*, vol. 447, no. 7146, pp. 799–816, 2007.

[104]　N. J. Fuda, M. B. Ardehali, and J. T. Lis, "Defining mechanisms that regulate RNA polymerase II

transcription in vivo," *Nature*, vol. 461, no. 7261. pp. 186–192, 10-Sep-2009.

[105] X. Lai *et al.*, "Pioneer Factors in Animals and Plants—Colonizing Chromatin for Gene Regulation," *Molecules*, vol. 23, no. 8, p. 1914, Jul. 2018.

[106] M. Iwafuchi-Doi and K. S. Zaret, "Pioneer transcription factors in cell reprogramming.," *Genes Dev.*, vol. 28, no. 24, pp. 2679–92, Dec. 2014.

[107] A. Bucceri, K. Kapitza, and F. Thoma, "Rapid accessibility of nucleosomal DNA in yeast on a second time scale.," *EMBO J.*, vol. 25, no. 13, pp. 3123–32, Jul. 2006.

[108] J. C. Reese, "Basal transcription factors," *Curr. Opin. Genet. Dev.*, vol. 13, no. 2, pp. 114–118, Apr. 2003.

[109] S. Sainsbury, C. Bernecky, and P. Cramer, "Structural basis of transcription initiation by RNA polymerase II," *Nat. Rev. Mol. Cell Biol.*, vol. 16, no. 3, pp. 129–143, Mar. 2015.

[110] Y. Zhou, H. Wu, M. Zhao, C. Chang, and Q. Lu, "The Bach Family of Transcription Factors: A Comprehensive Review," *Clin. Rev. Allergy Immunol.*, vol. 50, no. 3, pp. 345–356, Jun. 2016.

[111] G. E. Sonenshein, "Rel/NF-κB transcription factors and the control of apoptosis," *Semin. Cancer Biol.*, vol. 8, no. 2, pp. 113–119, Apr. 1997.

[112] S. Ogbourne and T. M. Antalis, "Transcriptional control and the role of silencers in transcriptional regulation in eukaryotes.," *Biochem. J.*, vol. 331, no. Pt 1, pp. 1–14, Apr. 1998.

[113] M. Levine, C. Cattoglio, and R. Tjian, "Looping back to leap forward: Transcription enters a new era," *Cell*, vol. 157, no. 1. Elsevier, pp. 13–25, 27-Mar-2014.

[114] A. Göndör and R. Ohlsson, "Enhancer functions in three dimensions: beyond the flat world perspective," *F1000Research*, vol. 7, p. 681, May 2018.

[115] M. Huan and B. Bartholomew, "Emerging Roles of Transcriptional Enhancers In Chromatin Looping And Promoter-Proximal Pausing Of RNA Polymerase II," *J. Biol. Chem.*, vol. 293, p. jbc.R117.813485, 2017.

[116] S. Lomvardas, G. Barnea, D. J. Pisapia, M. Mendelsohn, J. Kirkland, and R. Axel, "Interchromosomal Interactions and Olfactory Receptor Choice," *Cell*, vol. 126, no. 2, pp. 403–413, Jul. 2006.

[117] E. Trompouki *et al.*, "Lineage Regulators Direct BMP and Wnt Pathways to Cell-Specific Programs during Differentiation and Regeneration," *Cell*, vol. 147, no. 3, pp. 577–589, Oct. 2011.

[118] C. R. Clapier and B. R. Cairns, "The Biology of Chromatin Remodeling Complexes," *Annu. Rev. Biochem.*, vol. 78, no. 1, pp. 273–304, Jun. 2009.

[119] A. J. Ruthenburg, C. D. Allis, and J. Wysocka, "Methylation of Lysine 4 on Histone H3: Intricacy of Writing and Reading a Single Epigenetic Mark," *Mol. Cell*, vol. 25, no. 1, pp. 15–30, 2007.

[120] B. Piña, U. Brüggemeier, and M. Beato, "Nucleosome positioning modulates accessibility of regulatory proteins to the mouse mammary tumor virus promoter.," *Cell*, vol. 60, no. 5, pp. 719–31, Mar. 1990.

[121] K. S. Zaret and J. S. Carroll, "Pioneer transcription factors : establishing competence for gene expression Parameters affecting transcription factor access to target sites in chromatin Initiating events in chromatin : pioneer factors bind first," *Genes Dev.*, pp. 2227–2241, 2011.

[122] P. B. Becker and J. L. Workman, "Nucleosome remodeling and epigenetics," *Cold Spring Harb. Perspect. Biol.*, vol. 5, no. 9, p. a017905, Sep. 2013.

[123] A. N. Yadon and T. Tsukiyama, "SnapShot: Chromatin remodeling: ISWI," *Cell*, vol. 144, no. 3, pp. 453-453.e1, 2011.

[124] H. Huang *et al.*, "SnapShot: Histone Modifi cations," *Cell*, vol. 159, pp. 458-458.e1, 2014.

[125] A. F. Kebede *et al.*, "Histone propionylation is a mark of active chromatin," *Nat. Publ. Gr.*, 2017.

[126] M. Smolle *et al.*, "Chromatin remodelers Isw1 and Chd1 maintain chromatin structure during transcription by preventing histone exchange," *Nat. Struct. Mol. Biol.*, vol. 19, no. 9, pp. 884–892, 2012.

[127] A. H. Hassan, K. E. Neely, and J. L. Workman, "Histone acetyltransferase complexes stabilize SWI/SNF binding to promoter nucleosomes," *Cell*, vol. 104, no. 6, pp. 817–827, Mar. 2001.

[128] I. Sinha *et al.*, "Genome-wide mapping of histone modifications and mass spectrometry reveal H4 acetylation bias and H3K36 methylation at gene promoters in fission yeast," *Epigenomics*, vol. 2, no. 3, pp. 377–393, 2010.

[129] T. Suganuma and J. L. Workman, "Signals and Combinatorial Functions of Histone Modifications," *Annu. Rev. Biochem.*, vol. 80, no. 1, pp. 473–499, 2011.

[130] A. G. Ladurner, C. Inouye, R. Jain, and R. Tjian, "Bromodomains mediate an acetyl-histone encoded antisilencing function at heterochromatin boundaries," *Mol. Cell*, vol. 11, no. 2, pp. 365–376, Feb. 2003.

[131] C. E. Brown, T. Lechner, L. Howe, and J. L. Workman, "The many HATs of transcription coactivators," *Trends Biochem. Sci.*, vol. 25, no. 1, pp. 15–19, Jan. 2000.

[132] K. Ikeda, D. J. Steger, A. Eberharter, and J. L. Workman, "Activation Domain-Specific and General Transcription Stimulation by Native Histone Acetyltransferase Complexes," *Mol. Cell. Biol.*, vol. 19, no. 1, pp. 855 LP – 863, Jan. 1999.

[133] E. Larschan and F. Winston, "The S. cerevisiae SAGA complex functions in vivo as a coactivator for transcriptional activation by Gal4.," *Genes Dev.*, vol. 15, no. 15, pp. 1946–56, Aug. 2001.

[134] R. T. Utley *et al.*, "Transcriptional activators direct histone acetyltransferase complexes to nucleosomes," *Nature*, vol. 394, no. 6692, pp. 498–502, Jul. 1998.

[135] S. P. Baker and P. A. Grant, "The SAGA continues: Expanding the cellular role of a transcriptional co-activator complex," *Oncogene*, vol. 26, no. 37. NIH Public Access, pp. 5329–5340, 13-Aug-2007.

[136] A. Vezzoli *et al.*, "Molecular basis of histone H3K36me3 recognition by the PWWP domain of Brpf1," *Nat. Struct. Mol. Biol.*, vol. 17, no. 5, pp. 617–619, May 2010.

[137] Y. Doyon *et al.*, "ING tumor suppressor proteins are critical regulators of chromatin acetylation required for genome expression and perpetuation," *Mol. Cell*, vol. 21, no. 1, pp. 51–64, 2006.

[138] M.-E. Lalonde *et al.*, "Exchange of associated factors directs a switch in HBO1 acetyltransferase histone tail specificity.," *Genes Dev.*, vol. 27, no. 18, pp. 2009–24, Sep. 2013.

[139] S. D. Taverna *et al.*, "Yng1 PHD finger binding to H3 trimethylated at K4 promotes NuA3 HAT activity at K14 of H3 and transcription at a subset of targeted ORFs.," *Mol. Cell*, vol. 24, no. 5, pp. 785–96, Dec. 2006.

[140] T. M. Gilbert *et al.*, "A PWWP Domain-Containing Protein Targets the NuA3 Acetyltransferase Complex via Histone H3 Lysine 36 trimethylation to Coordinate Transcriptional Elongation at Coding Regions," *Mol. Cell. Proteomics* , vol. 13, no. 11, pp. 2883–2895, Nov. 2014.

[141] B. J. E. Martin, K. L. McBurney, V. E. Maltby, K. N. Jensen, J. Brind'Amour, and L. A. J. Howe, "Histone H3K4 and H3K36 methylation independently recruit the NuA3 histone acetyltransferase in Saccharomyces cerevisiae," *Genetics*, vol. 205, no. 3, pp. 1113–1123, 2017.

[142] H. Santos-Rosa *et al.*, "Active genes are tri-methylated at K4 of histone H3," *Nature*, vol. 419, no. 6905, pp. 407–411, Sep. 2002.

[143] D. S. Ginsburg, T. E. Anlembom, J. Wang, S. R. Patel, B. Li, and A. G. Hinnebusch, "NuA4 links methylation of histone H3 lysines 4 and 36 to acetylation of histones H4 and H3," *J. Biol. Chem.*, vol. 289, no. 47, pp. 32656–32670, Nov. 2014.

[144] Y. Wang, X. Li, and H. Hu, "H3K4me2 reliably defines transcription factor binding regions in different cells," *Genomics*, vol. 103, pp. 222–228, 2014.

[145] A. J. Bannister, R. Schneider, F. A. Myers, A. W. Thorne, C. Crane-Robinson, and T. Kouzarides, "Spatial distribution of di- and tri-methyl lysine 36 of histone H3 at active genes," *J. Biol. Chem.*, vol. 280, no. 18, pp. 17732–17736, 2005.

[146] D. K. Pokholok *et al.*, "Genome-wide map of nucleosome acetylation and methylation in yeast," *Cell*, vol. 122, no. 4, pp. 517–527, 2005.

[147] T. Jenuwein, "Translating the Histone Code," *Science (80-.).*, vol. 293, no. 5532, pp. 1074–1080, 2001.

[148] B. D. Strahl and C. D. Allis, "The language of covalent histone modifications," *Nature*, vol. 403, no. 6765. pp. 41–45, 2000.

[149] V. M. Weake and J. L. Workman, "Histone ubiquitination: triggering gene activity.," *Mol. Cell*, vol. 29, no. 6, pp. 653–63, Mar. 2008.

[150] G. S. Shieh *et al.*, "H2B ubiquitylation is part of chromatin architecture that marks exon-intron structure in budding yeast," *BMC Genomics*, vol. 12, no. 1, p. 627, 2011.

[151] H. H. Ng, R.-M. Xu, Y. Zhang, and K. Struhl, "Ubiquitination of histone H2B by Rad6 is required for efficient Dot1-mediated methylation of histone H3 lysine 79.," *J. Biol. Chem.*, vol. 277, no. 38, pp. 34655–7, Sep. 2002.

[152] M. Zofall and S. I. S. Grewal, "HULC, a Histone H2B Ubiquitinating Complex, Modulates Heterochromatin Independent of Histone Methylation in Fission Yeast," *J. Biol. Chem.* , vol. 282, no. 19, pp. 14065–14072, May 2007.

[153] N. J. Krogan *et al.*, "The Paf1 complex is required for histone H3 methylation by COMPASS and Dot1p: Linking transcriptional elongation to histone methylation," *Mol. Cell*, vol. 11, no. 3, pp. 721–729, 2003.

[154] J. Kim *et al.*, "RAD6-Mediated transcription-coupled H2B ubiquitylation directly stimulates H3K4 methylation in human cells.," *Cell*, vol. 137, no. 3, pp. 459–71, May 2009.

[155] S. B. Van Oss *et al.*, "The Histone Modification Domain of Paf1 Complex Subunit Rtf1 Directly Stimulates H2B Ubiquitylation through an Interaction with Rad6," *Mol. Cell*, vol. 64, no. 4, pp. 815–825, Nov. 2016.

[156] K. Tenney *et al.*, "Drosophila Rtf1 functions in histone methylation, gene expression, and Notch signaling.," *Proc. Natl. Acad. Sci. U. S. A.*, vol. 103, no. 32, pp. 11970–4, Aug. 2006.

[157] H. Vlaming *et al.*, "Direct screening for chromatin status on DNA barcodes in yeast delineates the regulome of H3K79 methylation by Dot1," *Elife*, vol. 5, no. DECEMBER2016, p. e18919, Dec.

2016.

[158] F. van Leeuwen, P. R. Gafken, and D. E. Gottschling, "Dot1p Modulates Silencing in Yeast by Methylation of the Nucleosome Core," *Cell*, vol. 109, no. 6, pp. 745–756, Jun. 2002.

[159] Q. Feng *et al.*, "Methylation of H3-Lysine 79 Is Mediated by a New Family of HMTases without a SET Domain," *Curr. Biol.*, vol. 12, no. 12, pp. 1052–1058, Jun. 2002.

[160] E. J. Worden, N. A. Hoffmann, C. W. Hicks, and C. Wolberger, "Mechanism of Cross-talk between H2B Ubiquitination and H3 Methylation by Dot1L," *Cell*, vol. 176, no. 6, pp. 1490-1501.e12, Mar. 2019.

[161] J. Kim *et al.*, "The n-SET Domain of Set1 Regulates H2B Ubiquitylation-Dependent H3K4 Methylation," *Mol. Cell*, vol. 49, no. 6, pp. 1121–1133, 2013.

[162] G. Napolitano, L. Lania, and B. Majello, "RNA Polymerase II CTD Modifications: How many tales from a single tail," *J. Cell. Physiol.*, vol. 229, no. 5, pp. 538–544, 2014.

[163] B. Zhu *et al.*, "Monoubiquitination of human histone H2B: The factors involved and their roles in HOX gene regulation," *Mol. Cell*, vol. 20, no. 4, pp. 601–611, 2005.

[164] O. Rozenblatt-Rosen *et al.*, "The parafibromin tumor suppressor protein is part of a human Paf1 complex.," *Mol. Cell. Biol.*, vol. 25, no. 2, pp. 612–20, Jan. 2005.

[165] R. J. Sims, C. F. Chen, H. Santos-Rosa, T. Kouzarides, S. S. Patel, and D. Reinberg, "Human but not yeast CHD1 binds directly and selectively to histone H3 methylated at lysine 4 via its tandem chromodomains," *J. Biol. Chem.*, vol. 280, no. 51, pp. 41789–41792, Dec. 2005.

[166] Y. Lee, D. Park, and V. R. Iyer, "The ATP-dependent chromatin remodeler Chd1 is recruited by transcription elongation factors and maintains H3K4me3/H3K36me3 domains at actively transcribed and spliced genes," *Nucleic Acids Res.*, vol. 45, no. 12, pp. 7180–7190, Jul. 2017.

[167] S. L. McDaniel and B. D. Strahl, "Shaping the cellular landscape with Set2/SETD2 methylation," *Cellular and Molecular Life Sciences*, vol. 74, no. 18. Springer International Publishing, pp. 3317–3334, 06-Sep-2017.

[168] E. J. Wagner and P. B. Carpenter, "Understanding the language of Lys36 methylation at histone H3," *Nat. Rev. Mol. Cell Biol.*, vol. 13, no. 2, pp. 115–126, 2012.

[169] B. D. Strahl *et al.*, "Set2 Is a Nucleosomal Histone H3-Selective Methyltransferase That Mediates Transcriptional Repression Set2 Is a Nucleosomal Histone H3-Selective Methyltransferase That Mediates Transcriptional Repression," *Mol. Cell. Biol.*, vol. 22, no. 5, pp. 1298–1306, 2002.

[170] Q. Qiao, Y. Li, Z. Chen, M. Wang, D. Reinberg, and R. M. Xu, "The structure of NSD1 reveals an autoregulatory mechanism underlying histone H3K36 methylation," *J. Biol. Chem.*, vol. 286, no. 10, pp. 8361–8368, Mar. 2011.

[171] E. Martinez-Garcia *et al.*, "The MMSET histone methyl transferase switches global histone methylation and alters gene expression in t(4;14) multiple myeloma cells," *Blood*, vol. 117, no. 1, pp. 211–220, Jan. 2011.

[172] S. Rahman *et al.*, "The Brd4 Extraterminal Domain Confers Transcription Activation Independent of pTEFb by Recruiting Multiple Proteins, Including NSD3," *Mol. Cell. Biol.*, vol. 31, no. 13, pp. 2641–2652, Jul. 2011.

[173] J. C. Black, C. Van Rechem, and J. R. Whetstine, "Histone Lysine Methylation Dynamics: Establishment, Regulation, and Biological Impact," *Mol. Cell*, vol. 48, pp. 491–507, 2012.

[174] J. R. Whetstine *et al.*, "Reversal of Histone Lysine Trimethylation by the JMJD2 Family of Histone Demethylases," *Cell*, vol. 125, no. 3, pp. 467–481, May 2006.

[175] P. G. Amendola, N. Zaghet, J. J. Ramalho, J. Vilstrup Johansen, M. Boxem, and A. E. Salcini, "JMJD-5/KDM8 regulates H3K36me2 and is required for late steps of homologous recombination and genome integrity," *PLOS Genet.*, vol. 13, no. 2, p. e1006632, Feb. 2017.

[176] K. O. Kizer, H. P. Phatnani, Y. Shibata, H. Hall, A. L. Greenleaf, and B. D. Strahl, "A Novel Domain in Set2 Mediates RNA Polymerase II Interaction and Couples Histone H3 K36 Methylation with Transcript Elongation," *Mol. Cell. Biol.*, vol. 25, no. 8, pp. 3305–3316, Apr. 2005.

[177] S. Suzuki *et al.*, "Histone H3K36 trimethylation is essential for multiple silencing mechanisms in fission yeast," *Nucleic Acids Res.*, vol. 44, no. 9, pp. 4147–4162, May 2016.

[178] S. M. Fuchs, K. O. Kizer, H. Braberg, N. J. Krogan, and B. D. Strahl, "RNA polymerase II carboxyl-terminal domain phosphorylation regulates protein stability of the Set2 methyltransferase and histone H3 di- and trimethylation at lysine 36.," *J. Biol. Chem.*, vol. 287, no. 5, pp. 3249–56, Jan. 2012.

[179] Y. Wang, Y. Niu, and B. Li, "Balancing acts of SRI and an auto-inhibitory domain specify Set2 function at transcribed chromatin," *Nucleic Acids Res.*, vol. 43, no. 10, pp. 4881–4892, May 2015.

[180] K. Zhu *et al.*, "SPOP-containing complex regulates SETD2 stability and H3K36me3-coupled alternative splicing," *Nucleic Acids Res.*, vol. 45, no. 1, pp. 92–105, Jan. 2017.

[181] Y. Chu, R. Simic, M. H. Warner, K. M. Arndt, and G. Prelich, "Regulation of histone modification and cryptic transcription by the Bur1 and Paf1 complexes," *EMBO J.*, vol. 26, no. 22, pp. 4646–4656, Nov. 2007.

[182] K. Zhang, J. M. Haversat, and J. Mager, "CTR9/PAF1c regulates molecular lineage identity, histone H3K36 trimethylation and genomic imprinting during preimplantation development," *Dev. Biol.*, vol. 383, no. 1, pp. 15–27, Nov. 2013.

[183] K. Yamagata and A. Kobayashi, "The cysteine-rich domain of TET2 binds preferentially to mono- and dimethylated histone H3K36," *J. Biochem.*, vol. 161, no. 4, p. mvx004, Jan. 2017.

[184] B. Li *et al.*, "Histone H3 Lysine 36 Dimethylation (H3K36me2) Is Sufficient to Recruit the Rpd3s Histone Deacetylase Complex and to Repress Spurious Transcription," *J. Biol. Chem.*, vol. 284, no. 12, pp. 7970–7976, Mar. 2009.

[185] M. J. Carrozza *et al.*, "Histone H3 methylation by Set2 directs deacetylation of coding regions by Rpd3S to suppress spurious intragenic transcription," *Cell*, vol. 123, no. 4, pp. 581–592, 2005.

[186] O. Bell *et al.*, "Localized H3K36 methylation states define histone H4K16 acetylation during transcriptional elongation in Drosophila," *EMBO J.*, vol. 26, no. 24, pp. 4974–4984, 2007.

[187] A. Dhayalan *et al.*, "The Dnmt3a PWWP domain reads histone 3 lysine 36 trimethylation and guides DNA methylation.," *J. Biol. Chem.*, vol. 285, no. 34, pp. 26114–20, Aug. 2010.

[188] C. Ballaré *et al.*, "Phf19 links methylated Lys36 of histone H3 to regulation of Polycomb activity," *Nat. Struct. Mol. Biol.*, vol. 19, no. 12, pp. 1257–1265, Dec. 2012.

[189] T. Hayakawa *et al.*, "RBP2 is an MRG15 complex component and down-regulates intragenic histone H3 lysine 4 methylation," *Genes to Cells*, vol. 12, no. 6, pp. 811–826, 2007.

[190] R. Guo *et al.*, "BS69/ZMYND11 reads and connects histone H3.3 lysine 36 trimethylation-decorated chromatin to regulated pre-mRNA processing," *Mol. Cell*, vol. 56, no. 2, pp. 298–310,

2014.

[191] S. X. Pfister *et al.*, "SETD2-Dependent Histone H3K36 Trimethylation Is Required for Homologous Recombination Repair and Genome Stability," *Cell Rep.*, vol. 7, no. 6, pp. 2006–2018, 2014.

[192] N. Makharashvili and T. T. Paull, "CtIP: A DNA damage response protein at the intersection of DNA metabolism," *DNA Repair (Amst).*, vol. 32, pp. 75–81, Aug. 2015.

[193] L. Li and Y. Wang, "Cross-talk between the H3K36me3 and H4K16ac histone epigenetic marks in DNA double-strand break repair," *J. Biol. Chem.*, vol. 292, no. 28, pp. 11951–11959, 2017.

[194] M. Daugaard *et al.*, "LEDGF (p75) promotes DNA-end resection and homologous recombination," *Nat. Struct. Mol. Biol.*, vol. 19, no. 8, pp. 803–810, Aug. 2012.

[195] S. Maurer-Stroh, N. J. Dickens, L. Hughes-Davies, T. Kouzarides, F. Eisenhaber, and C. P. Ponting, "The Tudor domain 'Royal Family': Tudor, plant Agenet, Chromo, PWWP and MBT domains," *Trends Biochem. Sci.*, vol. 28, no. 2, pp. 69–74, 2003.

[196] L. M. Slater, M. D. Allen, and M. Bycroft, "Structural variation in PWWP domains," *J. Mol. Biol.*, vol. 330, no. 3, pp. 571–576, 2003.

[197] Y. Qiu *et al.*, "Solution structure of the Pdp1 PWWP domain reveals its unique binding sites for methylated H4K20 and DNA.," *Biochem. J.*, vol. 442, no. 3, pp. 527–38, 2012.

[198] H. Wu *et al.*, "Structural and histone binding ability characterizations of human PWWP domains," *PLoS One*, vol. 6, no. 6, p. e18919, Jun. 2011.

[199] R. Sanchez and M.-M. Zhou, "The PHD finger: a versatile epigenome reader," *Trends Biochem. Sci.*, vol. 36, pp. 364–372, 2011.

[200] S. Qin and J. Min, "Structure and function of the nucleosome-binding PWWP domain," *Trends Biochem. Sci.*, vol. 39, no. 11, pp. 536–547, 2014.

[201] K. Zhang, K. Mosch, W. Fischle, and S. I. S. Grewal, "Roles of the Clr4 methyltransferase complex in nucleation, spreading and maintenance of heterochromatin," *Nat. Struct. Mol. Biol.*, vol. 15, no. 4, pp. 381–388, Apr. 2008.

[202] T. Wang *et al.*, "Crystal Structure of the Human SUV39H1 Chromodomain and Its Recognition of Histone H3K9me2/3," *PLoS One*, vol. 7, no. 12, p. e52977, Dec. 2012.

[203] I. Ezkurdia *et al.*, "Multiple evidence strands suggest that there may be as few as 19 000 human protein-coding genes," *Hum. Mol. Genet.*, vol. 23, no. 22, pp. 5866–5878, Nov. 2014.

[204] V. Wood *et al.*, "The genome sequence of Schizosaccharomyces pombe," *Nature*, vol. 415, no. 6874, p. 871, Feb. 2002.

[205] A. Lock *et al.*, "PomBase 2018: user-driven reimplementation of the fission yeast database provides rapid and intuitive access to diverse, interconnected information," *Nucleic Acids Res.*, Oct. 2018.

[206] J. Z. Jacobs, K. M. Ciccaglione, V. Tournier, and M. Zaratiegui, "Implementation of the CRISPR-Cas9 system in fission yeast," *Nat. Commun.*, vol. 5, no. 1, p. 5344, Dec. 2014.

[207] M. Rodríguez-López *et al.*, "A CRISPR/Cas9-based method and primer design tool for seamless genome editing in fission yeast," *Wellcome Open Res.*, vol. 1, p. 19, May 2017.

[208] G. M. Cooper, *The cell. A molecular approach*, vol. 26, no. 1. ASM Press, 1998.

[209] H. Raji and E. Hartsuiker, "Double-strand break repair and homologous recombination in

Schizosaccharomyces pombe," *Yeast*, vol. 23, no. 13. John Wiley & Sons, Ltd, pp. 963–976, 15-Oct-2006.

[210] C. Deng and M. R. Capecchi, "Reexamination of gene targeting frequency as a function of the extent of homology between the targeting vector and the target locus.," *Mol. Cell. Biol.*, vol. 12, no. 8, pp. 3365–3371, Aug. 1992.

[211] R. Egel, D. H. Beach, and A. J. Klar, "Genes required for initiation and resolution steps of mating-type switching in fission yeast.," *Proc. Natl. Acad. Sci. U. S. A.*, vol. 81, no. 11, pp. 3481–5, Jun. 1984.

[212] S. I. S. Grewal and A. J. S. Klar, "A recombinationally repressed region between mat2 and mat3 loci shares homology to centromeric repeats and regulates directionality of mating-type switching in fission yeast," *Genetics*, vol. 146, no. 4, pp. 1221–1238, 1997.

[213] G. Thon, P. Bjerling, C. M. Bünner, and J. Verhein-Hansen, "Expression-State Boundaries in the Mating-Type Region of Fission Yeast," *Genetics*, vol. 161, no. 2, pp. 611–622, 2002.

[214] Y. Hiraoka, E. Henderson, and E. H. Blackburn, "Not so peculiar: fission yeast telomere repeats," *Trends Biochem. Sci.*, vol. 23, no. 4, p. 126, Apr. 1998.

[215] R. Sepsiova *et al.*, "Evolution of telomeres in schizosaccharomyces pombe and its possible relationship to the diversification of telomere binding proteins," *PLoS One*, vol. 11, no. 4, p. e0154225, Apr. 2016.

[216] W. Palm and T. de Lange, "How Shelterin Protects Mammalian Telomeres," *Annu. Rev. Genet.*, vol. 42, no. 1, pp. 301–334, Dec. 2008.

[217] T. Miyoshi, J. Kanoh, M. Saito, and F. Ishikawa, "Fission yeast pot1-Tpp1 protects telomeres and regulates telomere length," *Science (80-.).*, vol. 320, no. 5881, pp. 1341–1344, Jun. 2008.

[218] T. Sugiyama and R. Sugioka-Sugiyama, "Red1 promotes the elimination of meiosis-specific mRNAs in vegetatively growing fission yeast," *EMBO J.*, vol. 30, no. 6, p. 1027—1039, Mar. 2011.

[219] A. Bah, H. Wischnewski, V. Shchepachev, and C. M. Azzalin, "The telomeric transcriptome of Schizosaccharomyces pombe," *Nucleic Acids Res.*, vol. 40, no. 7, pp. 2995–3005, Apr. 2012.

[220] K. R. Hansen, P. T. Ibarra, and G. Thon, "Evolutionary-conserved telomere-linked helicase genes of fission yeast are repressed by silencing factors, RNAi components and the telomere-binding protein Taz1," *Nucleic Acids Res.*, vol. 34, no. 1, pp. 78–88, 2006.

[221] M. Zofall, S. Yamanaka, F. E. Reyes-Turcu, K. Zhang, C. Rubin, and S. I. S. Grewal, "RNA Elimination Machinery Targeting Meiotic mRNAs Promotes Facultative Heterochromatin Formation," *Science (80-.).*, vol. 335, no. 6064, pp. 96–100, 2012.

[222] M. Gullerova and N. J. Proudfoot, "Cohesin complex promotes transcriptional termination between convergent genes in S. pombe.," *Cell*, vol. 132, no. 6, pp. 983–95, Mar. 2008.

[223] S. Yamanaka *et al.*, "RNAi triggered by specialized machinery silences developmental genes and retrotransposons," *Nature*, vol. 493, no. 7433, pp. 557–560, 2012.

[224] G. Wang *et al.*, "Conservation of heterochromatin protein 1 function.," *Mol. Cell. Biol.*, vol. 20, no. 18, pp. 6970–6983, 2000.

[225] M. Lachner, D. O'Carroll, S. Rea, K. Mechtler, and T. Jenuwein, "Methylation of histone H3 lysine 9 creates a binding site for HP1 proteins.," *Nature*, vol. 410, no. 6824, pp. 116–20, 2001.

[226] G. Thon and J. Verhein-Hansen, "Four chromo-domain proteins of Schizosaccharomyces pombe differentially repress transcription at various chromosomal locations," *Genetics*, vol. 155, no. 2, pp. 551–568, 2000.

[227] T. Schalch, G. Job, S. Shanker, J. F. Partridge, and L. Joshua-Tor, "The Chp1-Tas3 core is a multifunctional platform critical for gene silencing by RITS. TL - 18," *Nat. Struct. Mol. Biol.*, vol. 18 VN-r, no. 12, pp. 1351–1357, 2011.

[228] C. Keller, R. Adaixo, R. Stunnenberg, K. J. Woolcock, S. Hiller, and M. Bühler, "HP1 Swi6 Mediates the Recognition and Destruction of Heterochromatic RNA Transcripts," *Mol. Cell*, vol. 47, no. 2, pp. 215–227, 2012.

[229] M. Sadaie *et al.*, "Balance between distinct HP1 family proteins controls heterochromatin assembly in fission yeast.," *Mol. Cell. Biol.*, vol. 28, no. 23, pp. 6973–6988, 2008.

[230] M. Zofall and S. I. S. Grewal, "Swi6/HP1 Recruits a JmjC Domain Protein to Facilitate Transcription of Heterochromatic Repeats," *Mol. Cell*, vol. 22, no. 5, pp. 681–692, 2006.

[231] S. Braun, J. F. Garcia, M. Rowley, M. Rougemaille, S. Shankar, and H. D. Madhani, "The Cul4-Ddb1Cdt2 ubiquitin ligase inhibits invasion of a boundary-associated antisilencing factor into heterochromatin," *Cell*, vol. 144, no. 1, pp. 41–54, 2011.

[232] P. N. C. B. Audergon *et al.*, "Restricted epigenetic inheritance of H3K9 methylation.," *Sci. (New York, NY)*, vol. 348, no. 6230, pp. 132–135, 2015.

[233] K. M. Creamer *et al.*, "The Mi-2 Homolog Mit1 Actively Positions Nucleosomes within Heterochromatin To Suppress Transcription," *Mol. Cell. Biol.*, vol. 34, no. 11, pp. 2046–2061, 2014.

[234] G. D. Shankaranarayana, M. R. Motamedi, D. Moazed, and S. I. S. Grewal, "Sir2 regulates histone H3 lysine 9 methylation and heterochromatin assembly in fission yeast.," *Curr. Biol.*, vol. 13, no. 14, pp. 1240–6, Jul. 2003.

[235] B. J. Alper, G. Job, R. K. Yadav, S. Shanker, B. R. Lowe, and J. F. Partridge, "Sir2 is required for Clr4 to initiate centromeric heterochromatin assembly in fission yeast," *EMBO J.*, vol. 32, no. 17, pp. 2321–2335, Aug. 2013.

[236] J. Kanoh *et al.*, "The Fission Yeast spSet1p is a Histone H3-K4 Methyltransferase that Functions in Telomere Maintenance and DNA Repair in an ATM Kinase Rad3-dependent Pathway," *J. Mol. Biol.*, vol. 326, no. 4, pp. 1081–1094, Feb. 2003.

[237] S. L. Sanders, M. Portoso, J. Mata, J. Bähler, R. C. Allshire, and T. Kouzarides, "Methylation of histone H4 lysine 20 controls recruitment of Crb2 to sites of DNA damage.," *Cell*, vol. 119, no. 5, pp. 603–14, Nov. 2004.

[238] E. B. Gómez, J. M. Espinosa, and S. L. Forsburg, "Schizosaccharomyces pombe mst2+ encodes a MYST family histone acetyltransferase that negatively regulates telomere silencing.," *Mol. Cell. Biol.*, vol. 25, no. 20, pp. 8887–8903, 2005.

[239] T. Yamada *et al.*, "Roles of histone acetylation and chromatin remodeling factor in a meiotic recombination hotspot.," *EMBO J.*, vol. 23, no. 8, pp. 1792–803, Apr. 2004.

[240] E. B. Gómez, R. L. Nugent, S. Laria, and S. L. Forsburg, "Schizosaccharomyces pombe histone acetyltransferase Mst1 (KAT5) is an essential protein required for damage response and chromosome segregation.," *Genetics*, vol. 179, no. 2, pp. 757–71, Jun. 2008.

[241] B. Xhemalce and T. Kouzarides, "A chromodomain switch mediated by histone H3 Lys 4 acetylation regulates heterochromatin assembly.," *Genes Dev.*, vol. 24, no. 7, pp. 647–52, Apr. 2010.

[242] B. D. Reddy *et al.*, "Elimination of a specific histone H3K14 acetyltransferase complex bypasses the RNAi pathway to regulate pericentric heterochromatin functions," *Genes Dev.*, vol. 25, no. 3, pp. 214–219, Feb. 2011.

[243] D. G. E. Martin *et al.*, "The Yng1p Plant Homeodomain Finger Is a Methyl-Histone Binding Module That Recognizes Lysine 4-Methylated Histone H3 □," vol. 26, no. 21, pp. 7871–7879, 2006.

[244] X. Shi *et al.*, "Proteome-wide analysis in Saccharomyces cerevisiae identifies several PHD fingers as novel direct and selective binding modules of histone H3 methylated at either lysine 4 or lysine 36," *J. Biol. Chem.*, vol. 282, no. 4, pp. 2450–2455, 2007.

[245] Y. Wang *et al.*, "Histone H3 lysine 14 acetylation is required for activation of a DNA damage checkpoint in fission yeast," *J. Biol. Chem.*, vol. 287, no. 6, pp. 4386–4393, 2012.

[246] S. C. Trewick, E. Minc, R. Antonelli, T. Urano, and R. C. Allshire, "The JmjC domain protein Epe1 prevents unregulated assembly and disassembly of heterochromatin.," *EMBO J.*, vol. 26, no. 22, pp. 4670–4682, 2007.

[247] J. Wang, B. D. Reddy, and S. Jia, "Rapid epigenetic adaptation to uncontrolled heterochromatin spreading," *Elife*, vol. 2015, no. 4, pp. 1–17, 2015.

[248] P. Hentges, B. Van Driessche, L. Tafforeau, J. Vandenhaute, and A. M. Carr, "Three novel antibiotic marker cassettes for gene disruption and marker switching inSchizosaccharomyces pombe," *Yeast*, vol. 22, no. 13, pp. 1013–1019, Oct. 2005.

[249] E. R. Sanders, "Aseptic laboratory techniques: volume transfers with serological pipettes and micropipettors.," *J. Vis. Exp.*, no. 63, May 2012.

[250] A. Roguev, M. Wiren, J. S. Weissman, and N. J. Krogan, "High-throughput genetic interaction mapping in the fission yeast Schizosaccharomyces pombe.," *Nat. Methods*, vol. 4, no. 10, pp. 861–866, 2007.

[251] A. Untergasser *et al.*, "Primer3--new capabilities and interfaces.," *Nucleic Acids Res.*, vol. 40, no. 15, p. e115, Aug. 2012.

[252] S. R. Collins, M. Schuldiner, N. J. Krogan, and J. S. Weissman, "A strategy for extracting and analyzing large-scale quantitative epistatic interaction data.," *Genome Biol.*, vol. 7, no. 7, p. R63, 2006.

[253] R. R Development Core Team, *R: A Language and Environment for Statistical Computing*. 2018.

[254] D. S. Booth *et al.*, "RStudio: Integrated Development for R," *Nature*, 2018.

[255] A. J. Saldanha, "Java Treeview--extensible visualization of microarray data," *Bioinformatics*, vol. 20, no. 17, pp. 3246–3248, Nov. 2004.

[256] M. J. L. de Hoon, S. Imoto, J. Nolan, and S. Miyano, "Open source clustering software," *Bioinformatics*, vol. 20, no. 9, pp. 1453–1454, Jun. 2004.

[257] C. A. Schneider, W. S. Rasband, and K. W. Eliceiri, "NIH Image to ImageJ: 25 years of image analysis," *Nat. Methods*, vol. 9, no. 7, pp. 671–675, Jul. 2012.

[258] K. Ekwall, G. Cranston, and R. C. Allshire, "Fission yeast mutants that alleviate transcriptional

silencing in centromeric flanking repeats and disrupt chromosome segregation," *Genetics*, vol. 153, no. 3, pp. 1153–1169, 1999.

[259] M. J. Vogel, D. Peric-Hupkes, and B. van Steensel, "Detection of in vivo protein-DNA interactions using DamID in mammalian cells.," *Nat. Protoc.*, vol. 2, no. 6, pp. 1467–78, 2007.

[260] B. Steglich, G. J. Filion, B. van Steensel, and K. Ekwall, "The inner nuclear membrane proteins Man1 and Ima1 link to two different types of chromatin at the nuclear periphery in S. pombe," *Nucleus*, vol. 3, no. 1, pp. 77–87, Jan. 2012.

[261] K. J. Woolcock, D. Gaidatzis, T. Punga, and M. Bühler, "Dicer associates with chromatin to repress genome activity in Schizosaccharomyces pombe," *Nat. Struct. Mol. Biol.*, vol. 18, no. 1, pp. 94–100, 2011.

[262] C. Keller, R. Kulasegaran-Shylini, Y. Shimada, H. R. Hotz, and M. Bühler, "Noncoding RNAs prevent spreading of a repressive histone mark," *Nat. Struct. Mol. Biol.*, vol. 20, no. 8, pp. 994–1000, 2013.

[263] S. Marguerat, A. Schmidt, S. Codlin, W. Chen, R. Aebersold, and J. Bähler, "Quantitative analysis of fission yeast transcriptomes and proteomes in proliferating and quiescent cells," *Cell*, vol. 151, no. 3, pp. 671–683, 2012.

[264] J. ichi Nakayama *et al.*, "Alp13, an MRG family protein, is a component of fission yeast Clr6 histone deacetylase required for genomic integrity," *EMBO J.*, vol. 22, no. 11, pp. 2776–2787, Jun. 2003.

[265] K. O. Kizer, H. P. Phatnani, Y. Shibata, H. Hall, A. L. Greenleaf, and B. D. Strahl, "A Novel Domain in Set2 Mediates RNA Polymerase II Interaction and Couples Histone H3 K36 Methylation with Transcript Elongation," *Mol. Cell. Biol.*, vol. 25, no. 8, pp. 3305–3316, Apr. 2005.

[266] Y. Wang *et al.*, "Regulation of Set9-Mediated H4K20 Methylation by a PWWP Domain Protein," *Mol. Cell*, vol. 33, no. 4, pp. 428–437, 2009.

[267] B. Rao, Y. Shibata, B. D. Strahl, and J. D. Lieb, "Dimethylation of Histone H3 at Lysine 36 Demarcates Regulatory and Nonregulatory Chromatin Genome-Wide," *Mol. Cell. Biol.*, vol. 25, no. 21, pp. 9447–9459, Nov. 2005.

[268] E. S. Chen, K. Zhang, E. Nicolas, H. P. Cam, M. Zofall, and S. I. S. Grewal, "Cell cycle control of centromeric repeat transcription and heterochromatin assembly," *Nature*, vol. 451, no. 7179, pp. 734–737, Feb. 2008.

[269] A. Matsuda *et al.*, "Highly condensed chromatins are formed adjacent to subtelomeric and decondensed silent chromatin in fission yeast," vol. 6, p. 7753, Jul. 2015.

[270] C. J. Hogan *et al.*, "Fission yeast lec1-ino80-mediated nucleosome eviction regulates nucleotide and phosphate metabolism.," *Mol. Cell. Biol.*, vol. 30, no. 3, pp. 657–74, Feb. 2010.

[271] B. J. Monahan, J. Villén, S. Marguerat, J. Bähler, S. P. Gygi, and F. Winston, "Fission yeast SWI/SNF and RSC complexes show compositional and functional differences from budding yeast," *Nat. Struct. Mol. Biol.*, vol. 15, no. 8, pp. 873–880, Aug. 2008.

[272] M. Kimura and A. Ishihama, "Tfg3, a subunit of the general transcription factor TFIIF in Schizosaccharomyces pombe, functions under stress conditions," *Nucleic Acids Res.*, vol. 32, no. 22, pp. 6706–6715, 2004.

[273] V. Flury *et al.*, "The Histone Acetyltransferase Mst2 Protects Active Chromatin from Epigenetic

Silencing by Acetylating the Ubiquitin Ligase Brl1," *Mol. Cell*, vol. 67, no. 2, pp. 294-307.e9, Jul. 2017.

[274] I. V. Mikheyeva, P. J. R. Grady, F. B. Tamburini, D. R. Lorenz, and H. P. Cam, "Multifaceted Genome Control by Set1 Dependent and Independent of H3K4 Methylation and the Set1C/COMPASS Complex," *PLoS Genet.*, vol. 10, no. 10, 2014.

[275] A. W. Snowden, P. D. Gregory, C. C. Case, and C. O. Pabo, "Gene-specific targeting of H3K9 methylation is sufficient for initiating repression in vivo," *Curr. Biol.*, vol. 12, no. 24, pp. 2159–2166, Dec. 2002.

[276] R. C. Allshire and K. Ekwall, "Epigenetics regulation of chromatin states in *Schizosaccharomyces pombe*," *Cold Spring Harb Perspect. Biol.*, vol. 7, pp. 1–25, 2015.

[277] R. R. R. R. Barrales, M. Forn, P. R. P. R. P. R. Georgescu, Z. Sarkadi, and S. Braun, "Control of heterochromatin localization and silencing by the nuclear membrane protein Lem2," *Genes Dev.*, vol. 30, no. 2, pp. 1–16, Jan. 2016.

[278] D. E. Gottschling, "Summary: Epigenetics—from Phenomenon to Field," *Cold Spring Harb. Symp. Quant. Biol.*, vol. 69, pp. 507–520, Jan. 2004.

[279] D. Moazed, "Mechanisms for the inheritance of chromatin states," *Cell*, vol. 146, no. 4. Elsevier, pp. 510–518, 19-Aug-2011.

[280] V. E. Maltby *et al.*, "Histone H3 Lysine 36 Methylation Targets the Isw1b Remodeling Complex to Chromatin," *Mol. Cell. Biol.*, vol. 32, no. 17, pp. 3479–3485, Sep. 2012.

[281] A. Carpy *et al.*, "Absolute proteome and phosphoproteome dynamics during the cell cycle of Schizosaccharomyces pombe (Fission Yeast).," *Mol. Cell. Proteomics*, vol. 13, no. 8, pp. 1925–36, Aug. 2014.

[282] K. M. Kowalik, Y. Shimada, V. Flury, M. B. Stadler, J. Batki, and M. Bühler, "The Paf1 complex represses small-RNA-mediated epigenetic gene silencing.," *Nature*, vol. 520, no. 7546, pp. 248–252, 2015.

[283] M.-H. Kuo *et al.*, "Transcription-linked acetylation by Gcn5p of histones H3 and H4 at specific lysines," *Nature*, vol. 383, no. 6597. pp. 269–272, 1996.

[284] R. L. Nugent *et al.*, "Expression profiling of S. pombe acetyltransferase mutants identifies redundant pathways of gene regulation," *BMC Genomics*, vol. 11, no. 1, p. 59, 2010.

[285] J. C. Tanny, H. Erdjument-Bromage, P. Tempst, and C. D. Allis, "Ubiquitylation of histone H2B controls RNA polymerase II transcription elongation independently of histone H3 methylation," *Genes Dev.*, vol. 21, no. 7, p. 835—847, Apr. 2007.

[286] N. J. Krogan *et al.*, "Methylation of histone H3 by Set2 in Saccharomyces cerevisiae is linked to transcriptional elongation by RNA polymerase II.," *Mol. Cell. Biol.*, vol. 23, no. 12, pp. 4207–18, 2003.

[287] T. Cheutin, A. J. McNairn, T. Jenuwein, D. M. Gilbert, P. B. Singh, and T. Misteli, "Maintenance of stable heterochromatin domains by dynamic HP1 binding," *Science (80-.).*, vol. 299, no. 5607, pp. 721–725, 2003.

[288] X. Tadeo *et al.*, "Elimination of shelterin components bypasses RNAi for pericentric heterochromatin assembly," *Genes Dev.*, vol. 27, no. 22, pp. 2489–2499, 2013.